OPTIMUM DESIGN OF PARALLEL, HORIZONTAL AND LAMINAR FORCED
CONVECTION AIR-COOLED RECTANGULAR CHANNELS WITH
INSULATED LATERAL SURFACES

A THESIS SUBMITTED TO
THE GRADUATE SCHOOL OF NATURAL AND APPLIED SCIENCES
OF
MIDDLE EAST TECHNICAL UNIVERSITY

BY

MEHMET OZAN ÖZDEMİR

IN PARTIAL FULFILLMENT OF THE REQUIREMENTS
FOR
THE DEGREE OF MASTER OF SCIENCE
IN
MECHANICAL ENGINEERING

JULY 2009

Approval of the thesis:

OPTIMUM DESIGN OF PARALLEL, HORIZONTAL AND LAMINAR FORCED CONVECTION AIR-COOLED RECTANGULAR CHANNELS WITH INSULATED LATERAL SURFACES

submitted by **MEHMET OZAN ÖZDEMİR** in partial fulfillment of the requirements for the degree of **Master of Science in Mechanical Engineering Department, Middle East Technical University** by,

Prof. Dr. Canan Özgen   _____
Dean, Graduate School of **Natural and Applied Sciences**

Prof. Dr. Suha Oral   _____
Head of Department, **Mechanical Engineering**

Prof. Dr. Hafit Yüncü   _____
Supervisor, **Mechanical Engineering Dept., METU**

Examining Committee Members:

Prof. Dr. Faruk Arınç   _____
Mechanical Engineering Dept., METU

Prof. Dr. Hafit Yüncü   _____
Mechanical Engineering Dept., METU

Assoc. Prof. Dr. Atilla Bıyıkoğlu   _____
Mechanical Engineering Dept., Gazi Univ.

Assoc. Prof. Dr. Cemil Yamalı   _____
Mechanical Engineering Dept., METU

Assist. Prof. Dr. İlker Tarı   _____
Mechanical Engineering Dept., METU

Date: 15.07.2009

I hereby declare that all information in this document has been obtained and presented in accordance with academic rules and ethical conduct. I also declare that, as required by these rules and conduct, I have fully cited and referenced all material and results that are not original to this work.

Name, Last name: MEHMET OZAN ÖZDEMİR

Signature   :

ABSTRACT

OPTIMUM DESIGN OF PARALLEL, HORIZONTAL AND LAMINAR FORCED
CONVECTION AIR-COOLED RECTANGULAR CHANNELS WITH
INSULATED LATERAL SURFACES

Özdemir, Mehmet Ozan

M.S., Department of Mechanical Engineering

Supervisor: Prof. Dr. Hafit Yüncü

July 2009, 93 Pages

The objective of this thesis is to predict numerically the optimal spacing between parallel heat generating boards. The isothermal boards are stacked in a fixed volume of electronic package enclosed by insulated lateral walls, and they are cooled by laminar forced convection of air with prescribed pressure drop. Fixed pressure drop assumption is an acceptable model for installations in which several parallel boards in electronic equipment receive the coolant from the same source such as a fan.

In the numerical algorithm, the equations that govern the process of forced convection for constant property incompressible flow through one rectangular channel are solved. Numerical results of the flow and temperature field in each rectangular channel yield the optimal board-to-board spacing by which maximum heat dissipation rate from the package to the air is achieved. After the results of the optimization procedure are given, the correlations for the determination of the maximum heat transfer rate from the package and optimal spacing between boards

are, respectively, derived in terms of prescribed pressure difference, board length, and density and kinematic viscosity of air.

In conclusion, the obtained correlations are compared and assessed with the available two-dimensional studies in literature for infinite parallel plates. Furthermore, existing two-dimensional results are extended to a more generalized three-dimensional case at the end of the thesis.

Keywords: Optimization, Rectangular Channels, Laminar Air Flow, Forced Convection, Electronic Thermal Packaging

ÖZ

LAMİNER ZORLANMIŞ TAŞINIM YOLUYLA VE HAVA KULLANILARAK
SOĞUTULAN YATAY, PARALEL VE YAN YÜZEYLERİ YALITILMIŞ
DİKDÖRTGEN KANALLARIN OPTİMUM TASARIMI

Özdemir, Mehmet Ozan

Yüksek Lisans, Makine Mühendisliği Bölümü

Tez Yöneticisi: Prof. Dr. Hafit Yüncü

Temmuz 2009, 93 Sayfa

Bu tezin amacı, paralel ısı yayan plakaların optimum dizilişinin nümerik olarak incelenmesidir. İzotermal plakalar, yalıtılmış yan yüzeylerle çevrili olan sabit hacimli bir elektronik sistem paketinde bulunmakta ve öngörülmüş basınç farkı kullanılarak havanın laminer zorlanmış taşınımı ile soğutulmaktadır. Sabit veya öngörülmüş basınç varsayımı, elektronik malzemelerdeki birkaç paralel plakanın fan gibi ortak bir kaynak tarafından soğutulduğu donanımlar için kabul edilebilir bir modeldir.

Hazırlanan nümerik algoritmada, dikdörtgen kesitli bir kanaldaki sabit özellikli sıkıştırılamaz akış için zorlanmış taşınımı temsil eden denklemler çözülmüştür. Her bir dikdörtgen kesitli kanaldaki akış ve sıcaklık dağılımının nümerik sonuçları, plakalardan havaya olan ısı transferinin en yüksek seviyede elde edilmesi amacıyla plakaların optimum uzaklığının belirlenmesini sağlamıştır. Optimizasyon işleminin sonuçları verildikten sonra, en yüksek ısı transferi değerini ve paralel plakaların optimum uzaklığını veren bağıntılar, öngörülmüş basınç farkı, plaka uzunluğu, havanın yoğunluğu ve havanın kinematik viskozitesi cinsinden ayrı ayrı türetilmiştir.

Sonuç olarak; bu tezde elde edilen bilgiler, literatürde bulunan sonsuz genişliğe sahip izotermal paralel plakalar hakkındaki iki boyutlu çalışmalar ile karşılaştırılmış ve değerlendirilmiştir. Buna ilaveten, sabit hacimde bulunan paralel plakaların optimizasyonuna ilişkin iki boyutlu sonuçlar, ilgili tezin sonunda daha genellenmiş bir üç boyutlu modele genişletilmiştir.

Anahtar Kelimeler: Optimizasyon, Dikdörtgen Kanallar, Laminer Hava Akışı, Zorlanmış Taşınım, Elektronik Termal Paketleme

To My Grandparents

ACKNOWLEDGMENTS

TABLE OF CONTENTS

LIST OF TABLES

LIST OF FIGURES

FIGURES

NOMENCLATURE

A Face areas of the control volumes [m^2]

A_{cr} Cross-sectional area of the channels [equation (3.18)] [m^2]

A^* Dimensionless face areas of the control volumes

a Coefficients in discretized algebraic equations [equations from (4.15a) to (4.15f), from (4.17a) to (4.17f), from (4.19a) to (4.19f), from (4.25a) to (4.25f), from (4.28a) to (4.28f)]

B Coefficient in derived equation (5.15) for optimum spacing [Table 5.1 or Figure 5.21]

b Source term in discretized pressure correction equation [equation (4.25g)]

C Coefficient in derived equation (5.16) for maximum total heat transfer rate [Table 5.1 or Figure 5.22]

c_p Constant pressure specific heat of air (coolant) [J/kg.K]

D Diffusion conductance [equations from (4.7a) to (4.7f)] [kg/s]

D_h Hydraulic diameter [equation (3.17) or (5.6)] [m]

D^* Dimensionless diffusion conductance [equations from (4.9a) to (4.9f)]

E_p Average relative error in the approximation for dimensionless pressure (in SIMPLE algorithm) or for pressure correction (in Gauss-Seidel iterations) [equation (6.1a)]

E_u Average relative error in the approximation for dimensionless x-velocity component in SIMPLE or Gauss-Seidel iterations [equation (6.1b)]

E_v Average relative error in the approximation for dimensionless y-velocity component in SIMPLE or Gauss-Seidel iterations [equation (6.1c)]

E_w Average relative error in the approximation for dimensionless z-velocity component in SIMPLE or Gauss-Seidel iterations [equation (6.1d)]

E_θ Average relative error in the approximation for dimensionless temperature in Gauss-Seidel iterations [equation (6.1e)]

F Flow rate through a face of the control volume [equations from (4.5a) to(4.5f)] [kg/s]

F_{wall} Shear force applied to the wall along the face of the wall control volumes [equations (4.41a) and (4.41b)] [N]

F^* Dimensionless flow rate through a face of the control volume [equations from (4.6a) to (4.6f)]

F^*_{wall} Dimensionless shear force applied to the walls on the wall control volumes [equations (4.43a) and (4.43b)]

f Friction factor (dimensionless) [equation (4.34)]

H Height of the whole assembly occupied by the channels in z-direction [m]

h Heat transfer coefficient [W/m^2.K]

k Thermal conductivity [W/m.K]

Kn Knudsen number (dimensionless) [(Molecular mean free path, m)/ (Representative length scale, m)]

L Length of the channels in x-direction [m]

$\dot{m}$ Air (coolant) flow rate [equation (5.2)] [kg/s]

M_{inlet} Inlet mass flow rate of air [equation (4.40a)] [kg/s]

M_{outlet} Outlet mass flow rate of air evaluated after each iteration step [equation (4.40b)] [kg/s]

N_x Number of grids in x-direction

N_y Number of grids in y-direction

N_z Number of grids in z-direction

Nu Nusselt number (dimensionless) [equation (4.37)]

P Pressure [Pa]

P_e Pressure at the exit of the channel [Pa]

P_i Pressure at the inlet of the channel [Pa]

P_{cr} Perimeter of the channel cross-section [equation (3.19)] [m]

P' Dimensionless pressure correction

P^* Dimensionless pressure [equation (3.8)]

P^{**} Corrected dimensionless pressure [equation (4.26)]

Pe Peclet number (dimensionless); rate of strength of convective heat transfer to conductive heat transfer

Pr	Prandtl number (dimensionless) [equation (3.20)]
$\dot{Q}$	Total heat transfer rate from the boards to the flow [equation (5.8)] [W]
$\dot{Q}_{sc}$	Heat transfer rate from single channel to the flow [equation (5.3)] [W]
q_{wall}	Heat transfer rate from the wall to the control volume [equation (4.42)] [W]
q^{*}_{wall}	Dimensionless heat transfer rate from the wall to the control volume [equation (4.44)]
r	Ratio of upstream side gradient of ϕ to downstream side gradient of ϕ [equations (4.2) and (4.4)]
Re	Reynolds number (dimensionless)
Re_{D_h}	Reynolds number based on hydraulic diameter (dimensionless) [equation (3.16)]
s	Spacing between the isothermal walls or height of single channel in z direction [m]
s_{opt}	Optimum spacing between the isothermal walls or optimum height of single channel in z direction [equation (5.15)] [m]
T	Temperature [K]
T_e	Exit temperature of air (coolant) [K]
T_w	Uniform temperature of isothermal walls or parallel circuit boards [K]
T_∞	Free stream temperature of air (coolant) or inlet temperature of air (coolant) [K]
t	Time [s]
U_∞	Free stream velocity of air (coolant) or inlet velocity of air (coolant) [m/s]
u	Velocity component in x-direction [m/s]
$u^{'}$	Dimensionless correction for x-velocity component [equation (4.22a)]
u^{*}	Dimensionless x-velocity component [equation (3.9a)]
u^{**}	Corrected dimensionless x-velocity component [equation (4.23a)]
v	Velocity component in y-direction [m/s]
$v^{'}$	Dimensionless correction for y-velocity component [equation (4.22b)]
v^{*}	Dimensionless y-velocity component [equation (3.9b)]
v^{**}	Corrected dimensionless y-velocity component [equation (4.23b)]

W	Width of the whole assembly or each channel [m]
w	Velocity component in z-direction [m/s]
w'	Dimensionless correction for z-velocity component [equation (4.22c)]
w^*	Dimensionless z-velocity component [equation (3.9c)]
w^{**}	Corrected dimensionless z-velocity component [equation (4.23c)]
x	Longitudinal coordinate along the channel [m]
x^+	Dimensionless axial coordinate for the hydrodynamic entrance region in Figures from 4.8 to 4.11 [equation (4.49)]
x^*	Dimensionless longitudinal coordinate along the channel [equation (3.7a)]
y	Transverse coordinate along the width across the channel cross-section [m]
y^*	Dimensionless transverse coordinate along the width across the channel cross-section [equation (3.7b)]
z	Transverse coordinate along the height across the channel cross-section [m]
z^*	Dimensionless transverse coordinate along the height across the channel cross-section [equation (3.7c)]
α	Relaxation factor (dimensionless)
β	Aspect ratio of the channel cross-section [equation (4.35)]
Γ	Diffusion coefficient [equations (4.8a) and (4.8b), or Table 4.1]
ΔF	Difference in dimensionless mass flow rates across the faces of the control volume; total dimensionless mass flow rate into or out of the control volume [equations (4.15g), (4.17g), (4.19g) and (4.28g)]
ΔP^*	Dimensionless pressure drop along the channel [equation (4.36)]
Δx	Distance between the grid lines in x-direction [m]
Δx^*	Dimensionless distance between the grid lines in x-direction
Δy	Distance between the grid lines in y-direction [m]
Δy^*	Dimensionless distance between the grid lines in y-direction
Δz	Distance between the grid lines in z-direction [m]
Δz^*	Dimensionless distance between the grid lines in z-direction
δx	Distance between two any points in x-direction [m]
δy	Distance between two any points in y-direction [m]
δz	Distance between two any points in z-direction [m]

ε	Specified relative error limits for the iterative calculations of unknown variables; velocity components, pressure corrections and temperature [equations from (4.31a) to (4.31e)]
θ	Dimensionless temperature [equation (3.10)]
θ_e	Dimensionless temperature of the flow at exit of the channel
μ	Absolute viscosity [Pa.s]
v	Kinematic viscosity [equation (3.6)] [m^2/s]
ρ	Density [kg/m^3]
ϕ	General term for unknown variables; u, v, w, p and T
ψ	Limiter functions included in equations (4.1) and (4.3) for TVD schemes (dimensionless)

CHAPTER 1

INTRODUCTION

One of the most important aspects of electronic equipment management has always been recognized to be the dissipation of the heat produced in the electronic components. This operation is needed to avoid overheating of apparatus.

The electronic equipment cooling problem has become even more crucial during the years. As a consequence of the continuous evolution in the electronics industry year-by-year, production of more compact apparatus has been demanded more frequently. Thus, the quantity of heat to be dispersed is observed to be higher per unit area. With the above considerations, it is clear that there is a considerable importance in the optimization of cooling systems of electronic equipment. In this study, geometric optimization of parallel heat generating boards stacked in a fixed three-dimensional volume is to be investigated. As it may be appreciated, three dimensional studies for the optimization of cooling systems for electronic devices are very limited. This study may be an extension of existing two-dimensional studies to more generalized three-dimensional models and may also be used as a source for more detailed future studies about three-dimensional design of cooling systems.

Dissipating excessive heat generated within electronic systems is the main concern in the thermal design of the electronics. This operation is achieved by thermal packaging of system components. Generated heat is dissipated by the help of a coolant which flows through the spaces in the volume occupied by the components. The corresponding packaging should be appropriately designed so that heat transferred to the coolant is maximized by keeping the highest temperature within the

components below the allowable limit. Thermal packaging and its design are important for these reasons [1];

- Prevention of catastrophic failure due to the excessive temperatures within the electronic equipments

- Making operations of the electronic systems more reliable

- Reduction of life-cycle costs for the electronic equipments by means of a satisfactory thermal packaging

The need for thermal control of electronic equipments by means of packaging appeared in the 1960s when "SSI (small-scale integration)" chips began to be manufactured. At those times electronic systems were explored to be generating heat power of 0.1 to 0.3 W per 2 to 3 mm "SSI silicon semiconductor devices". However, heat generation within the components has significantly increased in parallel with technological developments year-by-year since then. After the beginning of mid-1980s, "ECL (emitter-coupled logic)" "LSI (large-scale integration)" was demanded with the cost of heat dissipation of 5 W per 5 mm chips [2]. Moreover, allowable maximum temperatures within the equipments decreased from 110-125 °C to 65-85 °C with high competence in reliability and performance. Hence, heat fluxes were obtained to be 25 x 10^4 W/m^2 from the "LSI" chips. This condition introduced the higher demand for better cooling systems and made the design of thermal packaging more challenging [1].

Next, in the mid-1990s, "CMOS (Complementary metal-oxide-semiconductor)" microprocessor chips were started to be manufactured owing to the domination of better speed and flexibility in the electronics industry. Consequently, power dissipation rates encountered in the devices increased to 15-30 W. Therefore, air was seen to be preferred as the coolant in the end of the 1990s because of the higher prices in electronics manufacturing and lower prices of air-cooling compared to the water-cooling. In addition, in the end of the 1990s, heat dissipation rates from the electronic chips were observed to be above 75 W with the estimated heat fluxes of $25x10^4$ W/m^2. To compensate this drastic condition, tolerated maximum temperatures within the systems were selected to be approximately 100 °C instead of

the aggressive studies to develop the efficiency of air-cooling [1]. It is declared in [3] and [4] that power dissipation requirements are expected to be 175 W for the operations at about 3 GHz in the beginning of 21st century. On the other hand, chip areas are predicted to expand from 3.8 cm^2 to 7.5 cm^2. Thus, heat fluxes from the chips are anticipated to rise to 30x10^4 W/m^2 rather than a harsh increase [3, 4]. However, search for thermal packaging with superior performance and capacity has been continuing along with the competence in the industry and the production of electronics having better qualities.

There are different cooling methods used in the thermal packaging of electronic components. These methods are summarized with their specifications in Table 1.1.

Table 1.1 General cooling techniques used in thermal packaging [5]

	Natural air convection (NAC)	Forced air convection (FAC)	FAC plus Water-cooled heat exchanger (WCHE)	Liquid-cooled (including evaporation, boiling)	
				Direct	**Indirect**
Coolant	air	air	air, water	inert insulator liquid	water etc.
Coolant mover	(buoyancy)	fan/blower	fan/blower, pump	pump	pump
Coolant velocity (m/s)	0.2	0.5-10			
Coolant capability	small	middle-large	middle-large	very large	large
Equipment volume	large	middle	middle	small	small
Acoustic noise	none	middle-large	middle	small	small
Reliability of cooling	high	middle	middle	small	small
Economy	high	middle-large	middle	small-middle	small-middle
Remarks (capabilities)	Capability increases with chimney effect			Capability depends on HE capacity	He-gas used to decrease contact

Although natural convection is also applied in thermal management of some memory devices, many "DRAMs (Dynamic Random Access Memories)" and "SRAMs (Static Random Access Memories)" are cooled by forced convection in a densely packed manner on a "PCB (Printed Circuit Board)" for considerable cooling performance. Forced convection is broadly applicable to these devices in order to obtain a maximum tolerable temperature of about 100 °C with densely packed memories each dissipating 1 W of heat power in practice [1]. Hence, forced convection of air, along with the technological advances in the industry, has been becoming more and more favorable due to its higher cooling capability as seen from Table 1.1.

Electronic systems are designed with different stages/levels of packaging from smallest element to the largest one. These levels are shown in Figure 1.1. As illustrated in Figure 1.1, there are four levels of packaging from smallest to largest;

1. Chip packages containing several chips

2. PCBs having a number of packages

3. Backplane level

4. System level
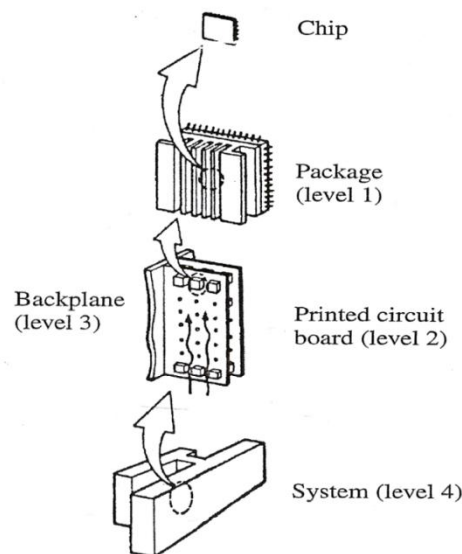
Figure 1.1 Levels of packaging in electronics [1]

Each level is considered separately during the design of thermal management since each one requires different cooling mechanisms [1]. The assembly or the model used in this thesis is selected to represent PCB level of packaging. Therefore, the results of this thesis can be applied for the cooling of PCBs.

In order to obtain the heat transfer from the PCBs to the coolant, there are a significant number of factors which are observed to be conduction within the packages and the PCB, convection to the air as the coolant, and the radiation in the surroundings [6]. Using heat transfer calculations, an optimum design for the thermal packaging should be found. However, different considerations are theoretically included in the optimization process. For instance, geometric parameters of the channels, shape of the channels and their cross-sections, thermal and physical properties of the air and the electronic components, and coolant mass flow rate are the crucial points that affect the optimization. Conversely, all these variables are not practically involved in the optimization process. Engineers are expected to consider the most effective variables of optimization by using his/her sense [7].

Optimization, which will be utilized in this thesis, can be expressed as the determination of the best geometrical arrangement by which the array of PCBs are located in the finite volume. Best arrangement, or layout, of PCBs corresponds to the design in which maximum heat dissipation from the electronic equipment, packed in a fixed volume, is achieved.

In this study, finite parallel boards at fixed wall temperature (T_w) stacked in a fixed volume (L x H x W) with insulated lateral walls are the main assembly in the calculations. Spacing of the boards (s) or the height of each channel (s) is tried to be optimized such that heat transfer rate to the air (coolant) is maximum. During the optimization, pressure drop across the channels is considered to be fixed. Note that constant pressure difference in forced convection of air is mainly provided by a fan or blower, as it may also be observed in Table 1.1 [5]. The flow is assumed to be laminar, incompressible and steady. The wall thicknesses are neglected. At the end of the study, optimum aspect ratio of the channels are introduced and discussed in

various aspects. In consequence, a general graphical relation for the design of three-dimensional thermal packaging is suggested with additional comments.

In this thesis, literature survey on the corresponding field is introduced in Chapter 2. Next, the model or the assembly used in the thesis, problem and the objectives of optimization are defined in detail in Chapter 3. Details of the solution are presented in Chapter 4. Results of the study are given in Chapter 5. Finally, obtained results are discussed and compared with the previously reported data in Chapter 6.

CHAPTER 2

LITERATURE SURVEY

A significant number of earlier studies have been devoted on searching for optimal spacing of infinite parallel plates and optimal arrangement of cooling passages of electronic equipment for laminar flow in literature. The common points or objectives in all of these efforts are to maximize the cooling performance and to gain maximum benefits from the thermal management process. In particular, recent progresses in the corresponding field can be divided into two main groups. The first group is the two-dimensional studies. The second group, which is limited in literature, is the optimization for three-dimensional geometries. To be convenient, two-dimensional studies are to be presented first. After two-dimensional studies are introduced, three-dimensional optimization processes are to be given in the current chapter.

First 2-D study to be considered was published by Bejan and Sciubba [8] for a stack of parallel boards in a fixed volume subjected to the laminar forced convection of air flow with fixed pressure drop. Thickness of the boards was assumed to be negligible. Optimum spacing of the boards with isothermal surfaces were determined by using an approximate way of intersection of asymptotes which was first presented in [9] and was explained in detail in [10]. In addition, more exact results were found in [8] for the cases of isothermal and uniform heat flux boundary conditions by using a numerical solution which was supported by the empirical formula in literature. Therefore, results produced from the method of intersection of asymptotes were validated by the numerical approach. As a consequence, they [8] demonstrated that there is an optimum spacing, which occurs when thermal entrance length of the flow is the same as the channel length, for the maximum heat transfer rate and this

optimum value is almost independent from the thermal boundary condition (isothermal or uniform heat flux) of the boards. Subsequently, Mereu, Sciubba and Bejan [11] extended the analysis reported in [8] for three different cases; fixed pressure drop, fixed flow-rate and fixed pumping power conditions. In [11], board thicknesses were not neglected and optimum spacing of the boards were again analytically found by the intersection of asymptotes. Result of this analytical solution was compared with the more exact numerical results by using a commercial finite element package. Mereu et al. [11] showed that optimum spacing is nearly independent from the board thickness. Next, experimental confirmation of Bejan and Sciubba's work [8] was carried out by Favre-Marinet, Le Person and Bejan [12]. Furthermore, Campo [13] focused on the stacked parallel boards subjected to uniform heat flux with two different conditions; bilateral heating (all two surfaces of boards active or heated) and unilateral heating (one surface heated, the other one insulated). Intersection of asymptotes was performed for the solution of each case by neglecting the plate thickness. Comparison of results for bilateral heating with Bejan and Sciubba's findings [8] is reported in [13]. Yüncü and Ekici [14] also investigated numerically the same layout of cooling system as the one in Bejan and Sciubba's publication [8] for laminar flow with isothermal and uniform heat flux boundary conditions. In [14], a finite volume based numerical algorithm is implemented for the discretization and solution of governing equations. On account of validation, Yüncü and Ekici [14] compared their results with the analytical and numerical outcomes of Bejan and Sciubba [8]. It was indicated in [14] that the correlations for the optimum spacing in [14] match with the ones in [8] within an error of 10% and 1% for the intersection of asymptotes and the empirically based numerical solution, respectively.

Morega and Bejan [15] advanced the solution of [8] for the stacked parallel plates with uniform heat flux to the model of parallel plates on which flush-mounted and protruding discrete heat sources are placed. Moreover, Bejan and Fautrelle [16] suggested locating additional smaller plates into the interstitial spaces between the parallel boards, which was first dealt with in [8]. They optimized the spacing and length of each type of boards (from small to large) analytically by performing intersection of asymptotes and constructal theory. Theoretical definitions and

explanations of constructal theory are given in [10] in detail. In fact, Bejan and Fautrelle [16] proved that maximum thermal performance of laminar forced convection across parallel boards can be increased by using multi-scale approach. The same problem as in [16] was solved numerically in [17] by implementing a commercial finite element package. Numerical results of [17] and analytical results of [16] were compared and discussed in [17].

Furukawa and Wang [18] performed "TO (thermal optimization)" in order to find the optimum layout of a stack of parallel boards on which discrete heat generating sources are placed. Air flow was considered as laminar and fully developed. "Entropy generation minimization (EGM)", which is expressed in [19] in detail, is implemented during the solution stage. Governing equations in [18] were handled numerically by the help of SIMPLER algorithm [20].

Types of heat transfer other than forced convection through two-dimensional geometries were also considered in [21] and [22]. Da Silva, Bejan and Lorente [21] analyzed the optimization of vertical boards which are subjected to laminar flow with natural convection. A commercial finite element package was employed in the numerical solution of system. They optimized not only the spacing of the walls, but also the angle between the walls and the distribution of heating along the boards. Next, Bello-Ochende and Bejan [22] showed that there exists an optimum spacing for the vertical isothermal parallel plates cooled by mixed convection, which is a more complex case than natural and forced convection. Similar to the procedure in [21], a commercial finite element program was operated. They also described the effects of Prandtl number (Pr), mixed convection ratio (ratio of natural convection to forced convection) and pressure drop on the optimum spacing of the plates. Hence, they derived a global correlation for the optimum spacing of vertical parallel plates subjected to mixed convection in a fixed total volume.

Besides the two-dimensional models and optimization processes, there is a limited number of projects involving three-dimensional layouts of channels or cooling systems in literature. First, A. Yılmaz, Büyükalaca and T. Yılmaz [23] considered a single three-dimensional duct having different cross-sectional shapes. They provided an analytical solution for convection heat transfer through one channel with

developing flow and fixed pressure drop by utilizing previously derived empirical formulae which govern frictional pressure losses and Nusselt number (Nu). Consequently, they derived a correlation for optimum hydraulic diameter of duct in terms of Prandtl number (Pr) and duct shape factor which is a representative value for different duct shapes.

Second, convection heat transfer through one rectangular microchannel was studied by Tunç and Bayazitoğlu [24] with the assumption of fully developed flow. All of the walls were designed to have uniform heat flux condition. They constituted a complete analytical solution by the traditional continuum approach which was shown to be conditionally valid (0.001<Kn<0.1) for the calculation of heat transfer through microchannels. As a result, they discussed the effects of channel aspect ratio, Knudsen number (Kn) and Prandtl number (Pr) on the resulting heat transfer values. At this point, note that Knudsen number is a dimensionless group which is physically defined as the ratio of molecular mean free path to the characteristic length scale. It is commonly used for checking the validity of continuum approach in fluid mechanics and heat transfer studies.

Finally, Muzychka [25] performed the approximate analytical way, intersection of asymptotes, with the purpose of optimizing three-dimensional arrays of isothermal ducts for the maximum heat transfer rate. Pressure drop across the channels and the total volume occupied by the channels were considered to be fixed and constant. The flow was assumed to be laminar. Calculations were done for parallel plates, rectangular channels, and elliptic, circular, polygonal and triangular ducts. Thus, approximate results of intersection of asymptotes revealed that isosceles triangle and square cross-sections are the most efficient for thermal packaging. In consequence, a universal correlation for optimum duct shape was derived for an arbitrary cross-section in [25]. Lastly, analytical results found in [25] were compared with the more exact results of [8] and [23] with purpose of validation.

In addition to the developments presented above, optimization studies in cooling systems for several geometries, different thermal boundary conditions and different types of flows can be reviewed in [1], [10], [26] and [27]. Since the demand for

superior performances in thermal packages increases almost every year, projects in this field become more complex and assorted.

As mentioned earlier, laminar forced air flow through parallel isothermal boards or rectangular channels with fixed pressure drop is considered in this thesis. Boards have the finite width, and the two ends of the boards are enclosed by the insulated walls in a fixed volume. Hence, optimum spacing of the parallel boards is determined after implementing a finite-volume based numerical code. The final correlations and figures are compared with the results of Bejan and Sciubba [8], and Yüncü and Ekici [14] for the case of two-dimensional infinite heat generating boards.

CHAPTER 3

WORKING MODEL AND GOVERNING EQUATIONS

3.1 COMPUTATIONAL DOMAIN AND OBJECTIVES

The geometry of the electronic package is illustrated in Figure 3.1. As shown in the corresponding figure, the model used in this thesis is composed of arrays of parallel and horizontal rectangular channels with insulated lateral walls. Electronic package with fixed volume has height H, length L and width W. A sufficiently large number of parallel electronic circuit boards cooled by forced convection are installed in the package. The board spacing s is considerably larger than the thickness of heat generating boards. Therefore, thickness of the surfaces is assumed to be negligible. Air flow with uniform velocity U_∞ and uniform temperature T_∞ is supplied at the inlet of the channels. Parallel heat generating circuit boards are kept at constant uniform temperature (T_w) and they are, in practice, equipped with several chip packages distributed on their surfaces. However, the effects of chip packages are assumed to be negligible in the numerical solution. The boards are flush-mounted and double-sided. In other words, heat is generated from both surfaces of the boards. Moreover, the pressure drop ($P_i - P_e$), by which air flow is driven, is fixed across the channels as the constraint of the optimization process. It was previously mentioned in Chapter 1 that fixed pressure difference between inlet and outlet of the channels is usually maintained by a fan or blower in practice [5]. In the end of the numerical operation, the main objective is to find the optimum height of a single channel (s_{opt}) or the spacing between the PCBs (s_{opt}) in order to dissipate maximum heat transfer rate from the isothermal surfaces.
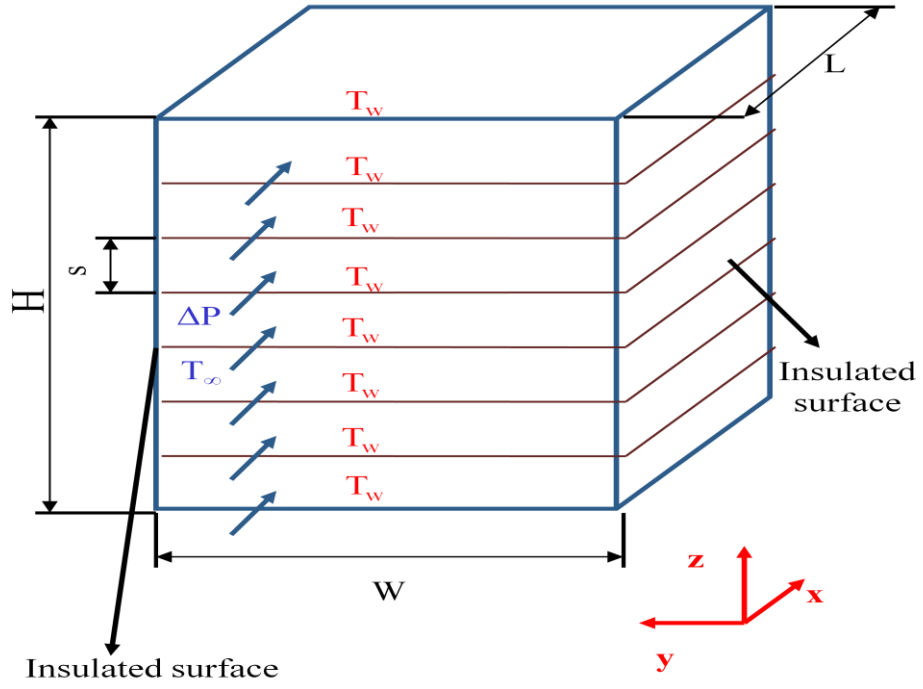
Figure 3.1 Configuration of the total assembly

Numerical calculations for finding temperature and velocity distributions are performed for a single channel (illustrated in Figure 3.2) in the current study. After the flow and heat transfer in a single channel are determined, the solution is extended to the whole assembly, which is shown in Figure 3.1.
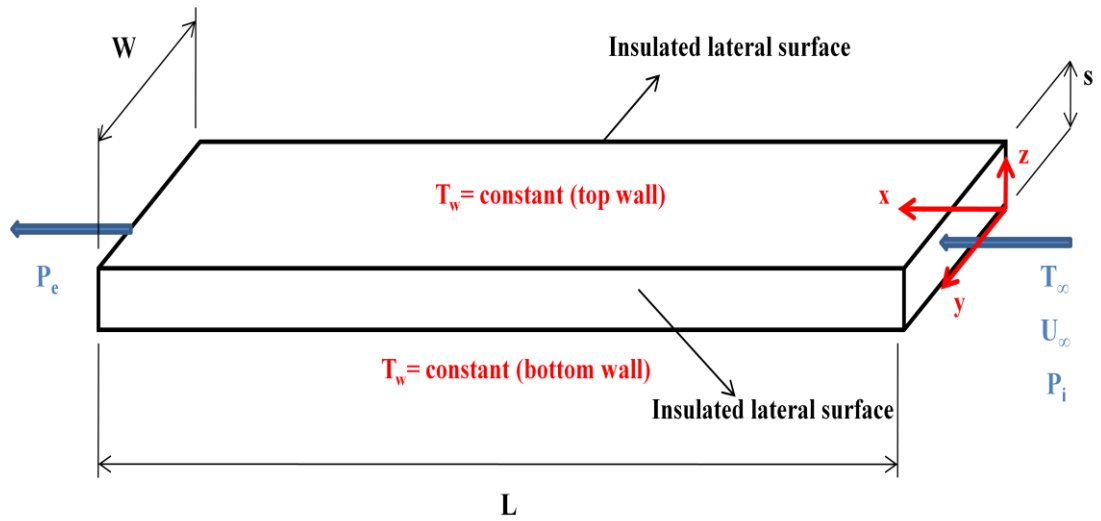
Figure 3.2 Representation of a single channel and boundary conditions with given coordinates

3.2 GOVERNING EQUATIONS

Before the numerical procedure, generalized continuity, momentum and energy equations should be simplified by certain assumptions. First of all, air flow is steady (time-independent) and laminar. Incompressible flow is assumed owing to the small temperature variations within the flow and moderate flow velocities. Viscous dissipation and wall thicknesses are neglected. In addition, channel walls are thought to be completely smooth without any roughness effects. Note also that air is a Newtonian fluid.

After the simplifications and the assumptions are applied to the general equations, the following governing equations are obtained:

$$\frac{\partial u}{\partial x}+\frac{\partial v}{\partial y}+\frac{\partial w}{\partial z}=0 \tag{3.1}$$

$$u\frac{\partial u}{\partial x}+v\frac{\partial u}{\partial y}+w\frac{\partial u}{\partial z}=-\frac{1}{\rho}\frac{\partial P}{\partial x}+\nu(\frac{\partial^2 u}{\partial x^2}+\frac{\partial^2 u}{\partial y^2}+\frac{\partial^2 u}{\partial z^2}) \tag{3.2}$$

$$u\frac{\partial v}{\partial x}+v\frac{\partial v}{\partial y}+w\frac{\partial v}{\partial z}=-\frac{1}{\rho}\frac{\partial P}{\partial y}+\nu(\frac{\partial^2 v}{\partial x^2}+\frac{\partial^2 v}{\partial y^2}+\frac{\partial^2 v}{\partial z^2}) \tag{3.3}$$

$$u\frac{\partial w}{\partial x}+v\frac{\partial w}{\partial y}+w\frac{\partial w}{\partial z}=-\frac{1}{\rho}\frac{\partial P}{\partial z}+\nu(\frac{\partial^2 w}{\partial x^2}+\frac{\partial^2 w}{\partial y^2}+\frac{\partial^2 w}{\partial z^2}) \tag{3.4}$$

$$\rho c_p(u\frac{\partial T}{\partial x}+v\frac{\partial T}{\partial y}+w\frac{\partial T}{\partial z})=k(\frac{\partial^2 T}{\partial x^2}+\frac{\partial^2 T}{\partial y^2}+\frac{\partial^2 T}{\partial z^2}) \tag{3.5}$$

The terms u, v and w in equations from (3.1) to (3.5) are the velocity components of the flow in x, y and z directions, respectively. P is the pressure, and ρ is the density. Moreover, ν is the kinematic viscosity. In addition, T is the temperature, c_p is the specific heat of air at constant pressure, and k is the thermal conductivity. Note that kinematic viscosity, ν, is also expressed as,

$$\nu=\frac{\mu}{\rho} \tag{3.6}$$

where μ is the absolute viscosity of air.

At this point, dimensionless parameters should be introduced. Coordinates of the working space, pressure, velocity components and temperature are brought to non-dimensional forms as reported below:

Coordinates of the working space:

x-coordinate:
$$x^* = \frac{x}{D_h}$$
(3.7a)

y-coordinate:
$$y^* = \frac{y}{D_h}$$
(3.7b)

z-coordinate:
$$z^* = \frac{z}{D_h}$$
(3.7c)

Pressure:

$$P^* = \frac{P}{\rho U_\infty^2}$$
(3.8)

Velocity components:

x-coordinate:
$$u^* = \frac{u}{U_\infty}$$
(3.9a)

y-coordinate:
$$v^* = \frac{v}{U_\infty}$$
(3.9b)

z-coordinate:
$$w^* = \frac{w}{U_\infty}$$
(3.9c)

Temperature:

$$\theta = \frac{T - T_\infty}{T_w - T_\infty}$$
(3.10)

After equations from (3.1) to (3.5) are modified and reorganized, resulting non-dimensional forms of the governing equations can be introduced as follows:

$$\frac{\partial u^*}{\partial x^*} + \frac{\partial v^*}{\partial y^*} + \frac{\partial w^*}{\partial z^*} = 0 \tag{3.11}$$

$$u^* \frac{\partial u^*}{\partial x^*} + v^* \frac{\partial u^*}{\partial y^*} + w^* \frac{\partial u^*}{\partial z^*} = -\frac{\partial P^*}{\partial x^*} + \frac{1}{\mathrm{Re}_{D_h}} \left(\frac{\partial^2 u^*}{\partial x^{*2}} + \frac{\partial^2 u^*}{\partial y^{*2}} + \frac{\partial^2 u^*}{\partial z^{*2}} \right) \tag{3.12}$$

$$u^* \frac{\partial v^*}{\partial x^*} + v^* \frac{\partial v^*}{\partial y^*} + w^* \frac{\partial v^*}{\partial z^*} = -\frac{\partial P^*}{\partial y^*} + \frac{1}{\mathrm{Re}_{D_h}} \left(\frac{\partial^2 v^*}{\partial x^{*2}} + \frac{\partial^2 v^*}{\partial y^{*2}} + \frac{\partial^2 v^*}{\partial z^{*2}} \right) \tag{3.13}$$

$$u^* \frac{\partial w^*}{\partial x^*} + v^* \frac{\partial w^*}{\partial y^*} + w^* \frac{\partial w^*}{\partial z^*} = -\frac{\partial P^*}{\partial z^*} + \frac{1}{\mathrm{Re}_{D_h}} \left(\frac{\partial^2 w^*}{\partial x^{*2}} + \frac{\partial^2 w^*}{\partial y^{*2}} + \frac{\partial^2 w^*}{\partial z^{*2}} \right) \tag{3.14}$$

$$u^* \frac{\partial \theta}{\partial x^*} + v^* \frac{\partial \theta}{\partial y^*} + w^* \frac{\partial \theta}{\partial z^*} = \frac{1}{\mathrm{Re}_{D_h} \mathrm{Pr}} \left(\frac{\partial^2 \theta}{\partial x^{*2}} + \frac{\partial^2 \theta}{\partial y^{*2}} + \frac{\partial^2 \theta}{\partial z^{*2}} \right) \tag{3.15}$$

Note that Reynolds number based on hydraulic diameter Re_{D_h} in equations from (3.12) to (3.15) is analytically expressed as,

$$\mathrm{Re}_{D_h} = \frac{U_\infty D_h}{\nu} \tag{3.16}$$

where hydraulic diameter, D_h, is given by,

$$D_h = \frac{4 A_{cr}}{P_{cr}} \tag{3.17}$$

In equation (3.17), A_{cr} is the cross-sectional area and P_{cr} is the perimeter of the cross-section. They are defined as shown below:

$$A_{cr} = sW \tag{3.18}$$

$$P_{cr} = 2(s + W) \tag{3.19}$$

Note also that Prandtl number, Pr, which is included in dimensionless energy equation, (3.15), is given by,

$$\mathrm{Pr} = \frac{\mu c_p}{k} \tag{3.20}$$
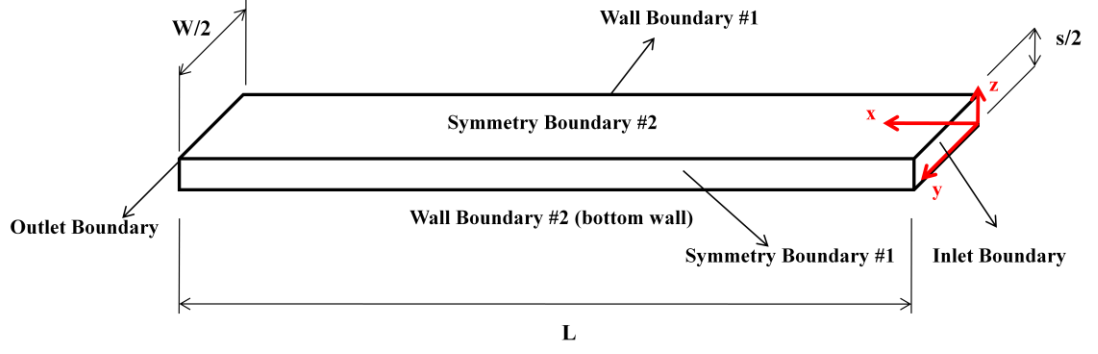
Figure 3.3 Computational domain used in the numerical algorithm with defined boundary conditions

3.3 BOUNDARY CONDITIONS

Since the differential equations from (3.11) to (3.15) are elliptic, the definition of the boundary conditions around all boundaries is required in the computational domain for the solution of these equations. Implementation and correct definition of boundary conditions are one of the most significant stages in the analytical and numerical calculations. In this section, each boundary condition is defined and introduced separately.

It should be emphasized that symmetrical properties of the computational domain in z and y directions are taken into account in the determination of boundary conditions. These symmetrical properties can easily be observed from Figure 3.2.

There are six main boundary conditions in the computational domain. These are called inlet, outlet, symmetry #1, symmetry #2, wall #1 and wall #2 in Figure 3.3.

3.3.1 Boundary Condition at the Inlet

As observed from Figure 3.2, a uniform velocity (U_∞) and temperature (T_∞) is maintained at the inlet of the channel. Therefore, inlet boundaries are,

$$\text{at } x = 0,\, 0 < y < \frac{W}{2} \text{ and } 0 < z < \frac{s}{2};\qquad u = U_\infty \qquad\qquad (3.21a)$$

$$v = 0 \qquad\qquad (3.21b)$$

$$w = 0 \tag{3.21c}$$

$$T = T_\infty \tag{3.21d}$$

in dimensional forms. Equations from (3.21a) to (3.21d) can be modified in order to obtain non-dimensional forms of inlet boundary conditions as shown below:

$$\text{at } x^* = 0,\ 0 < y^* < \frac{W}{2D_h} \text{ and } 0 < z^* < \frac{s}{2D_h}\ ; \qquad u^* = 1 \tag{3.22a}$$

$$v^* = 0 \tag{3.22b}$$

$$w^* = 0 \tag{3.22c}$$

$$\theta = 0 \tag{3.22d}$$

3.3.2 Boundary Condition at the Outlet

At the outlet of the channel, it should be pointed out that the parameter length L is sufficiently long to make the change of velocity and temperature profiles with respect to x zero. In other words, slope of the velocity components and temperature with respect to x is zero at the outlet. As the outlet conditions are investigated,

$$\text{at } x = L,\ 0 < y < \frac{W}{2} \text{ and } 0 < z < \frac{s}{2}\ ; \qquad \frac{\partial u}{\partial x} = 0 \tag{3.23a}$$

$$\frac{\partial v}{\partial x} = 0 \tag{3.23b}$$

$$\frac{\partial w}{\partial x} = 0 \tag{3.23c}$$

$$\frac{\partial T}{\partial x} = 0 \tag{3.23d}$$

in dimensional form. Next, the outlet boundary conditions are given as,

at $x^* = \dfrac{L}{D_h}$, $0 < y^* < \dfrac{W}{2D_h}$ and $0 < z^* < \dfrac{s}{2D_h}$; $\dfrac{\partial u^*}{\partial x^*} = 0$ (3.24a)

$$\dfrac{\partial v^*}{\partial x^*} = 0 \qquad (3.24b)$$

$$\dfrac{\partial w^*}{\partial x^*} = 0 \qquad (3.24c)$$

$$\dfrac{\partial \theta}{\partial x^*} = 0 \qquad (3.24d)$$

in non-dimensional form.

3.3.3 Symmetry Boundary Condition at y = W/2

The first symmetry condition occurs at the plane where $y = W/2$. At the boundaries of symmetry, there is no flow and scalar flux across the boundary [28]. Hence, the dimensional conditions at $y = W/2$ are written as follows:

at $y = \dfrac{W}{2}$, $0 < x < L$ and $0 < z < \dfrac{s}{2}$; $\dfrac{\partial u}{\partial y} = 0$ (3.25a)

$$v = 0 \qquad (3.25b)$$

$$\dfrac{\partial w}{\partial y} = 0 \qquad (3.25c)$$

$$\dfrac{\partial T}{\partial y} = 0 \qquad (3.25d)$$

Consequently, equations from (3.25a) to (3.25d) can be transformed into the non-dimensional forms as,

at $y^* = \dfrac{W}{2D_h}$, $0 < x^* < \dfrac{L}{D_h}$ and $0 < z^* < \dfrac{s}{2D_h}$; $\dfrac{\partial u^*}{\partial y^*} = 0$ (3.26a)

$$v^* = 0 \qquad (3.26b)$$

19

$$\frac{\partial w^*}{\partial y^*} = 0 \qquad\qquad (3.26c)$$

$$\frac{\partial \theta}{\partial y^*} = 0 \qquad\qquad (3.26d)$$

3.3.4 Symmetry Boundary Condition at z = s/2

The second symmetry condition occurs at the plane where z = s/2. In the same manner as the symmetry boundary condition at y = W/2, dimensional boundary conditions for the second symmetry can be defined as,

at $z = \dfrac{s}{2}$, $0 < x < L$ and $0 < y < \dfrac{W}{2}$; $\qquad \dfrac{\partial u}{\partial z} = 0 \qquad\qquad (3.27a)$

$$\frac{\partial v}{\partial z} = 0 \qquad\qquad (3.27b)$$

$$w = 0 \qquad\qquad (3.27c)$$

$$\frac{\partial T}{\partial z} = 0 \qquad\qquad (3.27d)$$

Next, equations from (3.27a) to (3.27d) can be converted into non-dimensional forms as given below:

at $z^* = \dfrac{s}{2D_h}$, $0 < x^* < \dfrac{L}{D_h}$ and $0 < y^* < \dfrac{W}{2D_h}$; $\qquad \dfrac{\partial u^*}{\partial z^*} = 0 \qquad\qquad (3.28a)$

$$\frac{\partial v^*}{\partial z^*} = 0 \qquad\qquad (3.28b)$$

$$w^* = 0 \qquad\qquad (3.28c)$$

$$\frac{\partial \theta}{\partial z^*} = 0 \qquad\qquad (3.28d)$$

3.3.5 Wall Boundary Condition at y = 0

The first wall boundary condition occurs at the lateral right wall, where y = 0. Since the right wall is very well insulated, there is no heat transfer across the wall. Therefore, gradient of temperature in y-direction is zero. The wall is solid and rigid. Thus, velocity perpendicular to the wall (v) is also considered to be zero. Finally, no slip conditions (u = w = 0) are assumed at the wall. As a result of the given considerations, the first wall boundary conditions are,

at y = 0, $0 < x < L$ and $0 < z < \dfrac{s}{2}$;

$$u = 0 \tag{3.29a}$$

$$v = 0 \tag{3.29b}$$

$$w = 0 \tag{3.29c}$$

$$\frac{\partial T}{\partial y} = 0 \tag{3.29d}$$

Then, the conditions are given as,

at $y^* = 0$, $0 < x^* < \dfrac{L}{D_h}$ and $0 < z^* < \dfrac{s}{2D_h}$;

$$u^* = 0 \tag{3.30a}$$

$$v^* = 0 \tag{3.30b}$$

$$w^* = 0 \tag{3.30c}$$

$$\frac{\partial \theta}{\partial y^*} = 0 \tag{3.30d}$$

in non-dimensional forms.

3.3.6 Wall Boundary Condition at z = 0

The second wall boundary condition occurs at the bottom wall, where z = 0. It is kept at constant wall temperature T_w. In addition, similar to the first wall boundary,

velocity perpendicular to the wall (w) is zero and no slip conditions ($u = v = 0$) are assumed at the wall. The given expressions can be represented analytically as shown,

at z = 0, 0 < x < L and $0 < y < \dfrac{W}{2}$; $\qquad u = 0$ $\hfill$ (3.31a)

$$v = 0 \hfill \text{(3.31b)}$$

$$w = 0 \hfill \text{(3.31c)}$$

$$T = T_w \hfill \text{(3.31d)}$$

Consequently, non-dimensional forms of the wall boundary conditions at z = 0 are defined as,

at $z^* = 0$, $0 < x^* < \dfrac{L}{D_h}$ and $0 < y^* < \dfrac{W}{2D_h}$; $\qquad u^* = 0$ $\hfill$ (3.32a)

$$v^* = 0 \hfill \text{(3.32b)}$$

$$w^* = 0 \hfill \text{(3.32c)}$$

$$\theta = 1 \hfill \text{(3.32d)}$$

CHAPTER 4

SOLUTION TECHNIQUE

Generally, there are two types of solution techniques for the design of thermo-fluid systems. These methods are the experimentations and theoretical calculations. Experimentations reflect the most realistic conditions because of the real working conditions provided in the experiments. However, experiments are usually carried out with small-scale models since it is mostly not possible to use the same dimensions as the actual model because of the finite volume and economic considerations. Hence, unlike actual models, all characteristics and features of the flow cannot be obtained accurately in the small-scale experiments. During small-scale modeling, some significant properties of the flow and the assembly are missed or ignored unexpectedly. On the contrary to the experimental studies, theoretical calculations are based on the mathematical model or equations. Theoretical calculations are cheaper and faster than experiments. Furthermore, they usually provide information for the entire domain rather than the certain points or few accessible areas which are measured in experiments. Finally, with the help of the solution procedure and assumptions, real practical conditions and ideal conditions can easily be simulated and compared in theoretical calculations [20].

Theoretical calculations can be performed by either analytical or numerical procedure. Analytical procedure is the solution of governing differential equations by classical mathematics. It is the most accurate method since it represents the whole model, thermal and fluid flow results analytically. However, use of classical mathematics is very limited in thermo-fluid problems. Classical mathematics is restricted to the very simple flows and flow geometries. Moreover, solving

differential equations reveals infinite series and special functions. In fact, obtaining these functions and interpreting them can be a harsh practice. On the other hand, in the numerical calculations, differential equations are converted into algebraic equations, which are easier to be handled and solved. In addition, numerical procedure can be applied to most of the complex geometries and heat transfer problems. Furthermore, in the numerical solutions, there are not any disadvantages for the design problems which can be represented by a proper mathematical model, and which do not have characteristics, such as complex geometries and highly variable thermo-fluid properties [20].

As a result of comparisons between solution techniques with respect to their main features, advantages and disadvantages, numerical calculations are determined to be the best solution for the working model given in the current study. Finite volume method (FVM), which is based on the control volume integration, is implemented in the numerical algorithm. In other words, conservation of flow variables is defined over each control volume in the governing equations. Before discretization, the derived equations from (3.11) to (3.15) are integrated over each control volume. Moreover, the dependant variables are expressed at the nodal points inside the control volumes in the corresponding method [28]. Note also that numerical calculations are performed by using a developed numerical code which is written in Visual C/C++.

4.1 NUMERICAL DISCRETIZATION OF COMPUTATIONAL DOMAIN AND GOVERNING EQUATIONS

Before the discretization process is explained, it should be noted that staggered grid arrangement is employed in the procedure. In this arrangement, scalar variables (pressure, temperature) are evaluated at the nodal points located in the main control volumes. Meanwhile, vectorial variables (velocities u, v, and w) are determined for the points in other control volumes, called staggered control volumes, and the nodal points of the staggered control volumes are located at the faces of the main control volumes of the arrangement. In other words, nodal points of the scalar and the

vectorial variables are not the same. In this way, the effect of pressure distribution on the velocities and the conservation of momentum is conveniently represented in the discretized equations [28, 29]. There are four types of control volumes in the domain; scalar volume (for continuity, pressure and temperature), u-control volume, v-control volume and w-control volume.

As seen from Figure 4.1, control volume and its nodal point are surrounded by neighboring nodes T, B, W, E, N and S. Additionally, faces of the control volume are represented with the small letters t, b, w, e, n and s.

4.1.1 Discretization Schemes for Steady State Convection-Diffusion Problems

For the discretization of continuity, momentum and energy equations, hybrid differencing scheme is implemented in the current study. In this section, different discretization schemes for three dimensional convection-diffusion problems are described separately. Consequently, it is explained why hybrid differencing scheme is selected for discretization.
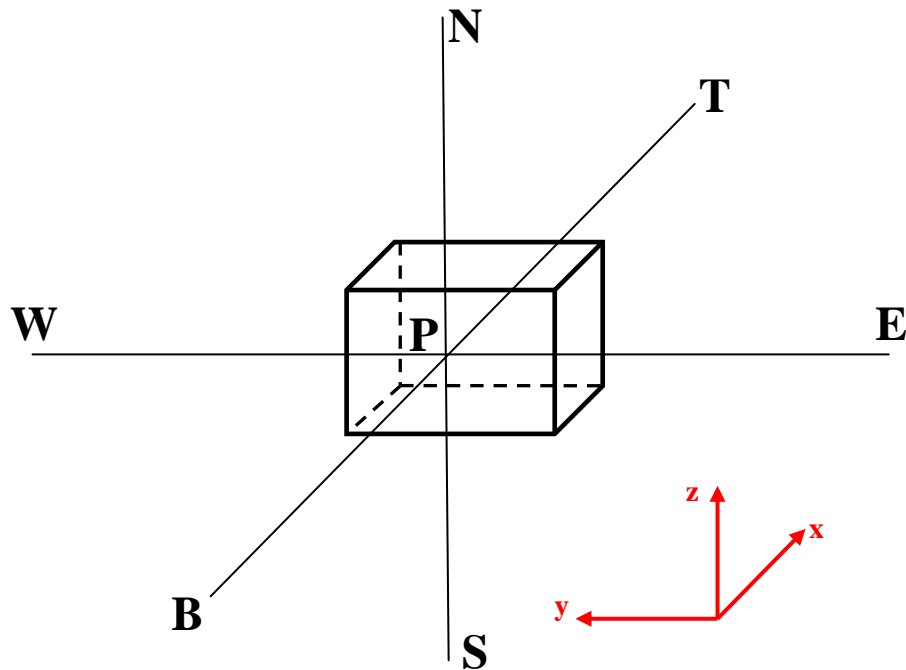
Figure 4.1 Control volume containing a nodal point P with neighboring nodes

25
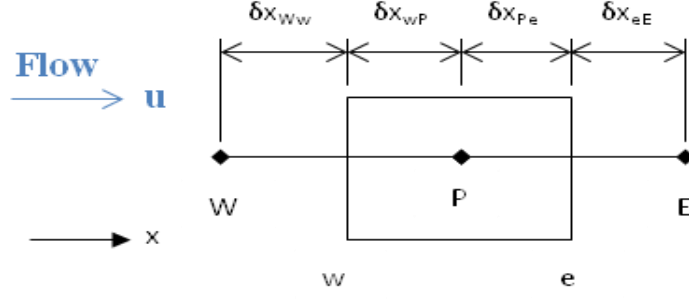
Figure 4.2 Control volume in simple 1-D flow for central, upwind and hybrid differencing schemes

Before continuing with types of different schemes, it should be pointed out that there are four important factors in the comparison of discretization schemes. These are conservativeness, boundedness, transportiveness and accuracy. Conservativeness states whether the selected method guarantees the conservation of flow. Next, if a method of discretization is bounded, it means that it absolutely provides a convergent and stable iterative solution. In addition, transportiveness means the ability of the flow whether it correctly predicts the direction of the flow and the relative strength of convection over diffusion. Finally, accuracy is the truncation error which is caused by the truncation of Taylor series expansion [28].

4.1.1.1 Central Differencing Scheme

In central differencing scheme, variables at the faces of the control volume, which are required at the discretization of the left hand sides of equations from (3.12) to (3.15), are evaluated by linear interpolation between the two nearest nodal points. For instance, a variable at the east face (e) is calculated by the interpolation between the values at points P and E in Figure 4.2.

Central differencing scheme yields a conservative solution. In addition, it possesses second-order accuracy. On the other hand, it is bounded only for the condition of $\left|Pe_{e,w,n,s,t,b}\right| = \left|F_{e,w,n,s,t,b}/D_{e,w,n,s,t,b}\right| < 2$ where Peclet number, Pe, is physically defined to be the measure which indicates the ratio of strength of convective heat transfer over conductive heat transfer. Note that F is the mass flow rate across a face through a

control volume and D is the diffusion conductance parameter for that face. Mathematical definitions of these parameters are given in part 4.1.3. Besides the conditionally boundedness hazard, the transportiveness property is not satisfied in central differencing formulation [28].

4.1.1.2 Upwind Differencing Scheme

Variables at the faces of the control volumes are determined by equalizing it to the value at the upstream nodal point along the flow direction in this formulation. For example, the value of the variable at the east face (e) in Figure 4.2 is taken to be equal to the value at the nodal point P.

Upwind differencing scheme is conservative and unconditionally bounded. Moreover, it possesses the transportiveness property since it indicates the flow direction during discretization. On the contrary to these positive features, the formulation has only first-order accuracy. Besides, the results which have relatively large magnitude of errors may be produced when the flow is not properly aligned with the grid lines. This undesirable condition is called as "false diffusion" [28]. For more sophisticated information, the details of false diffusion, upwind differencing and its characteristics can also be examined in [28].

4.1.1.3 Hybrid Differencing Scheme

As it may be realized from the name of the scheme, hybrid differencing is a compound of central and upwind differencing schemes. In hybrid differencing method, Peclet number Pe is determined at each face of the control volumes. At faces for which $|\text{Pe}| < 2$, central differencing scheme is implemented for the reason of its high accuracy. In contrast, if the condition for Peclet number Pe is not satisfied, upwind differencing is implemented for the corresponding face at the discretization stage.
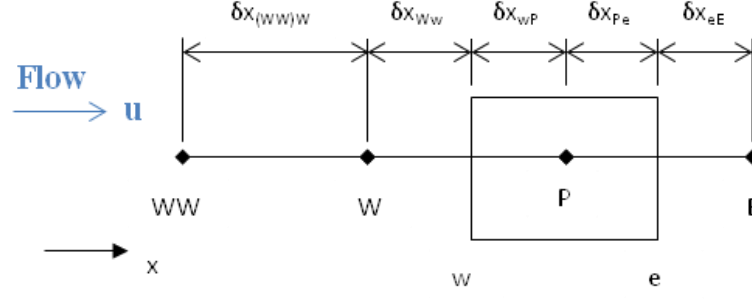
Figure 4.3 Control volume in simple 1-D flow for QUICK and TVD schemes

Since the desirable properties of both central differencing and upwind differencing are gathered in this method, better results than the two previous methods can be obtained. It is totally conservative and unconditionally bounded. Because it switches to central differencing for the condition stated above, it can provide relatively more accurate results than upwind differencing. Furthermore, it possesses the transportiveness property owing to the usage of upwind differencing for the case of $|Pe| \geq 2$ where central differencing is not preferred. The only disadvantage or drawback of this method is that its order of accuracy is 1 due to the truncation error in Taylor series formulation [28].

4.1.1.4 QUICK Differencing Scheme

Unlike central, upwind and hybrid differencing methods, quadratic interpolation by three points is performed in order to find the face values in QUICK (Quadratic Upstream Interpolation for Convective Kinetics) scheme. For instance, the value of a variable at the west face (w) for simple one-dimensional flow in Figure 4.3 is calculated by the quadratic interpolation between the nodal points WW, W and P.

Although it is more complex than the previously mentioned methods, QUICK scheme has third-order accuracy. Next, usage of consistent quadratic interpolation functions makes QUICK scheme fully conservative. In addition, it is equipped with the transportiveness property since the direction of the flow is considered during the determination of the interpolation function. On the other hand, the method does not

guarantee the boundedness and it may cause stability problems during the numerical solution process. In other words, undershoots and overshoots may be observed in the solution. In fact, the schemes with higher-order accuracy (third-order and more) may cause stability problems due to the consideration of high number of nodal points for the interpolation to calculate face values [28].

4.1.1.5   TVD (Total Variation Diminishing) Schemes

Although third and higher-order schemes are superior in accuracy, their possible stability problems have led the engineers to establish second-order accurate methods which possess all of the significant properties; conservativeness, boundedness and transportiveness. Therefore, TVD schemes can be said to be definitely convenient for general design problems and complex flows. There are different types of TVD schemes, differentiated by the various limiter functions ψ. In TVD schemes, a generalized interpolation function to evaluate a variable ϕ_e is [28],

$$\phi_e = \phi_P + \frac{1}{2}\psi(r_e)(\phi_E - \phi_P) \tag{4.1}$$

for the east face in Figure 4.3. Note that r_e is the ratio of the upstream side gradient to the downstream side gradient of the variable ϕ_e and for a uniform grid it is mathematically represented by [28],

$$r_e = \frac{\phi_P - \phi_W}{\phi_E - \phi_P} \tag{4.2}$$

Similarly, the variable equation for the west face can be derived as,

$$\phi_w = \phi_W + \frac{1}{2}\psi(r_w)(\phi_P - \phi_W) \tag{4.3}$$

with

$$r_w = \frac{\phi_W - \phi_{WW}}{\phi_P - \phi_W} \tag{4.4}$$

It is realized from equations (4.1) and (4.3) that limiter function is an expression which is only dependent on r. As mentioned above, limiter functions are different at each TVD scheme. Most commonly known limiter functions defined for the schemes are known to be Van Leer, Van Albada, Min-Mod, SUPERBEE, Sweby, QUICK and UMIST. Details of TVD schemes, limiter functions and their comparisons are given in [28].

4.1.2 Selection of the Discretization Scheme

After a brief analysis and definitions of discretization schemes for 3-D steady state convection-diffusion problems, the current problem in this study should be investigated. In the corresponding working model, the flow is laminar. Therefore, the flow itself is not very complex in nature. However, the computational domain is three-dimensional so that a reasonable discretization scheme should be implemented for satisfactory results with the consideration of computation time.

QUICK scheme is not selected for the modeling of discretized equations since it may cause stability problems in the solution. Moreover, upwind differencing is not considered because of the lowest accuracy it provides among all discretization schemes. Central differencing is also eliminated for the reasons that it is only conditionally bounded and it does not possess the transportiveness which may be detrimental to the numerical solution.

After the elimination procedure described above, there are two left methods to be considered. These are hybrid differencing and TVD schemes. TVD schemes are very convenient and accurate for the thermo-fluid problems with its second-order accuracy. However, it may require high computation time due to its more complex formulation relative to that in hybrid differencing. Furthermore, low accuracy (first-order) in hybrid differencing can be alleviated by an appropriate grid adaptation, and by the usage of non-uniform grid or mesh spacing and comparisons of the numerical solution obtained by the developed code with the available results for simple flows.

Therefore, hybrid differencing is selected for the discretization process. The operations, which can alleviate the low accuracy in hybrid differencing method, and which have been briefly indicated above, are given in the next sections. Grid adaptation and usage of non-uniform grids are presented in part 4.4 and comparison of the numerical results with the available data for simple flows is introduced in part 4.6.

4.1.3 Discretized Governing Equations

In this section, continuity, momentum and energy equations are discretized to bring the equations from (3.11) to (3.15) into the algebraic form which is the most convenient form in numerical and iterative solution. In addition to these equations, governing discretized equation for pressure corrections at each scalar node are determined for the reason that computed pressure and velocity values are corrected by these pressure corrections after each iteration step in the SIMPLE algorithm.
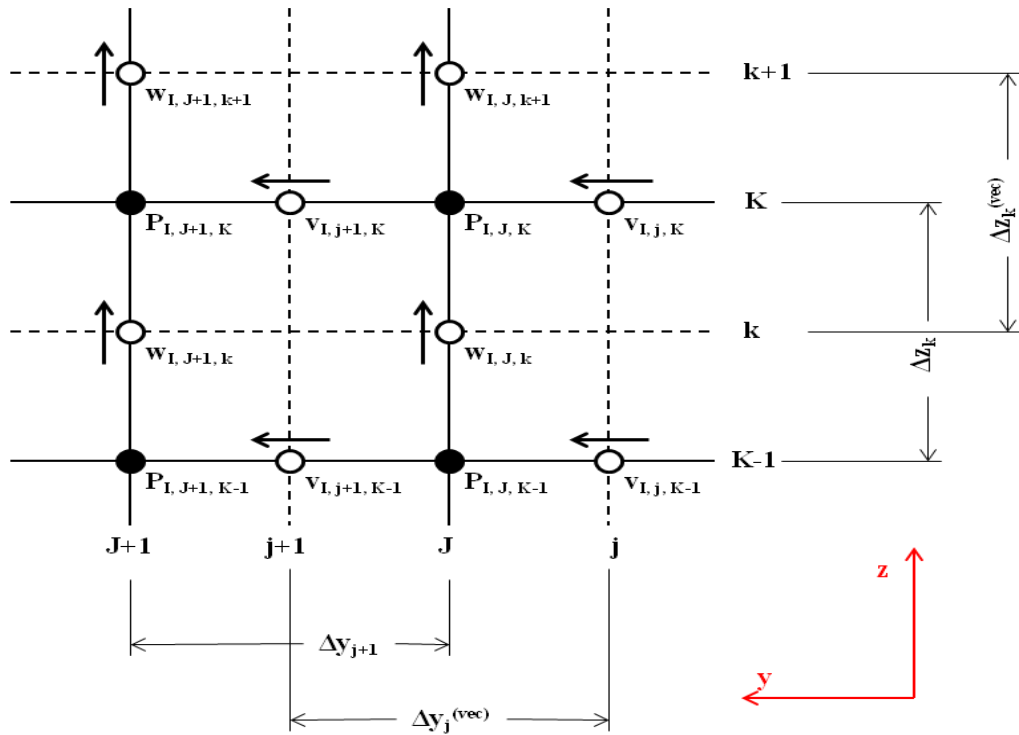
Figure 4.4 Representative section of the grid line arrangement in y-z plane

31

Note that backward staggered grid arrangement [28] is implemented in the numerical discretization. Staggered grid in three-dimensional problems is too complex to be represented by the simple notation, which is shown in Figure 4.1. Therefore, during discretization, there are six types of grid lines which are denoted by the letters I, J, K, i, j and k. I and i are in x-direction, J and j are in y-direction, and K and k are in z-direction. Note that scalar grid lines are represented by capital letters (I, J and K) and vectorial grid lines are represented by small letters (i, j and k). The general layout of grid lines considered in the current study is given in Figures 4.4, 4.5 and 4.6. While the distance terms with superscript (vec) are used for the definition of spacing between vectorial grid lines in these figures, the distances without superscripts denote the spacing between scalar grid lines.
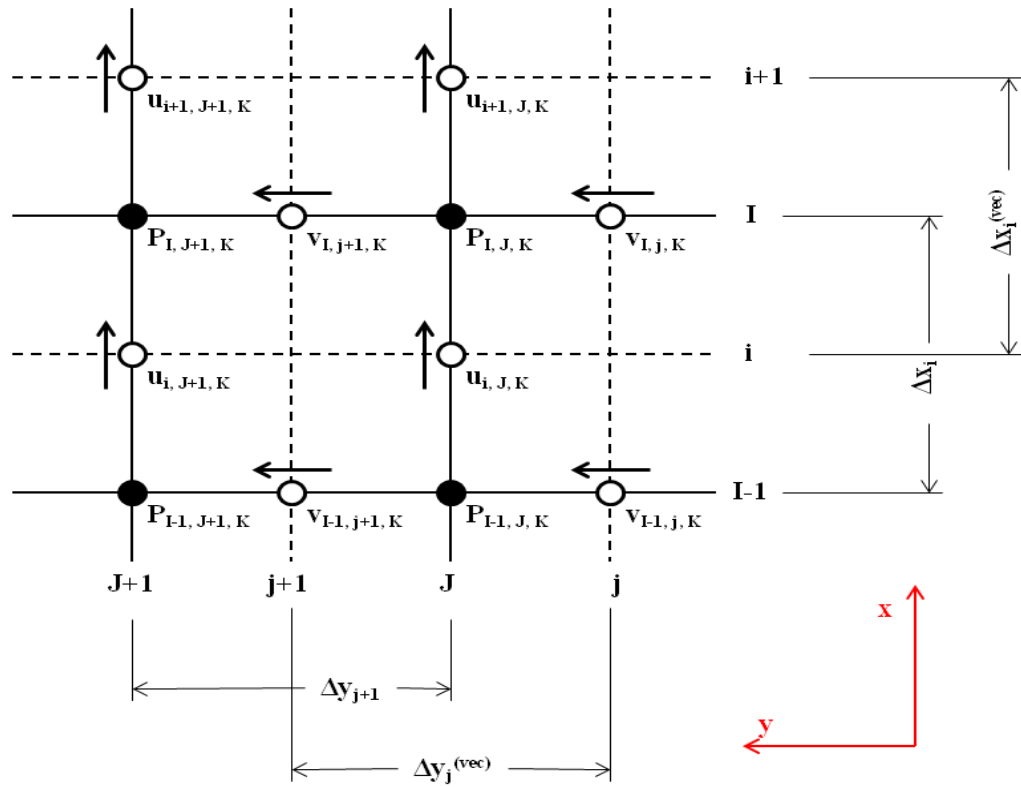
Figure 4.5 Representative section of the grid line arrangement in x-y plane
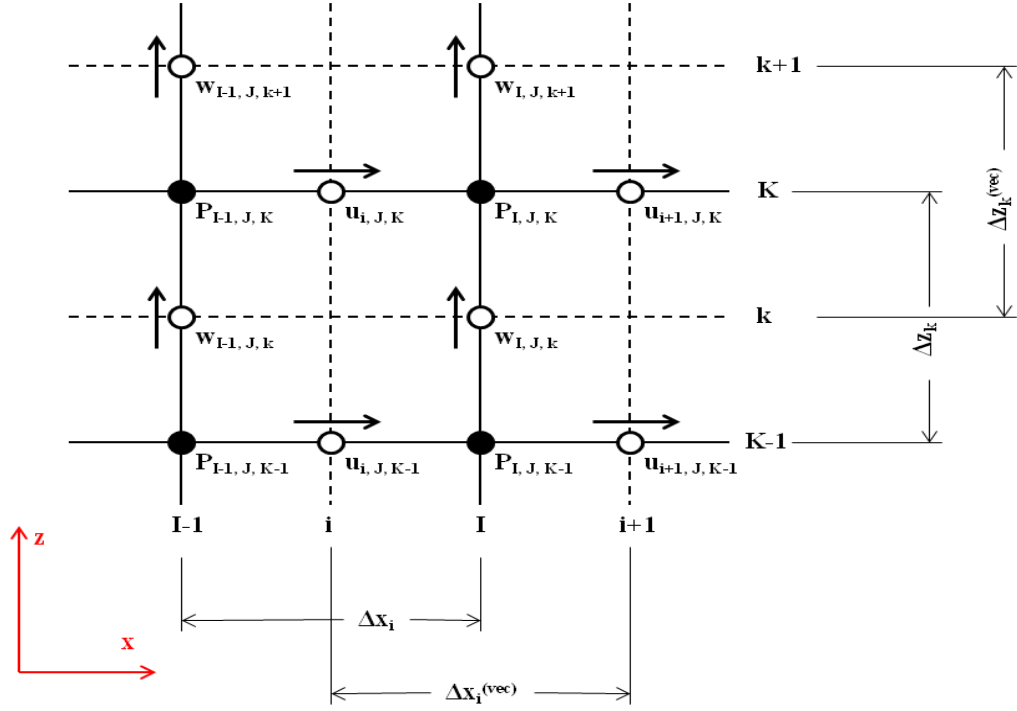
Figure 4.6 Representative section of the grid line arrangement in x-z plane

It is known from Chapter 3 that dimensionless velocities are defined by u^*, v^* and w^*, and they can be calculated by solving the discretized algebraic forms of the equations from (3.12) to (3.14) at each iteration. Pressure corrections (P') at scalar nodal points are also determined by solving the algebraic equations which will be derived later in part 4.1.3.5. Meanwhile, velocity corrections are denoted by u', v' and w' and they will also be discussed in part 4.1.3.5. Lastly, dimensionless temperature values (θ) at each node are obtained by the iterative solution of set of nodal algebraic energy equations, which will be presented in part 4.1.3.6, as the discretized form of the equation (3.15).

At this point, the parameter F that is the mass flow rate through a face of control volume should be declared. This parameter is mathematically represented using the simple notation by the expression,

$$F_b = \rho u_b A_b \tag{4.5a}$$

$$F_t = \rho u_t A_t \tag{4.5b}$$

33

$$F_e = \rho v_e A_e \tag{4.5c}$$

$$F_w = \rho v_w A_w \tag{4.5d}$$

$$F_s = \rho w_s A_s \tag{4.5e}$$

$$F_n = \rho w_n A_n \tag{4.5f}$$

Here, F is the mass flow rate through a face which is denoted by the letters e, w, n, s, t or b. The terms u, v and w are the velocities perpendicular to the associated faces. Finally, A is the cross-sectional area of that face. Furthermore, in non-dimensional form, F is described as,

$$F_b{}^* = \frac{u_b A_b}{U_\infty D_h{}^2} = u_b{}^* A_b{}^* \tag{4.6a}$$

$$F_t{}^* = \frac{u_t A_t}{U_\infty D_h{}^2} = u_t{}^* A_t{}^* \tag{4.6b}$$

$$F_e{}^* = \frac{u_e A_e}{U_\infty D_h{}^2} = u_e{}^* A_e{}^* \tag{4.6c}$$

$$F_w{}^* = \frac{u_w A_w}{U_\infty D_h{}^2} = u_w{}^* A_w{}^* \tag{4.6d}$$

$$F_s{}^* = \frac{u_s A_s}{U_\infty D_h{}^2} = u_s{}^* A_s{}^* \tag{4.6e}$$

$$F_n{}^* = \frac{u_n A_n}{U_\infty D_h{}^2} = u_n{}^* A_n{}^* \tag{4.6f}$$

Next, diffusion conductance D is to be explained. Diffusion conductance for each face of the finite volume can be analytically given as shown:

$$D_b = \frac{\Gamma_b}{\delta x_{BP}} A_b \tag{4.7a}$$

$$D_t = \frac{\Gamma_t}{\delta x_{PT}} A_t \tag{4.7b}$$

$$D_e = \frac{\Gamma_e}{\delta y_{PE}} A_e \tag{4.7c}$$

$$D_w = \frac{\Gamma_w}{\delta y_{WP}} A_w \tag{4.7d}$$

$$D_s = \frac{\Gamma_s}{\delta z_{SP}} A_s \tag{4.7e}$$

$$D_n = \frac{\Gamma_n}{\delta z_{PN}} A_n \tag{4.7f}$$

where Γ is the general diffusion coefficient [20] and in non-dimensional formulation it is given by,

$$\Gamma = \Gamma_b = \Gamma_t = \Gamma_e = \Gamma_w = \Gamma_s = \Gamma_n = \frac{1}{Re_{D_h}} \tag{4.8a}$$

$$\Gamma = \Gamma_b = \Gamma_t = \Gamma_e = \Gamma_w = \Gamma_s = \Gamma_n = \frac{1}{Re_{D_h} Pr} \tag{4.8b}$$

for momentum and energy equations, respectively. Hence, in dimensionless form, the mathematical expressions for diffusion conductance are,

$$D_b^* = \frac{1}{Re_{D_h} \delta x_{BP}^*} A_b^* \tag{4.9a}$$

$$D_t^* = \frac{1}{Re_{D_h} \delta x_{PT}^*} A_t^* \tag{4.9b}$$

$$D_e^* = \frac{1}{Re_{D_h} \delta y_{PE}^*} A_e^* \tag{4.9c}$$

$$D_w^* = \frac{1}{Re_{D_h} \delta y_{WP}^*} A_w^* \tag{4.9d}$$

$$D_s^* = \frac{1}{Re_{D_h} \delta z_{SP}^*} A_s^* \tag{4.9e}$$

$$D_n^* = \frac{1}{\mathrm{Re}_{D_h}\,\delta z^*_{PN}} A_n^* \qquad\qquad (4.9f)$$

for the momentum equations by using the simple notation. Diffusion conductance terms for energy equations can be determined easily by replacing "Re_{D_h}" in equations from (4.9a) to (4.9f) with the expression "$\mathrm{Re}_{D_h}\,\mathrm{Pr}$".

After the introduction of basic terms and their definitions, another important point about the discretization of governing equations from (3.11) to (3.15) should be presented. If the equations from (3.11) to (3.15) are carefully investigated, the similarity between the corresponding equations can be realized. In fact, these equations can be written in the following generalized form:

$$\frac{\partial(u^*\phi)}{\partial x^*} + \frac{\partial(v^*\phi)}{\partial y^*} + \frac{\partial(w^*\phi)}{\partial z^*} = \frac{\partial}{\partial x^*}(\Gamma\frac{\partial\phi}{\partial x^*}) + \frac{\partial}{\partial y^*}(\Gamma\frac{\partial\phi}{\partial y^*}) + \frac{\partial}{\partial z^*}(\Gamma\frac{\partial\phi}{\partial z^*}) + S_\phi \quad (4.10)$$

Table 4.1 General terms in equation (4.10) and their definitions for each governing equation

	ϕ	S_ϕ	Γ
Continuity equation	1	0	Not Defined
x-momentum equation	u^*	$-\dfrac{\partial P^*}{\partial x^*}$	$\dfrac{1}{\mathrm{Re}_{D_h}}$
y-momentum equation	v^*	$-\dfrac{\partial P^*}{\partial y^*}$	$\dfrac{1}{\mathrm{Re}_{D_h}}$
z-momentum equation	w^*	$-\dfrac{\partial P^*}{\partial z^*}$	$\dfrac{1}{\mathrm{Re}_{D_h}}$
Energy equation	θ	0	$\dfrac{1}{\mathrm{Re}_{D_h}\,\mathrm{Pr}}$

Note that ϕ is any variable, and S_ϕ is the source term associated with that variable and its equation. The generalized terms ϕ, S_ϕ, and Γ are summarized in Table 4.1.

It should be emphasized that source terms, S_ϕ, given in Table 4.1 are defined for the internal control volumes. Nevertheless, there are additional source terms at the boundaries of the computational domain. They are denoted by S_u and S_p and are zero for the internal volumes, as will be formulated in subsequent sections. The nonzero values of S_u and S_p are encountered in wall boundaries and are given in parts 4.5.3 and 4.5.4.

Accordingly, since the five governing equations can be written in a generalized form as in equation (4.10), one suitable numerical procedure can be implemented for the solution of flow field and temperature distribution. Note also that, for simplicity, energy equation or temperature distribution is determined after the continuity and momentum equations are solved. This condition is provided by the incompressibility of the air flow, which is considered due to the moderate flow velocity.

4.1.3.1 Continuity Equation

Continuity equation (3.11) can be discretized by integrating both sides of it over a scalar control volume. Discretized form of the continuity equation for a given scalar control volume can be expressed as,

$$(F^*_t - F^*_b) + (F^*_w - F^*_e) + (F^*_n - F^*_s) = 0 \qquad (4.11)$$

where subscripts t, b, w, e, n and s represent the faces of the scalar control volume. Then, substituting the definition of F into equation (4.11), the discretized continuity equation takes the form of,

$$(u^*_{i+1,J,K} - u^*_{i,J,K})A^*_{J,K} + (v^*_{I,j+1,K} - v^*_{I,j,K})A^*_{I,K} + (w^*_{I,J,k+1} - w^*_{I,J,k})A^*_{I,J} = 0 \quad (4.12)$$

The area notation, A^*, included in equation (4.12) represents the dimensionless face areas of the scalar control volume and is described as,

$$A^*_{J,K} = \frac{1}{4}(\Delta y^*_{\ j} + \Delta y^*_{\ j+1})(\Delta z^*_{\ k} + \Delta z^*_{\ k+1}) \qquad (4.13a)$$

$$A^*_{I,K} = \frac{1}{4}(\Delta x^*_{\ i} + \Delta x^*_{\ i+1})(\Delta z^*_{\ k} + \Delta z^*_{\ k+1}) \qquad (4.13b)$$

$$A^*_{I,J} = \frac{1}{4}(\Delta x^*_{\ i} + \Delta x^*_{\ i+1})(\Delta y^*_{\ j} + \Delta y^*_{\ j+1}) \qquad (4.13c)$$

for each face. It should be noted that Δx, Δy and Δz are the spacing values between the scalar grid lines (I, J and K) in x, y and z directions, respectively.

4.1.3.2 Momentum Equation in x-direction

Dimensionless momentum equation (3.12) in x-direction is integrated over the representative vectorial u-control volume (control volume for the velocity u). Discretized algebraic x-momentum equation over u-control volume is written as follows:

$$a_{i,J,K}u^*_{\ i,J,K} = a_{i,J+1,K}u^*_{\ i,J+1,K} + a_{i,J-1,K}u^*_{\ i,J-1,K} + a_{i+1,J,K}u^*_{\ i+1,J,K} + a_{i-1,J,K}u^*_{\ i-1,J,K} + a_{i,J,K+1}u^*_{\ i,J,K+1}$$
$$+ a_{i,J,K-1}u^*_{\ i,J,K-1} + \Delta F_u + (S_u)_u + \frac{1}{4}(P^*_{\ I-1,J,K} - P^*_{\ I,J,K})(\Delta y^*_{\ j} + \Delta y^*_{\ j+1})(\Delta z^*_{\ k} + \Delta z^*_{\ k+1}) \qquad (4.14)$$

where

$$a_{i-1,J,K} = \left\| \begin{array}{l} \frac{1}{4}[u^*_{\ i-1,J,K} + (u^*_{\ i,J,K} - u^*_{\ i-1,J,K})\frac{\Delta x^*_{\ i-1}}{\Delta x^*_{\ i-1} + \Delta x^*_{\ i}}](\Delta y^*_{\ j} + \Delta y^*_{\ j+1})(\Delta z^*_{\ k} + \Delta z^*_{\ k+1}), \\[2em] \frac{1}{2}\frac{(\Delta y^*_{\ j} + \Delta y^*_{\ j+1})(\Delta z^*_{\ k} + \Delta z^*_{\ k+1})}{\mathrm{Re}_{D_h}(\Delta x^*_{\ i-1} + \Delta x^*_{\ i})} \\[1em] \quad + \frac{1}{8}[u^*_{\ i-1,J,K} + (u^*_{\ i,J,K} - u^*_{\ i-1,J,K})\frac{\Delta x^*_{\ i-1}}{\Delta x^*_{\ i-1} + \Delta x^*_{\ i}}](\Delta y^*_{\ j} + \Delta y^*_{\ j+1})(\Delta z^*_{\ k} + \Delta z^*_{\ k+1}), \\[1em] 0 \end{array} \right\| \qquad (4.15a)$$

$$a_{i+1,J,K} = \left\| \begin{array}{l} -\dfrac{1}{4}[u^*_{i,J,K} + (u^*_{i+1,J,K} - u^*_{i,J,K})\dfrac{\Delta x^*_i}{\Delta x^*_i + \Delta x^*_{i+1}}](\Delta y^*_j + \Delta y^*_{j+1})(\Delta z^*_k + \Delta z^*_{k+1}), \\[4mm] \dfrac{1}{2}\dfrac{(\Delta y^*_j + \Delta y^*_{j+1})(\Delta z^*_k + \Delta z^*_{k+1})}{\mathrm{Re}_{D_h}(\Delta x^*_i + \Delta x^*_{i+1})} \\[4mm] \qquad -\dfrac{1}{8}[u^*_{i,J,K} + (u^*_{i+1,J,K} - u^*_{i,J,K})\dfrac{\Delta x^*_i}{\Delta x^*_i + \Delta x^*_{i+1}}](\Delta y^*_j + \Delta y^*_{j+1})(\Delta z^*_k + \Delta z^*_{k+1}), \\[4mm] 0 \end{array} \right\| \quad (4.15b)$$

$$a_{i,J-1,K} = \left\| \begin{array}{l} \dfrac{1}{4}\Delta x^*_i(v^*_{I-1,j,K} + v^*_{I,j,K})(\Delta z^*_k + \Delta z^*_{k+1}), \\[4mm] \dfrac{1}{2}\dfrac{\Delta x^*_i(\Delta z^*_k + \Delta z^*_{k+1})}{\mathrm{Re}_{D_h}\Delta y^*_j} + \dfrac{1}{8}\Delta x^*_i(v^*_{I-1,j,K} + v^*_{I,j,K})(\Delta z^*_k + \Delta z^*_{k+1}), \\[4mm] 0 \end{array} \right\| \quad (4.15c)$$

$$a_{i,J+1,K} = \left\| \begin{array}{l} -\dfrac{1}{4}\Delta x^*_i(v^*_{I-1,j+1,K} + v^*_{I,j+1,K})(\Delta z^*_k + \Delta z^*_{k+1}), \\[4mm] \dfrac{1}{2}\dfrac{\Delta x^*_i(\Delta z^*_k + \Delta z^*_{k+1})}{\mathrm{Re}_{D_h}\Delta y^*_{j+1}} - \dfrac{1}{8}\Delta x^*_i(v^*_{I-1,j+1,K} + v^*_{I,j+1,K})(\Delta z^*_k + \Delta z^*_{k+1}), \\[4mm] 0 \end{array} \right\| \quad (4.15d)$$

$$a_{i,J,K-1} = \left\| \begin{array}{l} \dfrac{1}{4}\Delta x^*_i(w^*_{I-1,J,k} + w^*_{I,J,k})(\Delta y^*_j + \Delta y^*_{j+1}), \\[4mm] \dfrac{1}{2}\dfrac{\Delta x^*_i(\Delta y^*_j + \Delta y^*_{j+1})}{\mathrm{Re}_{D_h}\Delta z^*_k} + \dfrac{1}{8}\Delta x^*_i(w^*_{I-1,J,k} + w^*_{I,J,k})(\Delta y^*_j + \Delta y^*_{j+1}), \\[4mm] 0 \end{array} \right\| \quad (4.15e)$$

$$a_{i,J,K+1} = \left\| \begin{array}{l} -\dfrac{1}{4}\Delta x^*_i(w^*_{I-1,J,k+1} + w^*_{I,J,k+1})(\Delta y^*_j + \Delta y^*_{j+1}), \\[4mm] \dfrac{1}{2}\dfrac{\Delta x^*_i(\Delta y^*_j + \Delta y^*_{j+1})}{\mathrm{Re}_{D_h}\Delta z^*_{k+1}} - \dfrac{1}{8}\Delta x^*_i(w^*_{I-1,J,k+1} + w^*_{I,J,k+1})(\Delta y^*_j + \Delta y^*_{j+1}), \\[4mm] 0 \end{array} \right\| \quad (4.15f)$$

$$\Delta F_u = \frac{1}{4}\{[u^*_{i,J,K} + (u^*_{i+1,J,K} - u^*_{i,J,K})\frac{\Delta x^*_i}{\Delta x^*_i + \Delta x^*_{i+1}}]$$

$$-[u^*_{i-1,J,K} + (u^*_{i,J,K} - u^*_{i-1,J,K})\frac{\Delta x^*_{i-1}}{\Delta x^*_{i-1} + \Delta x^*_i}]\}(\Delta y^*_j + \Delta y^*_{j+1})(\Delta z^*_k + \Delta z^*_{k+1})$$

$$+\frac{1}{4}\Delta x^*_i(\Delta z^*_k + \Delta z^*_{k+1})[(v^*_{I-1,j+1,K} + v^*_{I,j+1,K}) - (v^*_{I-1,j,K} + v^*_{I,j,K})]$$

$$+\frac{1}{4}\Delta x^*_i(\Delta y^*_j + \Delta y^*_{j+1})[(w^*_{I-1,J,k+1} + w^*_{I,J,k+1}) - (w^*_{I-1,J,k} + w^*_{I,J,k})]$$

(4.15g)

$$(S_u)_u = 0 \tag{4.15h}$$

$$a_{i,J,K} = a_{i-1,J,K} + a_{i+1,J,K} + a_{i,J-1,K} + a_{i,J+1,K} + a_{i,J,K-1} + a_{i,J,K+1} + \Delta F_u - (S_p)_u \tag{4.15i}$$

$$(S_p)_u = 0 \tag{4.15j}$$

4.1.3.3 Momentum Equation in y-direction

After the dimensionless momentum equation (3.13) in y-direction is integrated over the representative vectorial v-control volume (control volume for the velocity v), discretized momentum equation in y-direction is given by,

$$a_{I,j,K}v^*_{I,j,K} = a_{I-1,j,K}v^*_{I-1,j,K} + a_{I+1,j,K}v^*_{I+1,j,K} + a_{I,j-1,K}v^*_{I,j-1,K} + a_{I,j+1,K}v^*_{I,j+1,K} + a_{I,j,K-1}v^*_{I,j,K-1}$$

$$+a_{I,j,K+1}v^*_{I,j,K+1} + \Delta F_v + (S_u)_v + \frac{1}{4}(P^*_{I,J-1,K} - P^*_{I,J,K})(\Delta x^*_i + \Delta x^*_{i+1})(\Delta z^*_k + \Delta z^*_{k+1})$$

(4.16)

where

$$a_{I-1,j,K} = \left\Vert \begin{array}{l} \frac{1}{4}\Delta y^*_j(u^*_{i,J-1,K} + u^*_{i,J,K})(\Delta z^*_k + \Delta z^*_{k+1}), \\[2ex] \frac{1}{2}\frac{\Delta y^*_j(\Delta z^*_k + \Delta z^*_{k+1})}{\text{Re}_{D_h}\Delta x^*_i} + \frac{1}{8}\Delta y^*_j(u^*_{i,J-1,K} + u^*_{i,J,K})(\Delta z^*_k + \Delta z^*_{k+1}), \\[2ex] 0 \end{array} \right\Vert \tag{4.17a}$$

$$a_{I+1,j,K} = \left\|\begin{array}{l} -\dfrac{1}{4}\Delta y^{*}_{j}(u^{*}_{i+1,J-1,K}+u^{*}_{i+1,J,K})(\Delta z^{*}_{k}+\Delta z^{*}_{k+1}), \\[2ex] \dfrac{1}{2}\dfrac{\Delta y^{*}_{j}(\Delta z^{*}_{k}+\Delta z^{*}_{k+1})}{\mathrm{Re}_{D_{h}}\,\Delta x^{*}_{i+1}}-\dfrac{1}{8}\Delta y^{*}_{j}(u^{*}_{i+1,J-1,K}+u^{*}_{i+1,J,K})(\Delta z^{*}_{k}+\Delta z^{*}_{k+1}), \\[2ex] 0 \end{array}\right\| \qquad (4.17b)$$

$$a_{I,j-1,K} = \left\|\begin{array}{l} \dfrac{1}{4}[v^{*}_{I,j-1,K}+(v^{*}_{I,j,K}-v^{*}_{I,j-1,K})\dfrac{\Delta y^{*}_{j-1}}{\Delta y^{*}_{j-1}+\Delta y^{*}_{j}}](\Delta x^{*}_{i}+\Delta x^{*}_{i+1})(\Delta z^{*}_{k}+\Delta z^{*}_{k+1}), \\[2ex] \dfrac{1}{2}\dfrac{(\Delta x^{*}_{i}+\Delta x^{*}_{i+1})(\Delta z^{*}_{k}+\Delta z^{*}_{k+1})}{\mathrm{Re}_{D_{h}}(\Delta y^{*}_{j-1}+\Delta y^{*}_{j})} \\[2ex] \qquad +\dfrac{1}{8}[v^{*}_{I,j-1,K}+(v^{*}_{I,j,K}-v^{*}_{I,j-1,K})\dfrac{\Delta y^{*}_{j-1}}{\Delta y^{*}_{j-1}+\Delta y^{*}_{j}}](\Delta x^{*}_{i}+\Delta x^{*}_{i+1})(\Delta z^{*}_{k}+\Delta z^{*}_{k+1}), \\[2ex] 0 \end{array}\right\| \qquad (4.17c)$$

$$a_{I,j+1,K} = \left\|\begin{array}{l} -\dfrac{1}{4}[v^{*}_{I,j,K}+(v^{*}_{I,j+1,K}-v^{*}_{I,j,K})\dfrac{\Delta y^{*}_{j}}{\Delta y^{*}_{j}+\Delta y^{*}_{j+1}}](\Delta x^{*}_{i}+\Delta x^{*}_{i+1})(\Delta z^{*}_{k}+\Delta z^{*}_{k+1}), \\[2ex] \dfrac{1}{2}\dfrac{(\Delta x^{*}_{i}+\Delta x^{*}_{i+1})(\Delta z^{*}_{k}+\Delta z^{*}_{k+1})}{\mathrm{Re}_{D_{h}}(\Delta y^{*}_{j}+\Delta y^{*}_{j+1})} \\[2ex] \qquad -\dfrac{1}{8}[v^{*}_{I,j,K}+(v^{*}_{I,j+1,K}-v^{*}_{I,j,K})\dfrac{\Delta y^{*}_{j}}{\Delta y^{*}_{j}+\Delta y^{*}_{j+1}}](\Delta x^{*}_{i}+\Delta x^{*}_{i+1})(\Delta z^{*}_{k}+\Delta z^{*}_{k+1}), \\[2ex] 0 \end{array}\right\| \qquad (4.17d)$$

$$a_{I,j,K-1} = \left\|\begin{array}{l} \dfrac{1}{4}\Delta y^{*}_{j}(w^{*}_{I,J-1,k}+w^{*}_{I,J,k})(\Delta x^{*}_{i}+\Delta x^{*}_{i+1}), \\[2ex] \dfrac{1}{2}\dfrac{\Delta y^{*}_{j}(\Delta x^{*}_{i}+\Delta x^{*}_{i+1})}{\mathrm{Re}_{D_{h}}\,\Delta z^{*}_{k}}+\dfrac{1}{8}\Delta y^{*}_{j}(w^{*}_{I,J-1,k}+w^{*}_{I,J,k})(\Delta x^{*}_{i}+\Delta x^{*}_{i+1}), \\[2ex] 0 \end{array}\right\| \qquad (4.17e)$$

$$a_{I,j,K+1} = \left\|\begin{array}{l} -\dfrac{1}{4}\Delta y^{*}_{j}(w^{*}_{I,J-1,k+1}+w^{*}_{I,J,k+1})(\Delta x^{*}_{i}+\Delta x^{*}_{i+1}), \\[2ex] \dfrac{1}{2}\dfrac{\Delta y^{*}_{j}(\Delta x^{*}_{i}+\Delta x^{*}_{i+1})}{\mathrm{Re}_{D_{h}}\,\Delta z^{*}_{k+1}}-\dfrac{1}{8}\Delta y^{*}_{j}(w^{*}_{I,J-1,k+1}+w^{*}_{I,J,k+1})(\Delta x^{*}_{i}+\Delta x^{*}_{i+1}), \\[2ex] 0 \end{array}\right\| \qquad (4.17f)$$

$$\Delta F_v = \frac{1}{4} \Delta y^*_j (\Delta z^*_k + \Delta z^*_{k+1})[(u^*_{i+1,J-1,K} + u^*_{i+1,J,K}) - (u^*_{i,J-1,K} + u^*_{i,J,K})]$$

$$+ \frac{1}{4} \{[v^*_{I,j,K} + (v^*_{I,j+1,K} - v^*_{I,j,K}) \frac{\Delta y^*_j}{\Delta y^*_j + \Delta y^*_{j+1}}]$$

$$-[v^*_{I,j-1,K} + (v^*_{I,j,K} - v^*_{I,j-1,K}) \frac{\Delta y^*_{j-1}}{\Delta y^*_{j-1} + \Delta y^*_j}]\}(\Delta x^*_i + \Delta x^*_{i+1})(\Delta z^*_k + \Delta z^*_{k+1})$$

$$+ \frac{1}{4} \Delta y^*_j (\Delta x^*_i + \Delta x^*_{i+1})[(w^*_{I,J-1,k+1} + w^*_{I,J,k+1}) - (w^*_{I,J-1,k} + w^*_{I,J,k})]$$

(4.17g)

$$(S_u)_v = 0 \tag{4.17h}$$

$$a_{I,j,K} = a_{I-1,j,K} + a_{I+1,j,K} + a_{I,j-1,K} + a_{I,j+1,K} + a_{I,j,K-1} + a_{I,j,K+1} + \Delta F_v - (S_p)_v \tag{4.17i}$$

$$(S_p)_v = 0 \tag{4.17j}$$

4.1.3.4 Momentum Equation in z-direction

Like the two previous momentum equations, discretized z-momentum equation over w-control volume is derived as,

$$a_{I,J,k} w^*_{I,J,k} = a_{I-1,J,k} w^*_{I-1,J,k} + a_{I+1,J,k} w^*_{I+1,J,k} + a_{I,J-1,k} w^*_{I,J-1,k} + a_{I,J+1,k} w^*_{I,J+1,k} + a_{I,J,k-1} w^*_{I,J,k-1}$$

$$+ a_{I,J,k+1} w^*_{I,J,k+1} + \Delta F_w + (S_u)_w + \frac{1}{4}(P^*_{I,J,K-1} - P^*_{I,J,K})(\Delta x^*_i + \Delta x^*_{i+1})(\Delta y^*_j + \Delta y^*_{j+1})$$

(4.18)

where

$$a_{I-1,J,k} = \left\| \begin{array}{l} \frac{1}{4} \Delta z^*_k (u^*_{i,J,K-1} + u^*_{i,J,K})(\Delta y^*_j + \Delta y^*_{j+1}), \\[2mm] \frac{1}{2} \frac{\Delta z^*_k (\Delta y^*_j + \Delta y^*_{j+1})}{\mathrm{Re}_{D_h} \Delta x^*_i} + \frac{1}{8} \Delta z^*_k (u^*_{i,J,K-1} + u^*_{i,J,K})(\Delta y^*_j + \Delta y^*_{j+1}), \\[2mm] 0 \end{array} \right\| \tag{4.19a}$$

$$a_{I+1,J,k} = \left\|\begin{array}{l} -\dfrac{1}{4}\Delta z^{*}_{k}(u^{*}_{i+1,J,K-1}+u^{*}_{i+1,J,K})(\Delta y^{*}_{j}+\Delta y^{*}_{j+1}), \\[3mm] \dfrac{1}{2}\dfrac{\Delta z^{*}_{k}(\Delta y^{*}_{j}+\Delta y^{*}_{j+1})}{\mathrm{Re}_{D_{h}}\Delta x^{*}_{i+1}}-\dfrac{1}{8}\Delta z^{*}_{k}(u^{*}_{i+1,J,K-1}+u^{*}_{i+1,J,K})(\Delta y^{*}_{j}+\Delta y^{*}_{j+1}), \\[3mm] 0 \end{array}\right\| \qquad (4.19b)$$

$$a_{I,J-1,k} = \left\|\begin{array}{l} \dfrac{1}{4}\Delta z^{*}_{k}(v^{*}_{I,j,K-1}+v^{*}_{I,j,K})(\Delta x^{*}_{i}+\Delta x^{*}_{i+1}), \\[3mm] \dfrac{1}{2}\dfrac{\Delta z^{*}_{k}(\Delta x^{*}_{i}+\Delta x^{*}_{i+1})}{\mathrm{Re}_{D_{h}}\Delta y^{*}_{j}}+\dfrac{1}{8}\Delta z^{*}_{k}(v^{*}_{I,j,K-1}+v^{*}_{I,j,K})(\Delta x^{*}_{i}+\Delta x^{*}_{i+1}), \\[3mm] 0 \end{array}\right\| \qquad (4.19c)$$

$$a_{I,J+1,k} = \left\|\begin{array}{l} -\dfrac{1}{4}\Delta z^{*}_{k}(v^{*}_{I,j+1,K-1}+v^{*}_{I,j+1,K})(\Delta x^{*}_{i}+\Delta x^{*}_{i+1}), \\[3mm] \dfrac{1}{2}\dfrac{\Delta z^{*}_{k}(\Delta x^{*}_{i}+\Delta x^{*}_{i+1})}{\mathrm{Re}_{D_{h}}\Delta y^{*}_{j+1}}-\dfrac{1}{8}\Delta z^{*}_{k}(v^{*}_{I,j+1,K-1}+v^{*}_{I,j+1,K})(\Delta x^{*}_{i}+\Delta x^{*}_{i+1}), \\[3mm] 0 \end{array}\right\| \qquad (4.19d)$$

$$a_{I,J,k-1} = \left\|\begin{array}{l} \dfrac{1}{4}[w^{*}_{I,J,k-1}+(w^{*}_{I,J,k}-w^{*}_{I,J,k-1})\dfrac{\Delta z^{*}_{k-1}}{\Delta z^{*}_{k-1}+\Delta z^{*}_{k}}](\Delta x^{*}_{i}+\Delta x^{*}_{i+1})(\Delta y^{*}_{j}+\Delta y^{*}_{j+1}), \\[4mm] \dfrac{1}{2}\dfrac{(\Delta x^{*}_{i}+\Delta x^{*}_{i+1})(\Delta y^{*}_{j}+\Delta y^{*}_{j+1})}{\mathrm{Re}_{D_{h}}(\Delta z^{*}_{k-1}+\Delta z^{*}_{k})} \\[4mm] \qquad +\dfrac{1}{8}[w^{*}_{I,J,k-1}+(w^{*}_{I,J,k}-w^{*}_{I,J,k-1})\dfrac{\Delta z^{*}_{k-1}}{\Delta z^{*}_{k-1}+\Delta z^{*}_{k}}](\Delta x^{*}_{i}+\Delta x^{*}_{i+1})(\Delta y^{*}_{j}+\Delta y^{*}_{j+1}), \\[4mm] 0 \end{array}\right\| \qquad (4.19e)$$

$$a_{I,J,k+1} = \left\|\begin{array}{l} -\dfrac{1}{4}[w^{*}_{I,J,k}+(w^{*}_{I,J,k+1}-w^{*}_{I,J,k})\dfrac{\Delta z^{*}_{k}}{\Delta z^{*}_{k}+\Delta z^{*}_{k+1}}](\Delta x^{*}_{i}+\Delta x^{*}_{i+1})(\Delta y^{*}_{j}+\Delta y^{*}_{j+1}), \\[4mm] \dfrac{1}{2}\dfrac{(\Delta x^{*}_{i}+\Delta x^{*}_{i+1})(\Delta y^{*}_{j}+\Delta y^{*}_{j+1})}{\mathrm{Re}_{D_{h}}(\Delta z^{*}_{k}+\Delta z^{*}_{k+1})} \\[4mm] \qquad -\dfrac{1}{8}[w^{*}_{I,J,k}+(w^{*}_{I,J,k+1}-w^{*}_{I,J,k})\dfrac{\Delta z^{*}_{k}}{\Delta z^{*}_{k}+\Delta z^{*}_{k+1}}](\Delta x^{*}_{i}+\Delta x^{*}_{i+1})(\Delta y^{*}_{j}+\Delta y^{*}_{j+1}), \\[4mm] 0 \end{array}\right\| \qquad (4.19f)$$

$$\Delta F_w = \frac{1}{4}\Delta z^*_k (\Delta y^*_j + \Delta y^*_{j+1})[(u^*_{i+1,J,K-1} + u^*_{i+1,J,K}) - (u^*_{i,J,K-1} + u^*_{i,J,K})]$$

$$+ \frac{1}{4}\Delta z^*_k (\Delta x^*_i + \Delta x^*_{i+1})[(v^*_{I,j+1,K-1} + v^*_{I,j+1,K}) - (v^*_{I,j,K-1} + v^*_{I,j,K})]$$

$$+ \frac{1}{4}\{[w^*_{I,J,k} + (w^*_{I,J,k+1} - w^*_{I,J,k})\frac{\Delta z^*_k}{\Delta z^*_k + \Delta z^*_{k+1}}]$$

$$- [w^*_{I,J,k-1} + (w^*_{I,J,k} - w^*_{I,J,k-1})\frac{\Delta z^*_{k-1}}{\Delta z^*_{k-1} + \Delta z^*_k}]\}(\Delta x^*_i + \Delta x^*_{i+1})(\Delta y^*_j + \Delta y^*_{j+1})$$

(4.19g)

$$(S_u)_w = 0 \tag{4.19h}$$

$$a_{I,J,k} = a_{I-1,J,k} + a_{I+1,J,k} + a_{I,J-1,k} + a_{I,J+1,k} + a_{I,J,k-1} + a_{I,J,k+1} + \Delta F_w - (S_p)_w \tag{4.19i}$$

$$(S_p)_w = 0 \tag{4.19j}$$

4.1.3.5 Equations for Pressure Corrections and Velocity Corrections

As mentioned previously, evaluated pressure and velocities are corrected at the end of each iteration step. In this part, the procedure for the determination of pressure and velocity corrections is to be reported.

Before starting to explain the formulations for finding corrections, it should be noted that the equation (4.14) can also be written in terms of corrected dimensionless velocities u^{**} in x-direction as,

$$a_{i,J,K}u^{**}_{i,J,K} = a_{i,J+1,K}u^{**}_{i,J+1,K} + a_{i,J-1,K}u^{**}_{i,J-1,K} + a_{i+1,J,K}u^{**}_{i+1,J,K}$$

$$+ a_{i-1,J,K}u^{**}_{i-1,J,K} + a_{i,J,K+1}u^{**}_{i,J,K+1} + a_{i,J,K-1}u^{**}_{i,J,K-1}$$

$$+ \frac{1}{4}(\Delta y^*_j + \Delta y^*_{j+1})(\Delta z^*_k + \Delta z^*_{k+1})\{[u^*_{i,J,K} + (u^*_{i+1,J,K} - u^*_{i,J,K})\frac{\Delta x^*_i}{\Delta x^*_i + \Delta x^*_{i+1}}]$$

$$- [u^*_{i-1,J,K} + (u^*_{i,J,K} - u^*_{i-1,J,K})\frac{\Delta x^*_{i-1}}{\Delta x^*_{i-1} + \Delta x^*_i}]\} \tag{4.20}$$

$$+ \frac{1}{4}\Delta x^*_i (\Delta z^*_k + \Delta z^*_{k+1})[(v^*_{I-1,j+1,K} + v^*_{I,j+1,K}) - (v^*_{I-1,j,K} + v^*_{I,j,K})]$$

$$+ \frac{1}{4}\Delta x^*_i (\Delta y^*_j + \Delta y^*_{j+1})[(w^*_{I-1,J,k+1} + w^*_{I,J,k+1}) - (w^*_{I-1,J,k} + w^*_{I,J,k})]$$

$$+ \frac{1}{4}(P^{**}_{I-1,J,K} - P^{**}_{I,J,K})(\Delta y^*_j + \Delta y^*_{j+1})(\Delta z^*_k + \Delta z^*_{k+1})$$

44

Double starred (**) variables, which are included in equation (4.20), represent the corrected dimensionless velocity and pressure values. Next, if the equation (4.14) is subtracted from equation (4.20), it is obtained that

$$a_{i,J,K} u'_{i,J,K} = a_{i,J+1,K} u'_{i,J+1,K} + a_{i,J-1,K} u'_{i,J-1,K} + a_{i+1,J,K} u'_{i+1,J,K} + a_{i-1,J,K} u'_{i-1,J,K} + a_{i,J,K+1} u'_{i,J,K+1}$$
$$+ a_{i,J,K-1} u'_{i,J,K-1} + \frac{1}{4} (P'_{I-1,J,K} - P'_{I,J,K})(\Delta y^*_j + \Delta y^*_{j+1})(\Delta z^*_k + \Delta z^*_{k+1}) \tag{4.21}$$

where the primed variables (') are the pressure and velocity corrections. The term $a_{i,J+1,K} u'_{i,J+1,K} + a_{i,J-1,K} u'_{i,J-1,K} + a_{i+1,J,K} u'_{i+1,J,K} + a_{i-1,J,K} u'_{i-1,J,K} + a_{i,J,K+1} u'_{i,J,K+1} + a_{i,J,K-1} u'_{i,J,K-1}$ is ignored or discarded in SIMPLE algorithm [20]. Therefore, the definition for velocity correction in x-direction is,

$$u'_{i,J,K} = \frac{1}{4} \frac{(\Delta y^*_j + \Delta y^*_{j+1})(\Delta z^*_k + \Delta z^*_{k+1})}{a_{i,J,K}} (P'_{I-1,J,K} - P'_{I,J,K}) \tag{4.22a}$$

in a specified finite control volume. Similarly, for other velocity components,

$$v'_{I,j,K} = \frac{1}{4} \frac{(\Delta x^*_i + \Delta x^*_{i+1})(\Delta z^*_k + \Delta z^*_{k+1})}{a_{I,j,K}} (P'_{I,J-1,K} - P'_{I,J,K}) \tag{4.22b}$$

$$w'_{I,J,k} = \frac{1}{4} \frac{(\Delta x^*_i + \Delta x^*_{i+1})(\Delta y^*_j + \Delta y^*_{j+1})}{a_{I,J,k}} (P'_{I,J,K-1} - P'_{I,J,K}) \tag{4.22c}$$

Thus, the corrected velocities in x, y and z directions are analytically expressed by,

$$u^{**}_{i,J,K} = u^*_{i,J,K} + u'_{i,J,K} = u^*_{i,J,K} + \frac{1}{4} \frac{(\Delta y^*_j + \Delta y^*_{j+1})(\Delta z^*_k + \Delta z^*_{k+1})}{a_{i,J,K}} (P'_{I-1,J,K} - P'_{I,J,K}) \tag{4.23a}$$

$$v^{**}_{I,j,K} = v^*_{I,j,K} + v'_{I,j,K} = v^*_{I,j,K} + \frac{1}{4} \frac{(\Delta x^*_i + \Delta x^*_{i+1})(\Delta z^*_k + \Delta z^*_{k+1})}{a_{I,j,K}} (P'_{I,J-1,K} - P'_{I,J,K}) \tag{4.23b}$$

$$w^{**}_{I,J,k} = w^*_{I,J,k} + w'_{I,J,k} = w^*_{I,J,k} + \frac{1}{4} \frac{(\Delta x^*_i + \Delta x^*_{i+1})(\Delta y^*_j + \Delta y^*_{j+1})}{a_{I,J,k}} (P'_{I,J,K-1} - P'_{I,J,K}) \tag{4.23c}$$

As equations (4.23a), (4.23b) and (4.23c), which are written for corrected velocities, are substituted into the discretized continuity equation (4.11) and the resulting

equation is rearranged, the following relation for the determination of pressure corrections is obtained:

$$a_{I,J,K}P'_{I,J,K} = a_{I-1,J,K}P'_{I-1,J,K} + a_{I+1,J,K}P'_{I+1,J,K} + a_{I,J-1,K}P'_{I,J-1,K} + a_{I,J+1,K}P'_{I,J+1,K} + a_{I,J,K-1}P'_{I,J,K-1}$$
$$+ a_{I,J,K+1}P'_{I,J,K+1} + b_{I,J,K} \tag{4.24}$$

where

$$a_{I-1,J,K} = \frac{1}{16} \frac{[(\Delta y^*_j + \Delta y^*_{j+1})(\Delta z^*_k + \Delta z^*_{k+1})]^2}{a_{i,J,K}} \tag{4.25a}$$

$$a_{I+1,J,K} = \frac{1}{16} \frac{[(\Delta y^*_j + \Delta y^*_{j+1})(\Delta z^*_k + \Delta z^*_{k+1})]^2}{a_{i+1,J,K}} \tag{4.25b}$$

$$a_{I,J-1,K} = \frac{1}{16} \frac{[(\Delta x^*_i + \Delta x^*_{i+1})(\Delta z^*_k + \Delta z^*_{k+1})]^2}{a_{I,j,K}} \tag{4.25c}$$

$$a_{I,J+1,K} = \frac{1}{16} \frac{[(\Delta x^*_i + \Delta x^*_{i+1})(\Delta z^*_k + \Delta z^*_{k+1})]^2}{a_{I,j+1,K}} \tag{4.25d}$$

$$a_{I,J,K-1} = \frac{1}{16} \frac{[(\Delta x^*_i + \Delta x^*_{i+1})(\Delta y^*_j + \Delta y^*_{j+1})]^2}{a_{I,J,k}} \tag{4.25e}$$

$$a_{I,J,K+1} = \frac{1}{16} \frac{[(\Delta x^*_i + \Delta x^*_{i+1})(\Delta y^*_j + \Delta y^*_{j+1})]^2}{a_{I,J,k+1}} \tag{4.25f}$$

$$b_{I,J,K} = \frac{1}{4}(u^*_{i,J,K} - u^*_{i+1,J,K})(\Delta y^*_j + \Delta y^*_{j+1})(\Delta z^*_k + \Delta z^*_{k+1})$$
$$+ \frac{1}{4}(v^*_{I,j,K} - v^*_{I,j+1,K})(\Delta x^*_i + \Delta x^*_{i+1})(\Delta z^*_k + \Delta z^*_{k+1}) \tag{4.25g}$$
$$+ \frac{1}{4}(w^*_{I,J,k} - w^*_{I,J,k+1})(\Delta x^*_i + \Delta x^*_{i+1})(\Delta y^*_j + \Delta y^*_{j+1})$$

$$a_{I,J,K} = a_{I-1,J,K} + a_{I+1,J,K} + a_{I,J-1,K} + a_{I,J+1,K} + a_{I,J,K-1} + a_{I,J,K+1} \tag{4.25h}$$

Besides the correction of velocity values, nodal pressures at each control volume are also corrected by the following equation:

$$P^{**}_{I,J,K} = P^*_{I,J,K} + P'_{I,J,K} \tag{4.26}$$

4.1.3.6 Energy Equation

Dimensionless energy equation (3.15) is integrated over a scalar control volume in order to obtain,

$$a_{I,J,K}\theta_{I,J,K} = a_{I,J+1,K}\theta_{I,J+1,K} + a_{I,J-1,K}\theta_{I,J-1,K} + a_{I+1,J,K}\theta_{I+1,J,K} + a_{I-1,J,K}\theta_{I-1,J,K} + a_{I,J,K+1}\theta_{I,J,K+1}$$
$$+ a_{I,J,K-1}\theta_{I,J,K-1} + \Delta F_\theta + (S_u)_\theta \tag{4.27}$$

where

$$a_{I-1,J,K} = \left\| \begin{array}{l} \dfrac{1}{4}u^*_{i,J,K}(\Delta y^*_j + \Delta y^*_{j+1})(\Delta z^*_k + \Delta z^*_{k+1}), \\[3mm] \dfrac{1}{4}\dfrac{(\Delta y^*_j + \Delta y^*_{j+1})(\Delta z^*_k + \Delta z^*_{k+1})}{\mathrm{Re}_{D_h}\mathrm{Pr}\,\Delta x^*_i} + \dfrac{1}{8}u^*_{i,J,K}(\Delta y^*_j + \Delta y^*_{j+1})(\Delta z^*_k + \Delta z^*_{k+1}), \\[3mm] 0 \end{array} \right\| \tag{4.28a}$$

$$a_{I+1,J,K} = \left\| \begin{array}{l} -\dfrac{1}{4}u^*_{i+1,J,K}(\Delta y^*_j + \Delta y^*_{j+1})(\Delta z^*_k + \Delta z^*_{k+1}), \\[3mm] \dfrac{1}{4}\dfrac{(\Delta y^*_j + \Delta y^*_{j+1})(\Delta z^*_k + \Delta z^*_{k+1})}{\mathrm{Re}_{D_h}\mathrm{Pr}\,\Delta x^*_{i+1}} - \dfrac{1}{8}u^*_{i+1,J,K}(\Delta y^*_j + \Delta y^*_{j+1})(\Delta z^*_k + \Delta z^*_{k+1}), \\[3mm] 0 \end{array} \right\| \tag{4.28b}$$

$$a_{I,J-1,K} = \left\| \begin{array}{l} \dfrac{1}{4}v^*_{I,j,K}(\Delta x^*_i + \Delta x^*_{i+1})(\Delta z^*_k + \Delta z^*_{k+1}), \\[3mm] \dfrac{1}{4}\dfrac{(\Delta x^*_i + \Delta x^*_{i+1})(\Delta z^*_k + \Delta z^*_{k+1})}{\mathrm{Re}_{D_h}\mathrm{Pr}\,\Delta y^*_j} + \dfrac{1}{8}v^*_{I,j,K}(\Delta x^*_i + \Delta x^*_{i+1})(\Delta z^*_k + \Delta z^*_{k+1}), \\[3mm] 0 \end{array} \right\| \tag{4.28c}$$

$$a_{I,J+1,K} = \left\| \begin{array}{l} -\dfrac{1}{4}v^*_{I,j+1,K}(\Delta x^*_i + \Delta x^*_{i+1})(\Delta z^*_k + \Delta z^*_{k+1}), \\[3mm] \dfrac{1}{4}\dfrac{(\Delta x^*_i + \Delta x^*_{i+1})(\Delta z^*_k + \Delta z^*_{k+1})}{\mathrm{Re}_{D_h}\mathrm{Pr}\,\Delta y^*_{j+1}} - \dfrac{1}{8}v^*_{I,j+1,K}(\Delta x^*_i + \Delta x^*_{i+1})(\Delta z^*_k + \Delta z^*_{k+1}), \\[3mm] 0 \end{array} \right\| \qquad (4.28\text{d})$$

$$a_{I,J,K-1} = \left\| \begin{array}{l} \dfrac{1}{4}w^*_{I,J,k}(\Delta x^*_i + \Delta x^*_{i+1})(\Delta y^*_j + \Delta y^*_{j+1}), \\[3mm] \dfrac{1}{4}\dfrac{(\Delta x^*_i + \Delta x^*_{i+1})(\Delta y^*_j + \Delta y^*_{j+1})}{\mathrm{Re}_{D_h}\mathrm{Pr}\,\Delta z^*_k} + \dfrac{1}{8}w^*_{I,J,k}(\Delta x^*_i + \Delta x^*_{i+1})(\Delta y^*_j + \Delta y^*_{j+1}), \\[3mm] 0 \end{array} \right\| \qquad (4.28\text{e})$$

$$a_{I,J,K+1} = \left\| \begin{array}{l} -\dfrac{1}{4}w^*_{I,J,k+1}(\Delta x^*_i + \Delta x^*_{i+1})(\Delta y^*_j + \Delta y^*_{j+1}), \\[3mm] \dfrac{1}{4}\dfrac{(\Delta x^*_i + \Delta x^*_{i+1})(\Delta y^*_j + \Delta y^*_{j+1})}{\mathrm{Re}_{D_h}\mathrm{Pr}\,\Delta z^*_{k+1}} - \dfrac{1}{8}w^*_{I,J,k+1}(\Delta x^*_i + \Delta x^*_{i+1})(\Delta y^*_j + \Delta y^*_{j+1}), \\[3mm] 0 \end{array} \right\| \qquad (4.28\text{f})$$

$$\begin{aligned} \Delta F_\theta &= \frac{1}{4}(u^*_{i+1,J,K} - u^*_{i,J,K})(\Delta y^*_j + \Delta y^*_{j+1})(\Delta z^*_k + \Delta z^*_{k+1}) \\ &\quad + \frac{1}{4}(v^*_{I,j+1,K} - v^*_{I,j,K})(\Delta x^*_i + \Delta x^*_{i+1})(\Delta z^*_k + \Delta z^*_{k+1}) \\ &\quad + \frac{1}{4}(w^*_{I,J,k+1} - w^*_{I,J,k})(\Delta x^*_i + \Delta x^*_{i+1})(\Delta y^*_j + \Delta y^*_{j+1}) \end{aligned} \qquad (4.28\text{g})$$

$$(S_u)_\theta = 0 \qquad (4.28\text{h})$$

$$a_{I,J,K} = a_{I-1,J,K} + a_{I+1,J,K} + a_{I,J-1,K} + a_{I,J+1,K} + a_{I,J,K-1} + a_{I,J,K+1} + \Delta F_\theta - (S_p)_\theta \qquad (4.28\text{i})$$

$$(S_p)_\theta = 0 \qquad (4.28\text{j})$$

As indicated before, discretized algebraic energy equations are solved independent from the momentum equations. In other words, solution of temperature profile is independent from the solution of the velocity due to the incompressible flow consideration. It is known that the flow properties are constant throughout the

domain in incompressible flow. Therefore, the discretized energy equation (4.27) can be independently handled after the continuity and momentum equations are solved for the velocity profiles.

4.2 SOLUTION OF NODAL EQUATIONS

Equations (4.14), (4.16), (4.18) and (4.24), which have been derived in part 4.1.3, are to be simultaneously solved with the purpose of finding the iterated velocities and pressure corrections in SIMPLE algorithm. In addition, after the velocity and pressure field are definitely solved, temperature field or nodal temperatures in scalar control volumes are also calculated by the solution of the algebraic nodal energy equations (4.27). Numerical solution of n linear algebraic equations for n different unknown variables can be generally achieved by two different categories of methods; direct and indirect methods.

Direct methods are the solution techniques, such as Cramer's rule and Gauss Elimination, which are not iterative and are used to solve the nodal equations simultaneously. The associated error values caused by the direct methods are very small due to the non-iterative nature of the approaches. On the contrary, direct methods are very disadvantageous in terms of the high memory allocation and the high number of operations in order to give the simultaneous solution of n equations for n unknowns. The situation may be even more critical for the geometries having large number of nodes, i.e. where n is very large [28].

Indirect methods, by contrast, provide an iterative solution. The error consideration is more important in indirect methods on account of the iterative procedure. However, they are fast in terms of convergence if the solution procedure is properly designed. Furthermore, the algorithm in indirect methods is known to allocate lower memory compared to the direct methods since the only non-zero coefficients are stored in the memory [28].

The commonly known indirect methods are Jacobi and Gauss-Seidel. Both of these methods are initialized by guessed values. The only difference between is that while

in Jacobi, the evaluated number for a nodal point is not updated in the calculation of the other nodal values in the same iteration and it is updated in the next iteration step, in Gauss-Seidel, the evaluated number for a nodal point is immediately updated to be used for other nodes. As it can be predicted, Gauss- Seidel is more efficient or faster than Jacobi [28].

Other than the mentioned methods above, there is an additional method called tri-diagonal matrix algorithm (TDMA) which is mostly preferred in recent fluid dynamics applications. It is based on the direct or simultaneous solution of the algebraic equations for the most basic one-dimensional problems. Nevertheless, combination of direct and indirect methods should be implemented for the solution of two and three-dimensional problems. In three-dimensional cases, a line-by-line solution of the equations on each plane should be performed. In other words, a selected line of nodes are solved by the direct method. On the other hand, the complete solution of the plane and the volume (for three-dimensional cases) are applied iteratively [28].

TDMA is sufficiently fast for most of the applications. However, it should be noted that the speed of convergence of the algorithm depends on the sweep direction of the approach. To put it differently, it is important whether the control volumes or nodal points are ordered from south to north or west to east in matrix formation. Moreover, the corresponding approach is not applicable to the equations discretized by the QUICK algorithm. The details of the formulation of TDMA and the assessment of the algorithm can also be found in [28].

As a result, by consideration of the economical usage of the memory, classical direct methods are not included for the solution of algebraic equations in the problem. Moreover, TDMA is also eliminated in spite of its speed. The first reason for this is that formulation of TDMA is complex (usage of direct and indirect methods) and tedious in three-dimensional geometries. Furthermore, the flow is laminar and, therefore, not significantly complex in the current study. Although the required time for computations for the Gauss-Seidel or Jacobi might be longer than the time for TDMA method, the situation is not anticipated to be drastic because of the laminar flow condition. In addition, speed of convergence can be ameliorated by

implementing the relaxation process between the iterations. Hence, the numerical computations can be applied by classical indirect methods. Finally, Gauss-Seidel is selected for the solution of algebraic equations due to its being more efficient than Jacobi.

At this point, relaxation process should be presented. For most iterative processes in numerical calculations, the determined values are renewed by using a factor, which is called relaxation factor α. This operation is implemented in order to increase the speed of the convergence or to make the divergent algorithms convergent. To illustrate, nodal velocities, pressure corrections and temperatures are relaxed in Gauss-Seidel iterative method as shown:

$$u^{*\,(new)}_{i,J,K} = u^{*\,(old)}_{i,J,K} + \alpha_u (u^{*\,(calculated)}_{i,J,K} - u^{*\,(old)}_{i,J,K}) \tag{4.29a}$$

$$v^{*\,(new)}_{I,j,K} = v^{*\,(old)}_{I,j,K} + \alpha_v (v^{*\,(calculated)}_{I,j,K} - v^{*\,(old)}_{I,j,K}) \tag{4.29b}$$

$$w^{*\,(new)}_{I,J,k} = w^{*\,(old)}_{I,J,k} + \alpha_w (w^{*\,(calculated)}_{I,J,k} - w^{*\,(old)}_{I,J,k}) \tag{4.29c}$$

$$P'^{\,(new)}_{I,J,K} = P'^{\,(old)}_{I,J,K} + \alpha_P (P'^{\,(calculated)}_{I,J,K} - P'^{\,(old)}_{I,J,K}) \tag{4.29d}$$

$$\theta^{\,(new)}_{I,J,K} = \theta^{\,(old)}_{I,J,K} + \alpha_\theta (\theta^{\,(calculated)}_{I,J,K} - \theta^{\,(old)}_{I,J,K}) \tag{4.29e}$$

In the above expressions, superscript *calculated* denotes the determined values after the Gauss-Seidel iteration, *old* indicates the pre-determined solution in the previous iteration and *new* is the updated (relaxed) solution for the nodal point. Note that relaxed numbers are used as the initial values in the next iteration.

If α>1, the process is called over-relaxation. Otherwise, if 0<α<1, it is called under-relaxation. Unfortunately, there is no general expression or consideration to find the optimum relaxation factor α for the iteration process. The optimum value of α depends on the problem, size of the meshes and the numerical algorithm used for the solution of algebraic equations [20].

In this problem, the geometry of the channel and the grid spacing change from one model to another on account of the optimization process. Hence, there is not certain α

value considered in the study. Generally, in the current problem, the relaxation factors are selected such that $1.2<\alpha_p<1.9$, $1.1<\alpha_{u,v,w}<1.6$, $\alpha_\theta = 0.8$ for different numerical operations. Accordingly, fast convergence is gained by the relaxation in Gauss-Seidel iterative solutions of the algebraic equations (4.14), (4.16), (4.18), (4.24) and (4.27).

4.3 GENERAL SOLUTION ALGORITHM

For the solution of velocity and temperature profiles of the corresponding model and the flow, SIMPLE (Semi-Implicit Method for Pressure-Linked Equations) algorithm [28] is performed. The steps included in the algorithm are ordered in the form of flow chart in Figure 4.7.

Note that after pressure and velocities are corrected by equations (4.23a), (4.23b), (4.23c) and (4.26) as seen from Figure 4.7, corrected velocities and pressures are under-relaxed by the relaxation factors which differs for different models in the problem. Generally, it is considered that $0.01<\alpha^S_{u,v,w,P}<0.25$ in the numerical solution of the air flow. Thus, before the convergence check is carried out, velocity and pressure fields are under-relaxed as,

$$u^{**}_{i,J,K}{}^{(new)} = u^{*}_{i,J,K}{}^{(old)} + \alpha_u{}^S (u^{**}_{i,J,K}{}^{(calculated)} - u^{*}_{i,J,K}{}^{(old)}) \tag{4.30a}$$

$$v^{**}_{I,j,K}{}^{(new)} = v^{*}_{I,j,K}{}^{(old)} + \alpha_v{}^S (v^{**}_{I,j,K}{}^{(calculated)} - v^{*}_{I,j,K}{}^{(old)}) \tag{4.30b}$$

$$w^{**}_{I,J,k}{}^{(new)} = w^{*}_{I,J,k}{}^{(old)} + \alpha_w{}^S (w^{**}_{I,J,k}{}^{(calculated)} - w^{*}_{I,J,k}{}^{(old)}) \tag{4.30c}$$

$$P^{**}_{I,J,K}{}^{(new)} = P^{*}_{I,J,K}{}^{(old)} + \alpha_P{}^S (P^{**}_{I,J,K}{}^{(calculated)} - P^{*}_{I,J,K}{}^{(old)}) \tag{4.30d}$$

The capital superscript S denotes that the relaxation factors in equations (4.30a), (4.30b), (4.30c) and (4.30d) belong to the SIMPLE algorithm in order to the differentiate them from the relaxation factors in Gauss-Seidel iterative method. Moreover, it should be pointed out that prescribed error limits ε_P and $\varepsilon_{u,\,v,\,w}$ are the same for both Gauss-Seidel iterations and SIMPLE algorithm, and they are

concluded, by dropping superscripts star (*) and prime (') in velocity and pressure components, as given below:

$$\frac{\sum\limits_{K=1}^{N_z-2}\sum\limits_{J=1}^{N_y-2}\sum\limits_{I=1}^{N_x-2}(P^n_{I,J,K}-P^{n-1}_{I,J,K})}{\sum\limits_{K=1}^{N_z-2}\sum\limits_{J=1}^{N_y-2}\sum\limits_{I=1}^{N_x-2}P^n_{I,J,K}}\leq \varepsilon_P=0.001 \qquad (4.31a)$$

$$\frac{\sum\limits_{K=1}^{N_z-2}\sum\limits_{J=1}^{N_y-2}\sum\limits_{i=1}^{N_x-3}(u^n_{i,J,K}-u^{n-1}_{i,J,K})}{\sum\limits_{K=1}^{N_z-2}\sum\limits_{J=1}^{N_y-2}\sum\limits_{i=1}^{N_x-3}u^n_{i,J,K}}\leq \varepsilon_u=0.00001 \qquad (4.31b)$$

$$\frac{\sum\limits_{K=1}^{N_z-2}\sum\limits_{j=1}^{N_y-3}\sum\limits_{I=1}^{N_x-2}(v^n_{I,j,K}-v^{n-1}_{I,j,K})}{\sum\limits_{K=1}^{N_z-2}\sum\limits_{j=1}^{N_y-3}\sum\limits_{I=1}^{N_x-2}v^n_{I,j,K}}\leq \varepsilon_v=0.00001 \qquad (4.31c)$$

$$\frac{\sum\limits_{k=1}^{N_z-3}\sum\limits_{J=1}^{N_y-2}\sum\limits_{I=1}^{N_x-2}(w^n_{I,J,k}-w^{n-1}_{I,J,k})}{\sum\limits_{k=1}^{N_z-3}\sum\limits_{J=1}^{N_y-2}\sum\limits_{I=1}^{N_x-2}w^n_{I,J,k}}\leq \varepsilon_w=0.00001 \qquad (4.31d)$$

where n-1 is the previous iteration and the term represented by n-1 is the solution of the previous iteration. Therefore, if the inequalities stated above are satisfied, iterations in Gauss-Seidel or SIMPLE algorithm are stopped. In addition, convergence check for the determination of temperature distribution by using the Gauss-Seidel iterations can be given as,

$$\frac{\sum\limits_{K=1}^{N_z-2}\sum\limits_{J=1}^{N_y-2}\sum\limits_{I=1}^{N_x-2}(\theta^n_{I,J,K}-\theta^{n-1}_{I,J,K})}{\sum\limits_{K=1}^{N_z-2}\sum\limits_{J=1}^{N_y-2}\sum\limits_{I=1}^{N_x-2}\theta^n_{I,J,K}}\leq \varepsilon_\theta=0.0000001 \qquad (4.31e)$$

Finally, as the inequality described by (4.31e) is achieved, Gauss-Seidel iterations for solving the discretized energy equations are treated to be sufficient for convergence.
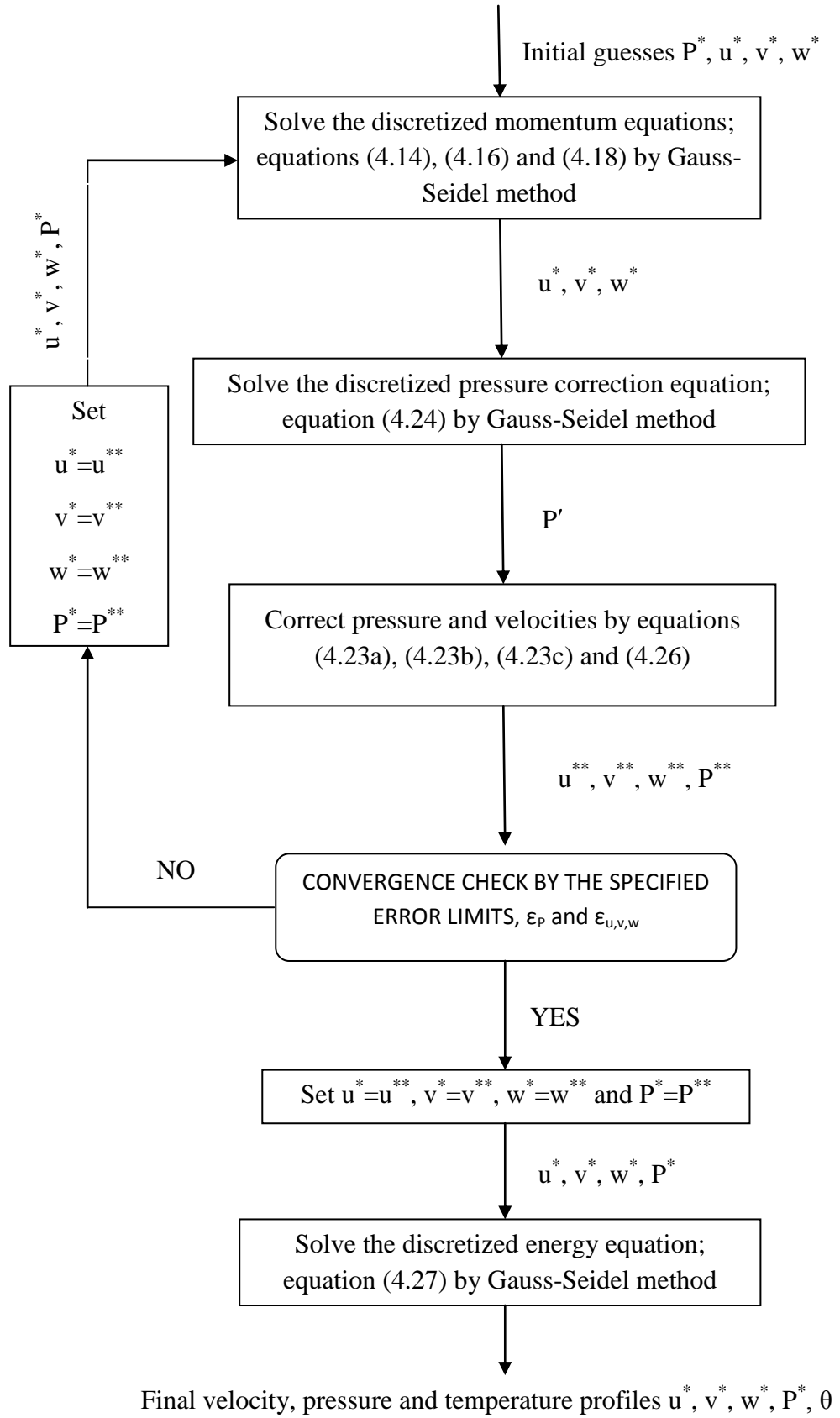
Initial guesses P^*, u^*, v^*, w^*

Solve the discretized momentum equations; equations (4.14), (4.16) and (4.18) by Gauss-Seidel method

u^*, v^*, w^*

Solve the discretized pressure correction equation; equation (4.24) by Gauss-Seidel method

P'

Correct pressure and velocities by equations (4.23a), (4.23b), (4.23c) and (4.26)

u^{**}, v^{**}, w^{**}, P^{**}

CONVERGENCE CHECK BY THE SPECIFIED ERROR LIMITS, ε_P and $\varepsilon_{u,v,w}$

NO

YES

u^*, v^*, w^*, P^*

Set
$u^*=u^{**}$
$v^*=v^{**}$
$w^*=w^{**}$
$P^*=P^{**}$

Set $u^*=u^{**}$, $v^*=v^{**}$, $w^*=w^{**}$ and $P^*=P^{**}$

u^*, v^*, w^*, P^*

Solve the discretized energy equation; equation (4.27) by Gauss-Seidel method

Final velocity, pressure and temperature profiles u^*, v^*, w^*, P^*, θ

Figure 4.7 Flow chart for the SIMPLE algorithm used in the problem

54

4.4 MESH GENERATION

As it is stated before, staggered grid arrangement with non-uniform grid spacing is used in the generation of the mesh layout. Mesh elements are in the shape of rectangular prism. They are created such that the distances between the scalar nodes are related as,

$$\Delta x_{i+1} = 1.05 \Delta x_i \qquad for\ 1 < i < (N_x - 1) \tag{4.32a}$$

$$\Delta y_{j+1} = 1.05 \Delta y_j \qquad for\ 1 < j < (N_y - 1) \tag{4.32b}$$

$$\Delta z_{k+1} = 1.05 \Delta z_k \qquad for\ 1 < k < (N_z - 1) \tag{4.32c}$$

As it may be recognized from equations from (4.32a) to (4.32c), meshes are designed to be finer at the regions where the gradients of the flow velocities and temperatures are larger with respect to the directions x, y and z. These regions are the entrance of the channel and the locations near the walls.

Furthermore, the velocity grid lines are situated at the middle of the scalar grid lines. Therefore, spacing of the velocity grid lines is represented by,

$$\Delta x_i^{(vec)} = \frac{\Delta x_i + \Delta x_{i+1}}{2} \qquad for\ 1 < i < (N_x - 2) \tag{4.33a}$$

$$\Delta y_j^{(vec)} = \frac{\Delta y_j + \Delta y_{j+1}}{2} \qquad for\ 1 < j < (N_y - 2) \tag{4.33b}$$

$$\Delta z_k^{(vec)} = \frac{\Delta z_k + \Delta z_{k+1}}{2} \qquad for\ 1 < k < (N_z - 2) \tag{4.33c}$$

where the superscript *vec* shows that $\Delta x_i^{(vec)}$, $\Delta y_j^{(vec)}$, and $\Delta z_k^{(vec)}$ are defined for the distances between the velocity nodes, which are the points for the vector variables.

The criteria which are taken into account during the selection of number of grids in the numerical computation are presented in Table 4.1, Table 4.2 and Table 4.3. Note that f and β are the friction factor and the aspect ratio of the cross-section, and they are defined as follows:

$$f = 2\Delta P^* \frac{D_h}{L} \tag{4.34}$$

$$\beta = \frac{s}{W} \tag{4.35}$$

Dimensionless pressure drop, ΔP^*, in equation (4.34) is defined by,

$$\Delta P^* = \frac{\Delta P}{\rho U_\infty^2} \tag{4.36}$$

where ΔP is the pressure drop across the channel.

Table 4.2 Grid adaptation with respect to the fully developed friction factors

# of Grids (N_x x N_y x N_z)	$(fRe_{D_h})_{fd}$		
	$\beta=0.001$	$\beta=0.5$	$\beta=1$
40x10x10	23.879	15.558	14.38
60x10x10	23.88	15.553	14.35
80x10x10	23.882	15.55	14.35
40x15x15	23.98	15.556	14.34
100x10x10	23.883	15.538	14.34
50x15x15	23.98	15.55	14.33
120x10x10	23.883	15.54	14.32
Shah and London [30]	**23.968**	**15.54806**	**14.22708**

Table 4.3 Grid adaptation with respect to the fully developed Nusselt numbers

# of Grids (N_x x N_y x N_z)	$(Nu)_{fd}$		
	$\beta=0.001$	$\beta=0.5$	$\beta=1$
40x10x10	7.46	4.6882	3.717
60x10x10	7.52	4.6878	3.716
80x10x10	7.522	4.676	3.7153
40x15x15	7.524	4.634	3.713
100x10x10	7.5276	4.67	3.7134
50x15x15	7.526	4.6329	3.713
120x10x10	7.5278	4.67	3.713
Schmidt [31]	**7.5295**	**4.619**	**3.703**

Table 4.4 Average times performed by CPU for the numerical solution of fluid flow and heat transfer

# of Grids (N_x x N_y x N_z)	CPU Time (seconds)		
	β=0.001	β=0.5	β=1
40x10x10	598	727	404
60x10x10	654	1074	555
80x10x10	578	675	740
40x15x15	1825	1535	1622
100x10x10	795	699	664
50x15x15	1970	1353	2508
120x10x10	890	567	702

The Nusselt number Nu, which is introduced in Table 4.3, is a dimensionless number, and it is given as,

$$Nu = \frac{hD_h}{k} \tag{4.37}$$

where h is the heat transfer coefficient.

It can be seen from Tables 4.2, 4.3 and 4.4 that computations involving 15x15 grids in y and z-directions give generally better results than the model of 10x10 cross-section grids. However, computation time increases drastically for 15x15 grids in the cross-section. Moreover, the error encountered in the cross-sections with 10x10 grid arrangements can be alleviated by integrating more grids in x-direction along the channel. Indeed, the numerical errors in friction factors for mesh arrangement of 120x10x10 are about 0.05%-0.7% based on the comparison with the values reported by Shah and London [30]. Similarly, for the same mesh configuration (120x10x10), the errors in Nusselt numbers, which are computed numerically, are about 0.02%-1.10% based on the comparison with the fully developed Nusselt numbers suggested by Schmidt [31]. Thus, 120x10x10 mesh configuration is concluded to be reasonable for the numerical solution of the air flow and heat transfer in the current study.

4.5 DISCRETIZED BOUNDARY CONDITIONS

As it is shown in part 3.3, there are four kinds of boundaries in the current problem. There are one inlet, one outlet, two walls and two symmetries at the boundaries of the domain. In this section, it is expressed how each kind of boundary is integrated into the discretization and the numerical solver.

4.5.1 Boundary Condition at the Inlet

At the inlet control volumes, velocities u, v and w, and temperature T at the back (denoted by B in Figure 4.1) of the volume are known. Therefore, discretized u-, v-, w-momentum equations and energy equation at the inlet are solved normally by substituting the inlet velocities and temperature. Finally, inlet boundary conditions in terms of numerical definitions can be summarized as shown:

$$u^*_{0,J,K} = 1 \qquad for\, 1 \leq J \leq (N_y - 1)\, and\, 1 \leq K \leq (N_z - 1) \qquad (4.38a)$$

$$v^*_{0,j,K} = 0 \qquad for\, 0 \leq j \leq (N_y - 2)\, and\, 1 \leq K \leq (N_z - 1) \qquad (4.38b)$$

$$w^*_{0,J,k} = 0 \qquad for\, 1 \leq J \leq (N_y - 1)\, and\, 0 \leq k \leq (N_z - 2) \qquad (4.38c)$$

$$\theta_{0,J,K} = 0 \qquad for\, 1 \leq J \leq (N_y - 1)\, and\, 1 \leq K \leq (N_z - 1) \qquad (4.38d)$$

In addition to the given conditions, connection of the discretized pressure correction equation (4.24) with the inlet pressure node (denoted by B in Figure 4.1) at the inlet scalar control volume is effaced by setting the back side coefficient at pressure correction equation to zero since there is no need to correct the velocities and the pressures at the inlet side.

4.5.2 Boundary Condition at the Outlet

As discussed in part 3.3.2, gradients of the velocity components and temperature along the flow direction (x) is zero at the outlet. Hence, the velocities and

temperatures at the outlet control volumes are taken to be equal to the velocities and temperatures at the outlet boundary. However, it should be emphasized that there is one exception [28] to be considered. While calculating outlet side (denoted by T in Figure 4.1) velocity of the u-control volume, it is equalized to the "(inlet mass flow rate / outlet mass flow rate) u_p" in order to ensure the continuity, instead of simply taking it equal to the u-velocity at node P. The given information is formulated as follows:

$$u^*_{N_x-2,J,K} = \frac{M_{inlet}}{M_{outlet}} u^*_{N_x-3,J,K} \qquad for\ 1 \le J \le (N_y-1)\ and\ 1 \le K \le (N_z-1) \qquad (4.39a)$$

$$v^*_{N_x-1,j,K} = v^*_{N_x-2,j,K} \quad for\ 0 \le j \le (N_y-2)\ and\ 1 \le K \le (N_z-1) \qquad (4.39b)$$

$$w^*_{N_x-1,J,k} = w^*_{N_x-2,J,k} \quad for\ 1 \le J \le (N_y-1)\ and\ 0 \le k \le (N_z-2) \qquad (4.39c)$$

$$\theta_{N_x-1,J,K} = \theta_{N_x-2,J,K} \quad for\ 1 \le J \le (N_y-1)\ and\ 1 \le K \le (N_z-1) \qquad (4.39d)$$

where

$$M_{inlet} = \rho U_\infty s W \qquad (4.40a)$$

$$M_{outlet} = \rho \sum_{K=1}^{N_z-2} \sum_{J=1}^{N_y-2} [u_{N_x-3,J,K}(\Delta y_J + \Delta y_{J+1})(\Delta z_K + \Delta z_{K+1})] \qquad (4.40b)$$

It is clear that u-, v-, w-momentum equations and the energy equation are solved by simply substituting equations from (4.39a) to (4.39d) at the outlet control volumes without the need for any other modifications. Hence, the link of the pressure correction equation to the outlet side (namely T) is disconnected by setting the corresponding coefficient of the outlet side to zero since the corrections for velocity components and for the pressure are not required similar to the inlet boundary condition.

4.5.3 Wall Boundary Condition at y = 0

Since the walls of the channels are solid, v-velocities across this boundary (shown as E in Figure 4.1) are simply set to zero and the discretized v-momentum equation for the control volume near the wall is solved without any other operations. Nonetheless, for u- and w-control volumes or for their momentum equations, shear force F_{wall} applied to the wall is taken into account. Besides, heat transfer rate from the wall is considered to define the wall boundary condition for the energy equation.

Shear forces applied to the wall along the u-, and w-control volumes with laminar flow consideration can be, respectively, defined as,

$$(F_{wall})^u_{i,K} = -\mu \frac{u_{i,1,K}\Delta x_i(\Delta z_K + \Delta z_{K+1})}{\Delta y_1} \quad for\ 1 \le i \le (N_x - 3)\ and\ 1 \le K \le (N_z - 2) \tag{4.41a}$$

$$(F_{wall})^w_{I,k} = -\mu \frac{w_{I,1,k}\Delta z_k(\Delta x_I + \Delta x_{I+1})}{\Delta y_1} \quad for\ 1 \le I \le (N_x - 2)\ and\ 1 \le k \le (N_z - 3) \tag{4.41b}$$

Next, heat transfer rate from the wall to the control volume is,

$$(q_{wall})_{I,K} = -\frac{1}{2}\frac{\mu c_P}{Pr}\frac{(T_{I,1,K} - T_w)(\Delta x_I + \Delta x_{I+1})(\Delta z_K + \Delta z_{K+1})}{\Delta y_1} \tag{4.42}$$
$$for\ 1 \le I \le (N_x - 2)\ and\ 1 \le K \le (N_z - 2)$$

Equations (4.41a), (4.41b) and (4.42) can be non-dimensionalized as follows:

$$(F^*_{wall})^u_{i,K} = \frac{(F_{wall})^u_{i,K}}{\rho U_\infty^2 D_h^2} = -\frac{1}{Re_{D_h}}\frac{u^*_{i,1,K}\Delta x^*_i(\Delta z^*_K + \Delta z^*_{K+1})}{\Delta y^*_1} \tag{4.43a}$$
$$for\ 1 \le i \le (N_x - 3)\ and\ 1 \le K \le (N_z - 2)$$

$$(F^*_{wall})^w_{I,k} = \frac{(F_{wall})^w_{I,k}}{\rho U_\infty^2 D_h^2} = -\frac{1}{Re_{D_h}}\frac{w^*_{I,1,k}\Delta z^*_k(\Delta x^*_I + \Delta x^*_{I+1})}{\Delta y^*_1} \tag{4.43b}$$
$$for\ 1 \le I \le (N_x - 2)\ and\ 1 \le k \le (N_z - 3)$$

$$(q^*_{wall})_{I,K} = \frac{(q_{wall})_{I,K}}{\rho c_P U_\infty D_h^2(T_w - T_\infty)} = -\frac{1}{2}\frac{1}{Re_{D_h}Pr}\frac{(\theta_{I,1,K} - 1)(\Delta x^*_I + \Delta x^*_{I+1})(\Delta z^*_K + \Delta z^*_{K+1})}{\Delta y^*_1} \tag{4.44}$$
$$for\ 1 \le I \le (N_x - 2)\ and\ 1 \le K \le (N_z - 2)$$

Note that equations (4.43a), (4.43b) and (4.44) are converted into source forms and they are added to the general source terms S_u and S_p in the discretized momentum equations. In consequence, necessary relations at the wall boundary for $y = 0$ can be summarized as given below:

$$(S_p)_u = -\frac{1}{\mathrm{Re}_{D_h}} \frac{\Delta x^*_i (\Delta z^*_K + \Delta z^*_{K+1})}{\Delta y^*_1} \quad for\ 1 \le i \le (N_x - 3)\ and\ 1 \le K \le (N_z - 2) \quad (4.45a)$$

$$(S_u)_u = 0 \quad for\ 1 \le i \le (N_x - 3)\ and\ 1 \le K \le (N_z - 2) \tag{4.45b}$$

$$v^*_{I,0,K} = 0 \quad for\ 0 \le I \le (N_x - 1)\ and\ 1 \le K \le (N_z - 1) \tag{4.45c}$$

$$(S_p)_w = -\frac{1}{\mathrm{Re}_{D_h}} \frac{\Delta z^*_k (\Delta x^*_I + \Delta x^*_{I+1})}{\Delta y^*_1} \quad for\ 1 \le I \le (N_x - 2)\ and\ 1 \le k \le (N_z - 3) \tag{4.45d}$$

$$(S_u)_w = 0 \quad for\ 1 \le I \le (N_x - 2)\ and\ 1 \le k \le (N_z - 3) \tag{4.45e}$$

$$(S_p)_\theta = -\frac{1}{2} \frac{1}{\mathrm{Re}_{D_h}\ \mathrm{Pr}} \frac{(\Delta x^*_I + \Delta x^*_{I+1})(\Delta z^*_K + \Delta z^*_{K+1})}{\Delta y^*_1}$$
$$for\ 1 \le I \le (N_x - 2)\ and\ 1 \le K \le (N_z - 2) \tag{4.45f}$$

$$(S_u)_\theta = -\frac{1}{2} \frac{1}{\mathrm{Re}_{D_h}\ \mathrm{Pr}} \frac{(\Delta x^*_I + \Delta x^*_{I+1})(\Delta z^*_K + \Delta z^*_{K+1})}{\Delta y^*_1}$$
$$for\ 1 \le I \le (N_x - 2)\ and\ 1 \le K \le (N_z - 2) \tag{4.45g}$$

Finally, note also that the link to the wall boundary side (denoted by E in Figure 4.1) at the scalar control volume in the discretized pressure correction equation is disconnected by setting the east side coefficient to zero since the velocity and pressure correction are not needed in the wall boundaries.

4.5.4 Wall Boundary Condition at z = 0

The procedure in wall boundary at $z = 0$ is very similar to that in wall boundary presented in part 4.5.3. Hence, after the same procedure is carried out, the following source terms and boundaries are reported:

$$(S_p)_u = -\frac{1}{\text{Re}_{D_h}} \frac{\Delta x^*_i (\Delta y^*_J + \Delta y^*_{J+1})}{\Delta z^*_1} \quad for\ 1 \le i \le (N_x - 3)\ and\ 1 \le J \le (N_y - 2) \quad (4.46a)$$

$$(S_u)_u = 0 \quad for\ 1 \le i \le (N_x - 3)\ and\ 1 \le J \le (N_y - 2) \quad\quad (4.46b)$$

$$(S_p)_v = -\frac{1}{\text{Re}_{D_h}} \frac{\Delta y^*_j (\Delta x^*_I + \Delta x^*_{I+1})}{\Delta z^*_1} \quad for\ 1 \le I \le (N_x - 2)\ and\ 1 \le j \le (N_y - 3) \quad (4.46c)$$

$$(S_u)_v = 0 \quad for\ 1 \le I \le (N_x - 2)\ and\ 1 \le j \le (N_y - 3) \quad\quad (4.46d)$$

$$w^*_{I,J,0} = 0 \quad for\ 0 \le I \le (N_x - 1)\ and\ 1 \le J \le (N_y - 1) \quad\quad (4.46e)$$

$$(S_p)_\theta = -\frac{1}{2} \frac{1}{\text{Re}_{D_h} \text{Pr}} \frac{(\Delta x^*_I + \Delta x^*_{I+1})(\Delta y^*_J + \Delta y^*_{J+1})}{\Delta z^*_1}$$
$$for\ 1 \le I \le (N_x - 2)\ and\ 1 \le J \le (N_y - 2) \quad\quad (4.46f)$$

$$(S_u)_\theta = -\frac{1}{2} \frac{1}{\text{Re}_{D_h} \text{Pr}} \frac{(\Delta x^*_I + \Delta x^*_{I+1})(\Delta y^*_J + \Delta y^*_{J+1})}{\Delta z^*_1}$$
$$for\ 1 \le I \le (N_x - 2)\ and\ 1 \le J \le (N_y - 2) \quad\quad (4.46g)$$

In addition, the link to the wall is disconnected in the discretized pressure correction equation, i.e. the south side coefficient in the discretized equation of the scalar control volume is taken to be zero.

4.5.5 Symmetry Boundary Condition at y = W/2

As mentioned previously in part 3.3.3, there is no flow and heat flux across the symmetry line. Thus, equations from (3.26a) to (3.26d) have been written in Chapter 3. These equations can be reconsidered in the algebraic forms as presented below:

$$u^*_{i,N_y-1,K} = u^*_{i,N_y-2,K} \quad for\ 0 \le i \le (N_x - 2)\ and\ 1 \le K \le (N_z - 1) \quad (4.47a)$$

$$v^*_{I,N_y-2,K} = 0 \quad for\ 0 \le I \le (N_x - 1)\ and\ 1 \le K \le (N_z - 1) \quad (4.47b)$$

$$w^*_{I,N_y-1,k} = w^*_{I,N_y-2,k} \quad for\ 0 \le I \le (N_x-1)\ and\ 0 \le k \le (N_z-2) \tag{4.47c}$$

$$\theta_{I,N_y-1,K} = \theta_{I,N_y-2,K} \quad for\ 0 \le I \le (N_x-1)\ and\ 1 \le K \le (N_z-1) \tag{4.47d}$$

Finally, the connection of the discretized pressure correction equation with the symmetry side (or the west (W) point in Figure 4.1) is cut by setting the corresponding coefficient in the pressure correction equation to zero. The reason for this is that velocity and pressure corrections are not required in the symmetry boundary.

4.5.6 Symmetry Boundary Condition at z = s/2

Similar to the formulation performed in part 4.5.5,

$$u^*_{i,J,N_z-1} = u^*_{i,J,N_z-2} \quad for\ 0 \le i \le (N_x-2)\ and\ 1 \le J \le (N_y-1) \tag{4.48a}$$

$$v^*_{I,j,N_z-1} = v^*_{I,j,N_z-2} \quad for\ 0 \le I \le (N_x-1)\ and\ 0 \le j \le (N_y-2) \tag{4.48b}$$

$$w^*_{I,J,N_z-2} = 0 \quad for\ 0 \le I \le (N_x-1)\ and\ 1 \le J \le (N_y-1) \tag{4.48c}$$

$$\theta_{I,J,N_z-1} = \theta_{I,J,N_z-2} \quad for\ 0 \le I \le (N_x-1)\ and\ 1 \le J \le (N_y-1) \tag{4.48d}$$

Like the symmetry boundary at y = W/2, the link of the scalar control volume for the pressure corrections to the north side (N in Figure 4.1) is eliminated by setting the north side coefficient to zero in the discretized pressure correction equation.

4.6 VALIDATION OF THE NUMERICAL SOLVER

In order to prove the validity of the present solution method, solution of the developed numerical code for certain cases is compared by the available results in literature. First, pressure drop and the friction factor values in developing laminar flow obtained from the numerical code are confirmed. Next, heat transfer or the

Nusselt number values for the fully developed laminar flow are attested after the comparison with available reported values.

4.6.1 Friction Factor in Developing Laminar Flow

Developing friction factor values resulted from the numerical code are checked by using the data yielded by Curr, Sharma and Tatchell's numerical investigation [32] for rectangular ducts in Figures from 4.8 to 4.11. Recall that friction factor f, aspect ratio β and Reynolds number based on hydraulic diameter Re_{D_h} have been previously defined in equations (4.34), (4.35) and (3.16), respectively. Note also that in Figure 4.8, β is taken to be $0.001 \approx 0$ for self-developed code since $\beta = s/W = 0$ is almost impossible in 3-D numerical solution. In addition, the term x^+ is the dimensionless axial coordinate for the hydrodynamic entrance region, and x^+ is defined as follows:

$$x^+ = \frac{x}{D_h \, Re} \tag{4.49}$$
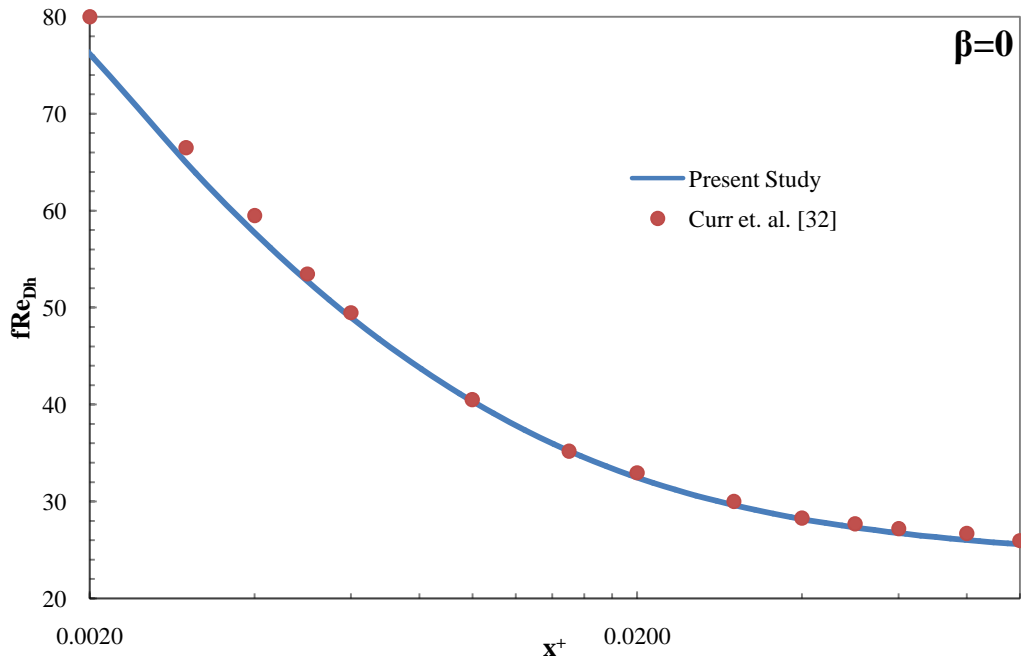
Figure 4.8 Friction factor in developing laminar flow (β=0 or infinite parallel plates condition)
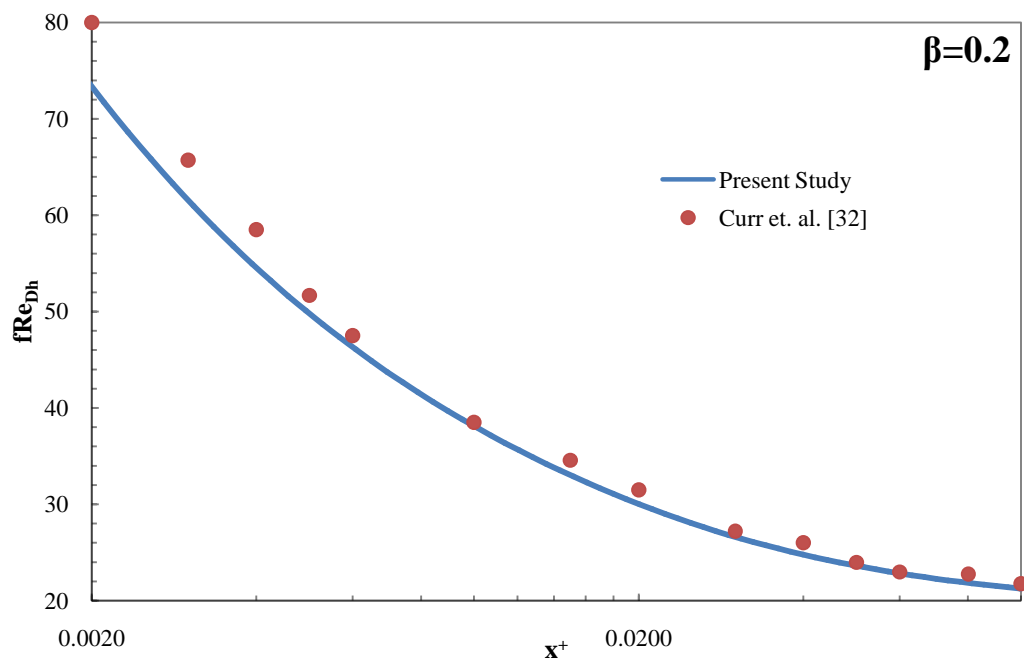
Figure 4.9 Friction factor in developing laminar flow (β=0.2)
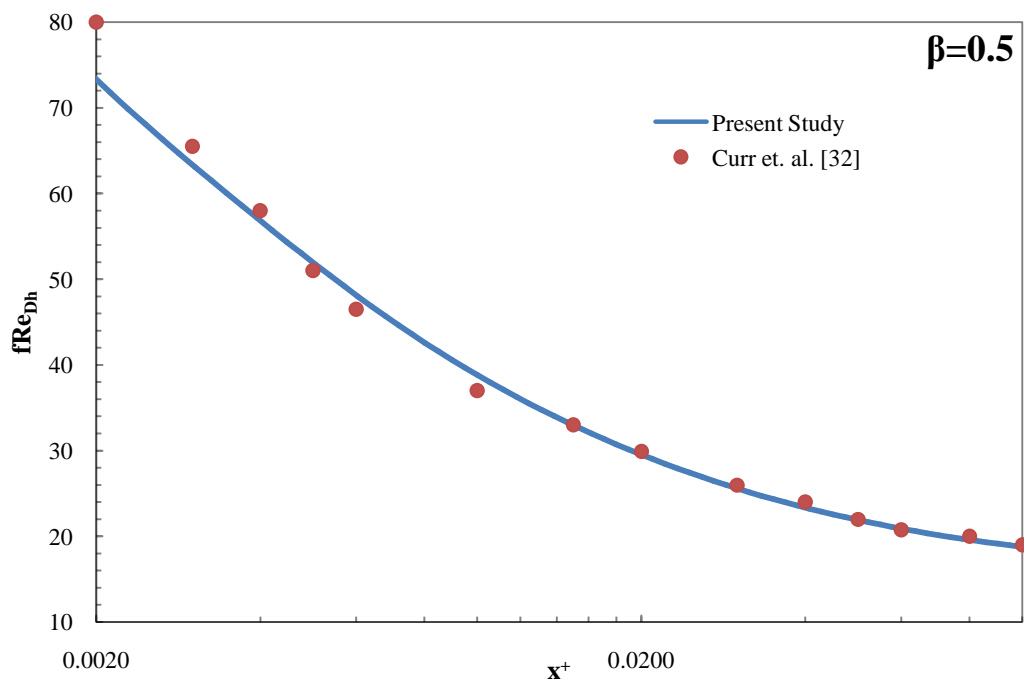
Figure 4.10 Friction factor in developing laminar flow (β=0.5)
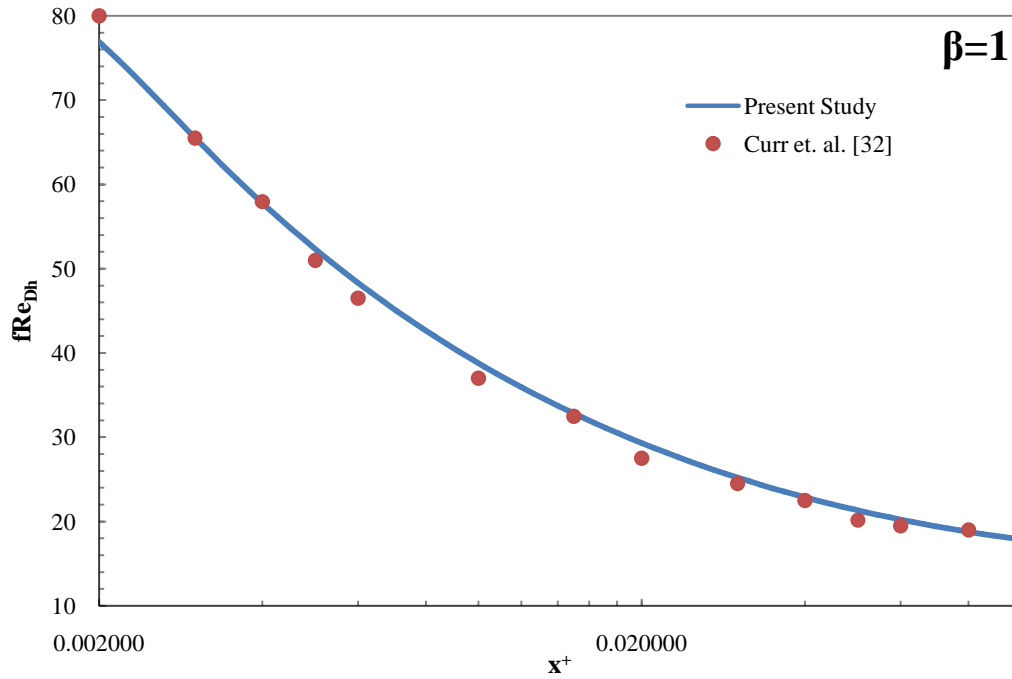
Figure 4.11 Friction factor in developing laminar flow (β=1)

When the Figures from 4.8 to 4.11 are carefully investigated, it is obvious that the relatively larger errors in friction factor are encountered at the entrance of the channel. However, the two results are seen to be in such a good agreement that the magnitude of the maximum percentage error is about 9% in terms of the absolute value. Therefore, results of the developed code can be said to be satisfactory according to the friction factor comparison with Curr et al.'s numerical study [32].

4.6.2 Nusselt Number in Thermally Fully Developed Flow

Fully developed Nusselt numbers for different aspect ratios of channel cross-section obtained from the current numerical code are assessed by comparing them with Schmidt's findings [31], which are based on the finite difference method for a rectangular duct with insulated lateral surfaces. The two results are presented in Figure 4.12. Recall that Nusselt number Nu has been previously defined in equation (4.37).
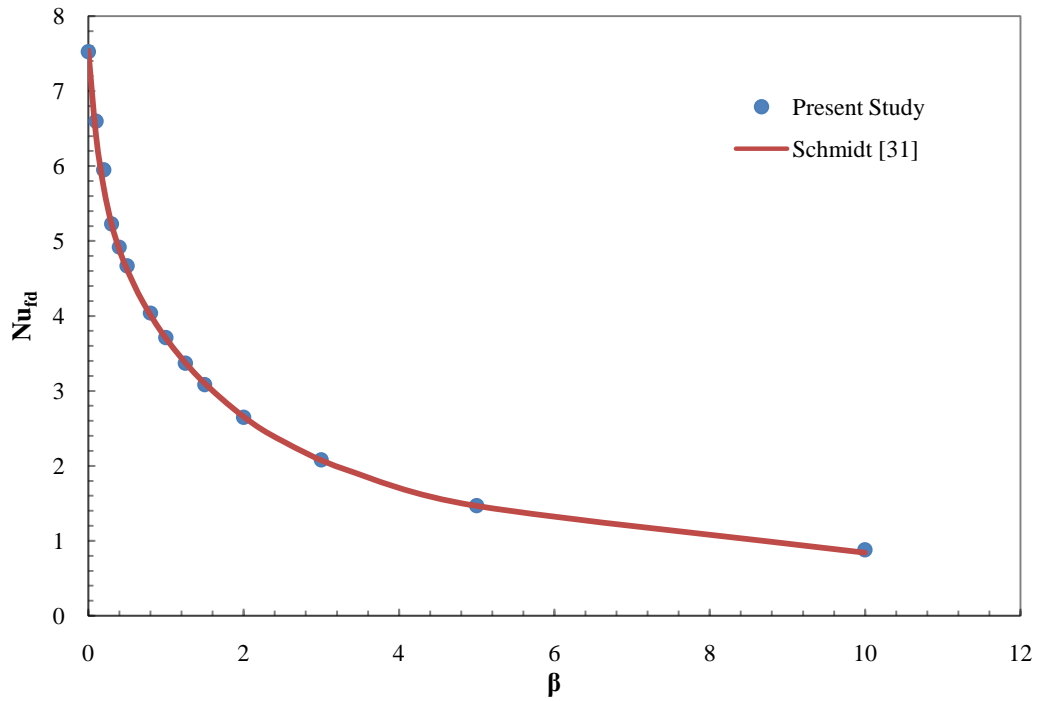
Figure 4.12 Nusselt number in thermally fully developed laminar flow for different channel aspect ratios

As it is clearly observed from Figure 4.12, the results of the developed code and the data from Schmidth [31] are in a good agreement. In consequence, the developed code used in the current study can predict the results of Schmidt [31] at most within 4.5% deviation in magnitude. Hence, the numerical code can be performed for the optimization process with a sufficient accuracy in the evaluation of fully developed Nusselt number Nu.

As a result, satisfactory results have been obtained from parts 4.6.1 and 4.6.2. Therefore, the developed numerical code can be implemented for the solution of the current problem.

CHAPTER 5

OPTIMIZATION PROCEDURE

In this chapter, the procedure applied before the optimization process, and the results of the optimization are given in detail. The chapter is classified into three parts. Necessary dimensionless parameters and their derivation are presented in the first part. Next, maximization procedure and numerical results are given in the second part. Finally, the graphs and the correlations obtained from the optimization of numerical results are introduced in the third part.

5.1 DIMENSIONLESS PARAMETERS IN THE OPTIMIZATION PROCESS

There are two significant dimensionless parameters considered in the optimization. These are the dimensionless heat transfer rate from the boards and the dimensionless pressure difference group across the channel. In this part, the two parameters are derived and defined separately.

5.1.1 Dimensionless Heat Transfer Rate

To begin with, heat transfer rate from one channel is calculated by,

$$\dot{Q}_{sc} = \dot{m} c_p (T_e - T_\infty) \tag{5.1}$$

where T_e is the flow temperature at the channel outlet, and $\dot{m}$ is the mass flow rate of air. Mass flow rate of air is defined as,

$$\dot{m} = M_{inlet} = \rho U_\infty sW \tag{5.2}$$

Substituting equation (5.2), heat transfer rate from one channel becomes,

$$\dot{Q}_{sc} = \rho U_\infty c_p sW(T_e - T_\infty) \tag{5.3}$$

Since there are H/s channels in the whole assembly, total heat transfer rate from the boards is given by,

$$\dot{Q} = \rho U_\infty c_p sW(T_e - T_\infty)\frac{H}{s} \tag{5.4}$$

From equation (3.10),

$$T_e - T_\infty = \theta_e(T_w - T_\infty) \tag{5.5}$$

With the help of equations from (3.17) to (3.19), hydraulic diameter D_h can be expressed as,

$$D_h = \frac{2sW}{s+W} \tag{5.6}$$

By using equations (5.5) and (5.6), equation (5.4) takes the following form:

$$\dot{Q} = \frac{1}{2}\rho U_\infty D_h H c_p \theta_e(T_w - T_\infty)\frac{s+W}{s} \tag{5.7}$$

At this point, recall the definition of Prandtl number, equation (3.20), definition of Reynolds number, equation (3.16), and kinematic viscosity, equation (3.6). Hence, by using equations (3.6), (3.16) and (3.20), and rearranging equation (5.7), total heat transfer rate is,

$$\dot{Q} = \frac{1}{2}\text{Re}_{D_h} kH \Pr \theta_e(T_w - T_\infty)[1 + \frac{1}{(\frac{s}{L}).(\frac{L}{W})}] \tag{5.8}$$

Note that air properties k and Pr, and the parameters H and (T_w-T_∞) are constant during the numerical solution. Therefore, the constants can be transferred to the left

hand side of equation (5.8) in order to obtain the dimensionless total heat transfer rate as,

$$\frac{\dot{Q}}{kH \Pr(T_w - T_\infty)} = \frac{1}{2} \mathrm{Re}_{D_h} \theta_e [1 + \frac{1}{(\frac{s}{L}).(\frac{L}{W})}] \tag{5.9}$$

It should be emphasized that Reynolds number Re_{D_h} and dimensionless temperature difference θ_e at the channel exit are the functions of geometrical parameters and the pressure drop across the channel. In other words, if the pressure drop across the channel, and the parameters s/L and L/W are given, dimensionless heat transfer rate to the coolant (air), equation (5.9), can be easily evaluated. In the optimization process, dimensionless term $\dot{Q} / kH \Pr(T_w - T_\infty)$ is to be maximized with respect to s/L for different L/W values and fixed pressure drop across the channel.

5.1.2 Dimensionless Pressure Drop

In derivation of dimensionless pressure drop across the channels, definitions and suggestions reported by Bhattacharjee and Grosshandler [33], and Petrescu [34] are taken into account. Group of dimensionless pressure drop in the current optimization process is determined to be

$$\frac{\Delta P L^2}{\rho v^2} = constant \tag{5.10}$$

The importance of this parameter can be more explicitly understood if the equation (4.36) is reconsidered. By taking equation (3.16) into account, equation (4.36) can also be reorganized as,

$$\Delta p^* = \frac{\Delta p D_h^2}{\rho \frac{U_\infty^2 D_h^2}{v^2} v^2} = \frac{\Delta p}{\rho v^2} (\frac{D_h}{\mathrm{Re}_{D_h}})^2 \tag{5.11}$$

Equation (5.11) can be converted into the following form:

70

$$\Delta p = \Delta p^* \rho v^2 (\frac{\mathrm{Re}_{D_h}}{D_h})^2 \tag{5.12}$$

After equation (5.12) is substituted into equation (5.10) and necessary simplifications are carried out, the following relation is obtained:

$$\frac{\Delta P L^2}{\rho v^2} = \Delta p^* \mathrm{Re}_{D_h}^2 (\frac{L}{D_h})^2 = constant \tag{5.13}$$

As the definition of hydraulic diameter D_h, equation (5.6), is recalled, equation (5.13) becomes,

$$\frac{\Delta P L^2}{\rho v^2} = \frac{1}{4} \Delta p^* \mathrm{Re}_{D_h}^2 [\frac{L}{W} + \frac{1}{(\frac{s}{L})}]^2 = constant \tag{5.14}$$

It is known that Re_{D_h} is a function of the pressure difference and the corresponding geometrical parameters. Therefore, if the fixed dimensionless pressure drop Δp^*, and the parameters L/W and s/L are determined, the term $\Delta P L^2 / \rho v^2$ can be calculated. As a result, the selected dimensionless term $\Delta P L^2 / \rho v^2$ for pressure drop is convenient to be included in the optimization procedure.

5.2 MAXIMIZATION PROCEDURE AND NUMERICAL RESULTS

The procedure applied for the determination of heat transfer rate $\dot{Q} / kH \Pr(T_w - T_\infty)$ with respect to the parameter s/L can be summarized by the following steps:

1) Choose the value of L/W.

2) Choose the value of dimensionless pressure difference group $\Delta P L^2 / \rho v^2$.

3) Determine or assume the value of s/L.

4) Guess the Reynolds number Re_{D_h} for $\mathrm{Re}_{D_h} \le 2300$ (since the flow is laminar).

5) Calculate the dimensionless pressure drop ΔP^* from equation (5.14).

6) Solve the continuity and momentum equations, equations from (3.11) to (3.14), by Gauss-Seidel method in order to determine the dimensionless velocity

components u^*, v^*, w^*, and dimensionless pressure corrections P' at every nodal points.

7) Calculate corrected dimensionless pressure and velocity components P^{**}, u^{**}, v^{**} and w^{**} at every nodal points by using equations from (4.23a) to (4.23c), and equation (4.26).

8) Calculate the dimensionless pressure drop ΔP^* across the channel from the determined pressure field.

9) If the converged results for velocity and pressure fields are experienced, go to step 10. Otherwise, return back to step 6 by taking ΔP^* determined at step 8 as the new guessed value.

10) Solve the dimensionless energy equation, equation (3.15), by Gauss-Seidel method in order to obtain temperature distribution in the computational domain or dimensionless temperature values θ at each nodal point.

11) Calculate the dimensionless total heat transfer rate $\dot{Q}/kH\Pr(T_w - T_\infty)$ from equation (5.9).

12) Go to step 3 and choose a new s/L value.

13) As the smooth curve for the variation of total heat transfer rate as a function of board-to-board spacing at the prescribed pressure drop and at a certain L/W are obtained with the peak point, go to step 2 and choose another value of dimensionless pressure group, $\Delta P L^2 / \rho \nu^2$.

14) If the resulting data for a certain L/W value is seen to be sufficient for the generation of the smooth curves, as in Figure 5.4, with the optimum (peak) points, go to step 1 and choose another L/W value.

15) If the whole data is sufficient, stop the procedure.

Recall that the procedure for SIMPLE algorithm, which is presented in Figure 4.7, is applied between steps 6 and 7, and between steps 9 and 10 for the solution of flow and temperature fields. More detailed explanation of the operations between the corresponding steps can be found in the previous chapter.

In addition, it should be noted that calculations at steps from 1 to 14 have been repeated for eight different L/W values, which are sorted as 0.5, 1, 3, 5, 6, 8, 10 and 20. Therefore, "total heat transfer rate $\dot{Q}/kH\Pr(T_w - T_\infty)$ versus board-to-board

spacing s/L" curves for prescribed dimensionless pressure drop values $\Delta PL^2 / \rho v^2$ are plotted for eight different L/W values by repeating the whole procedure eight times.

The samples of "total heat transfer rate versus board-to-board spacing" curves for three cases, L/W=0.5, L/W=5 and L/W=10, are given in Figures 5.1, 5.2 and 5.3, respectively. In each of three graphs, peak points of the "total heat transfer rate versus board-to-board spacing" curves at some pressure difference values $\Delta PL^2 / \rho v^2$, which are indicated in the figures, can be clearly detected. Hence, the total heat transfer rate given by equation (5.9) is maximized by finding the optimum s/L ratio at specified group of dimensionless pressure drop $\Delta PL^2 / \rho v^2$ for each value of L/W. In other words, peak points of the curves in Figures 5.1, 5.2 and 5.3 are noted in terms of maximum total heat transfer rate and optimum board-to-board spacing at corresponding pressure difference and L/W value.
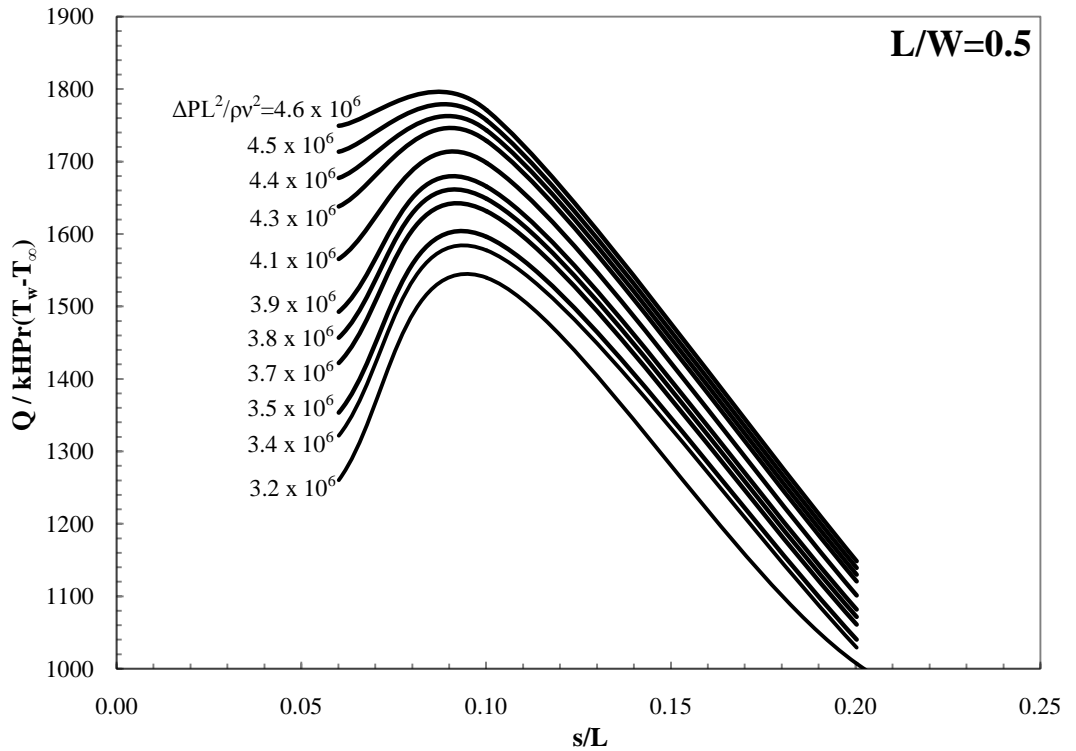
Figure 5.1 The total heat transfer rate versus board-to-board spacing (L/W=0.5)
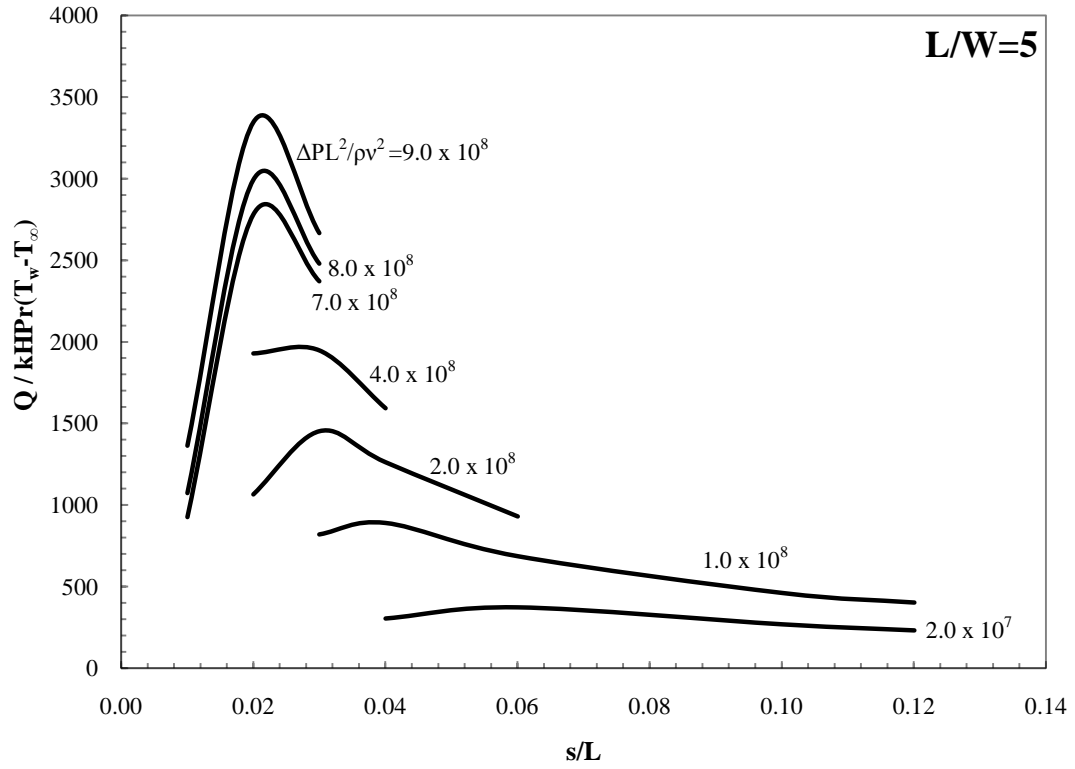
Figure 5.2 The total heat transfer rate versus board-to-board spacing (L/W=5)
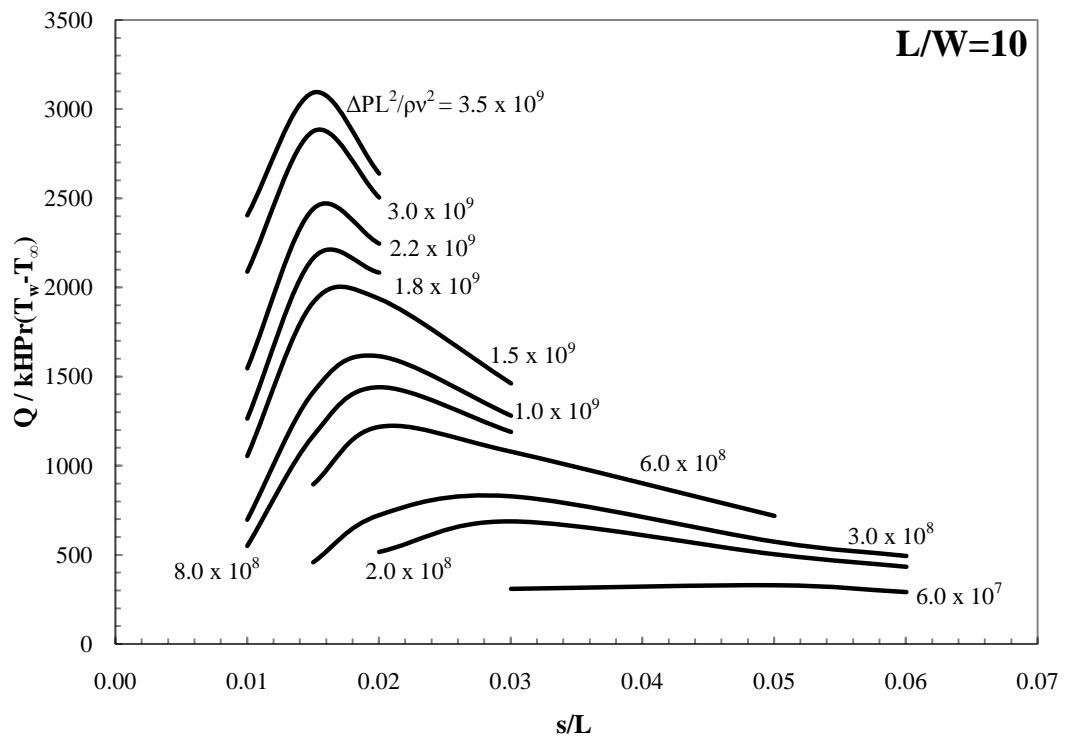
Figure 5.3 The total heat transfer rate versus board-to-board spacing (L/W=10)

74
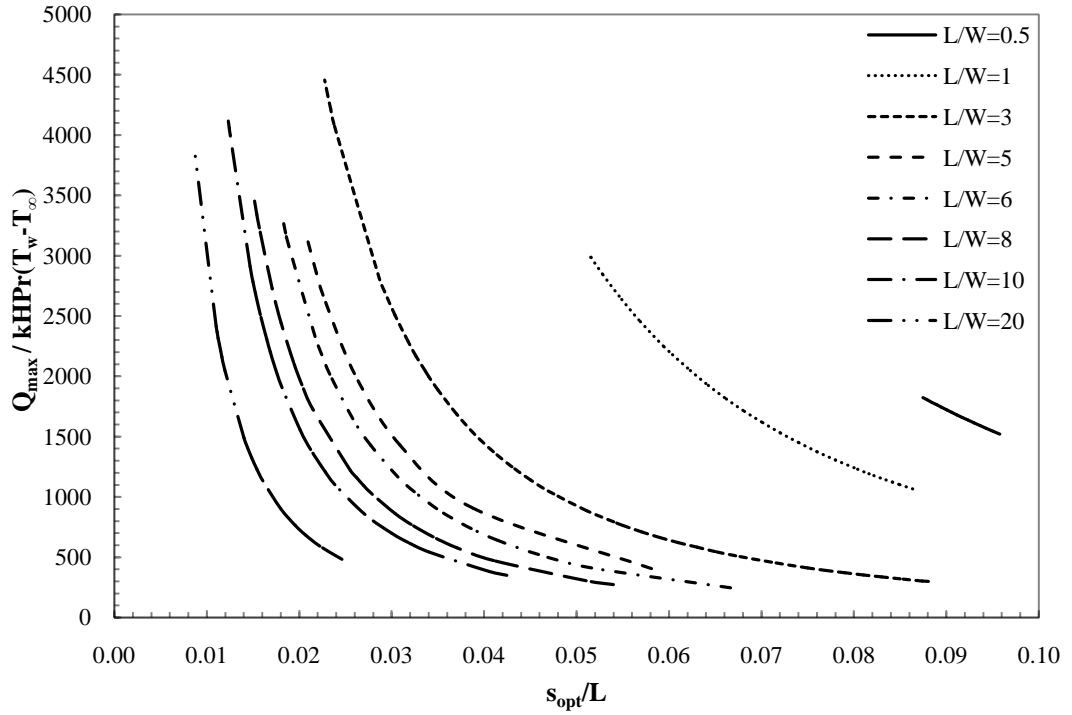
Figure 5.4 Maximum total heat transfer rate versus optimum board-to-board spacing for different L/W values

"$\dot{Q} / kH \Pr(T_w - T_\infty)$ versus s/L" curves for other L/W values are obtained in the same manner. Consequently, optimum (peak) points are noted for each model with respect to given L/W's. All of the peak points in terms of maximum total heat transfer rate and optimum board-to-board spacing are presented in Figure 5.4. It should be underlined that there is seen to be a general trend and relation between the curves.

5.3 OPTIMIZATION RESULTS

With the help of the peak points noted from the curves of "total heat transfer rate versus board-to-board spacing" in part 5.2, the points of data for the optimum spacing s_{opt}/L versus dimensionless group $\Delta P L^2 / \rho \nu^2$ are reported at each L/W in Figures from 5.5 to 5.12. Smooth curves are fitted into these points with maximum error of 13.5% in magnitude. Equations of the corresponding curves are indicated in the figures.
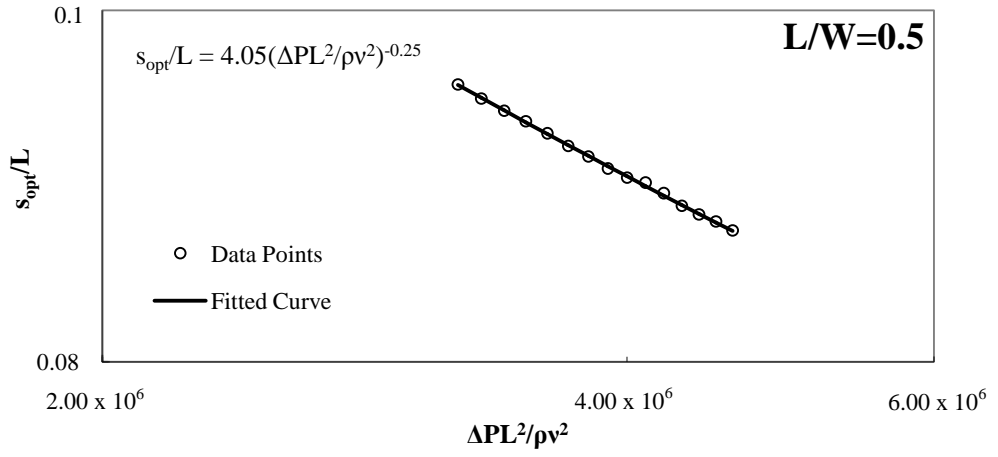
Figure 5.5 The optimum board-to-board spacing versus pressure drop (L/W=0.5)
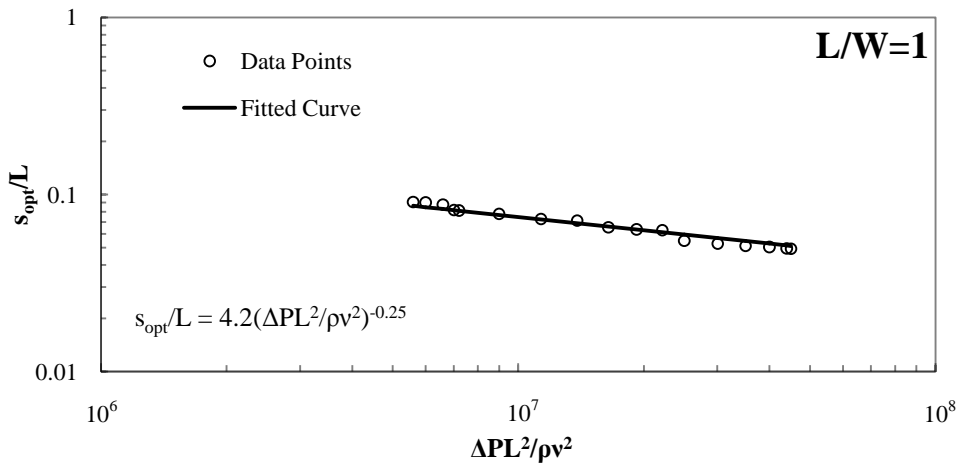
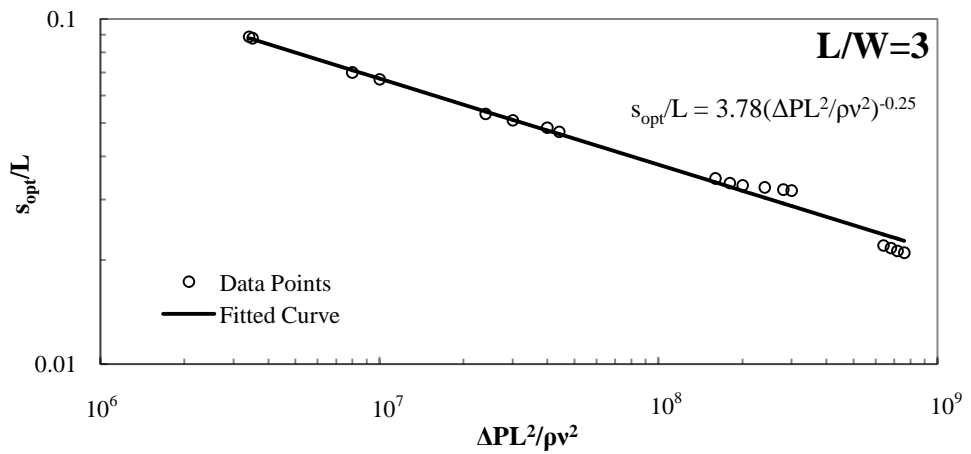**Figure 5.6** The optimum board-to-board spacing versus pressure drop (L/W=1)

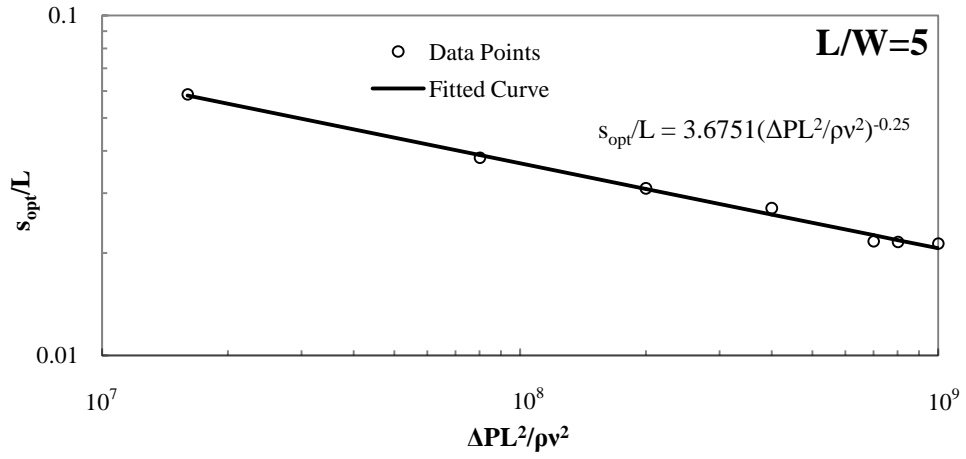**Figure 5.7** The optimum board-to-board spacing versus pressure drop (L/W=3)

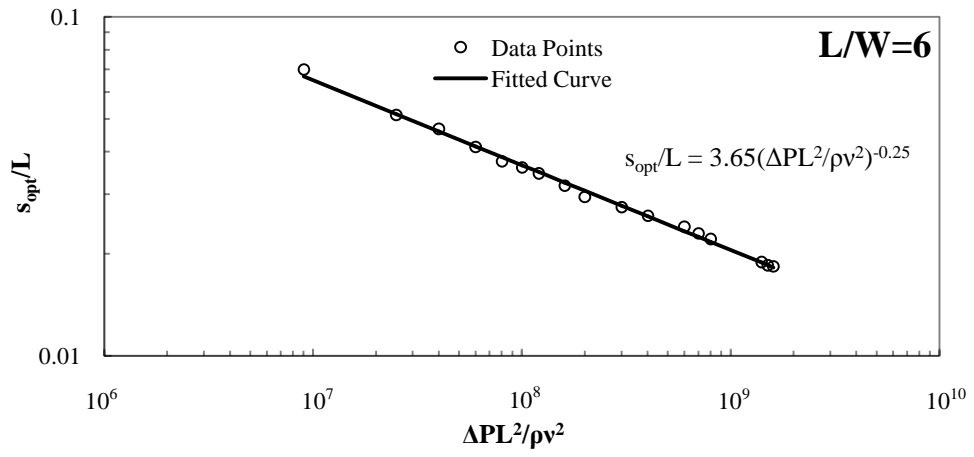**Figure 5.8** The optimum board-to-board spacing versus pressure drop (L/W=5)

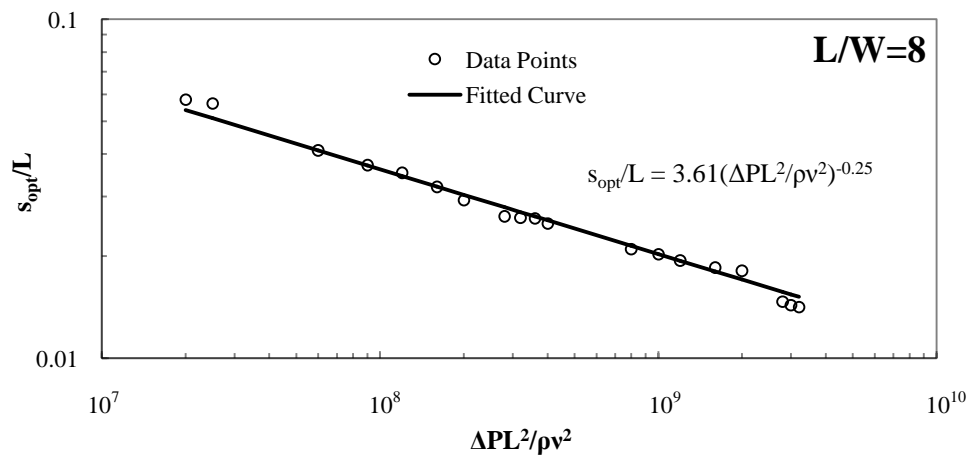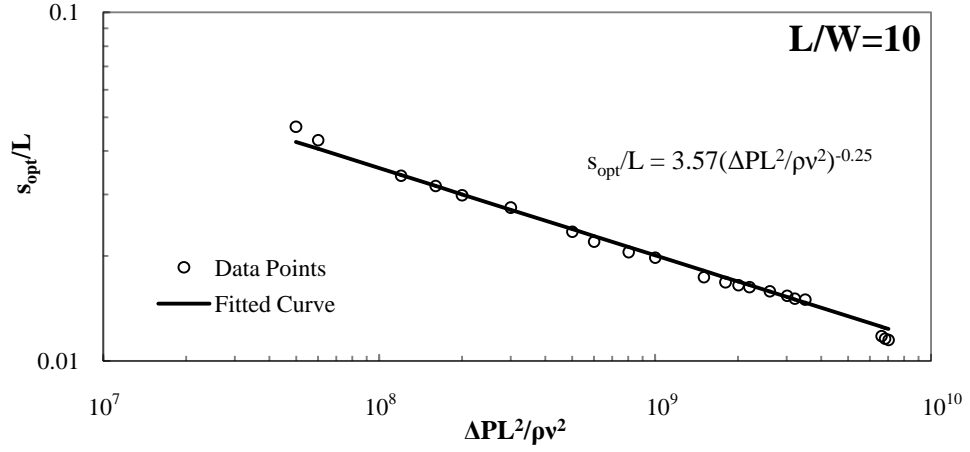**Figure 5.9** The optimum board-to-board spacing versus pressure drop (L/W=6)

Figure 5.10 The optimum board-to-board spacing versus pressure drop (L/W=8)

77

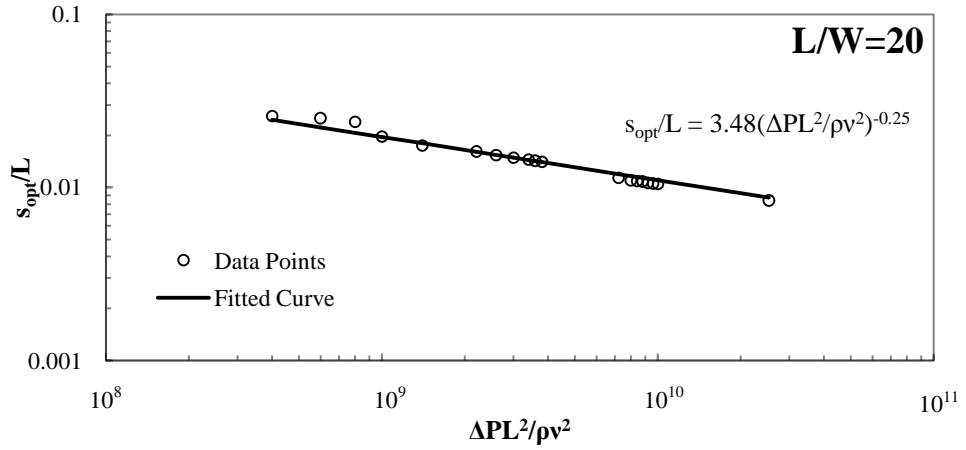**Figure 5.11** The optimum board-to-board spacing versus pressure drop (L/W=10)

Figure 5.12 The optimum board-to-board spacing versus pressure drop (L/W=20)

One can also plot the data indicating the trend of maximum dimensionless heat transfer rate with respect to the dimensionless pressure group $\Delta PL^2 / \rho v^2$. These data are additionally included in Figures from 5.13 to 5.20 along with their fitted curves and the corresponding relations. Note that the maximum error in curve fitting is 11.4% in magnitude.
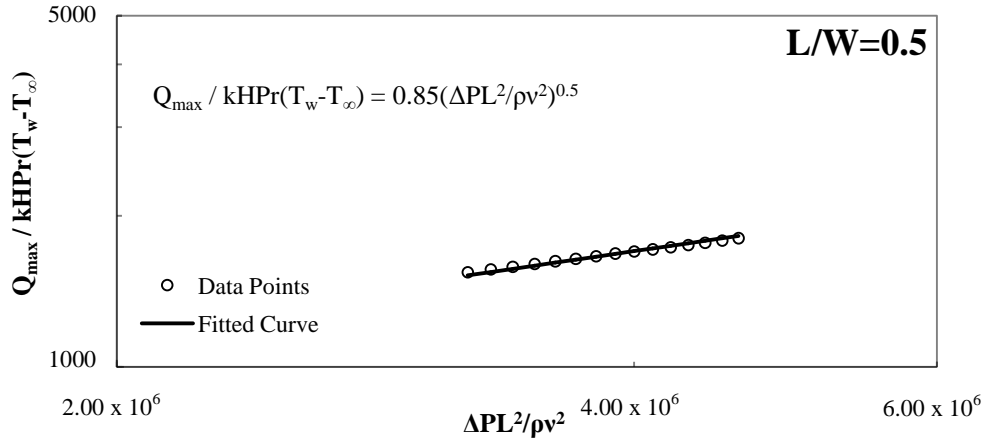
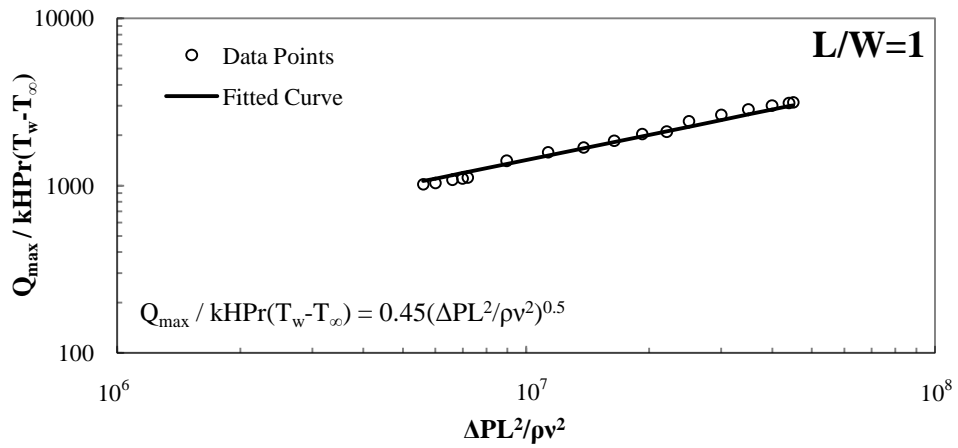**Figure 5.13** Maximum total heat transfer rate versus pressure drop (L/W=0.5)

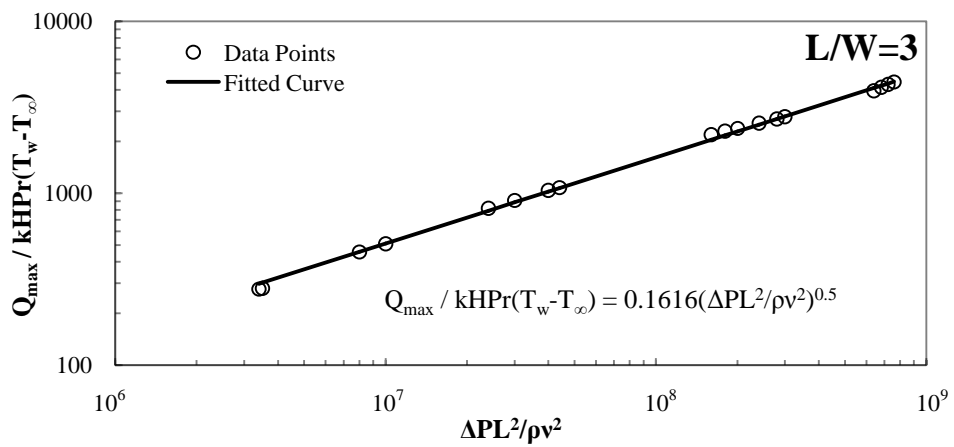**Figure 5.14** Maximum total heat transfer rate versus pressure drop (L/W=1)

Figure 5.15 Maximum total heat transfer rate versus pressure drop (L/W=3)

Figure 5.16 Maximum total heat transfer rate versus pressure drop (L/W=5)

Figure 5.17 Maximum total heat transfer rate versus pressure drop (L/W=6)

Figure 5.18 Maximum total heat transfer rate versus pressure drop (L/W=8)
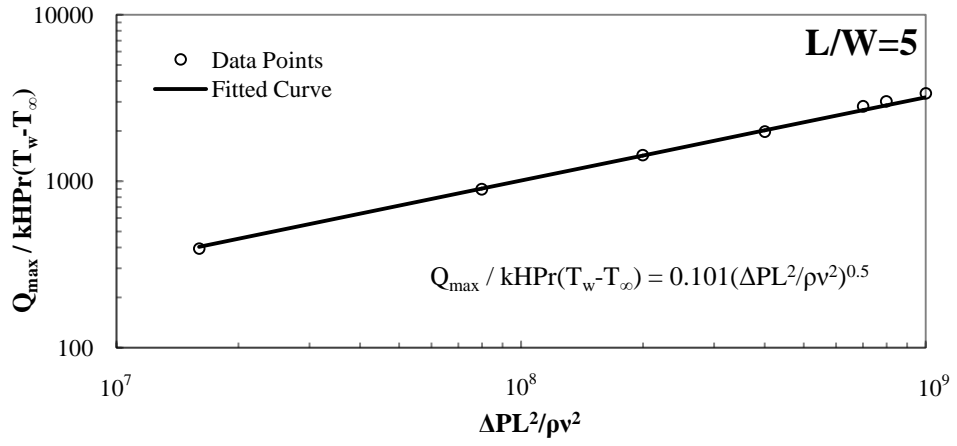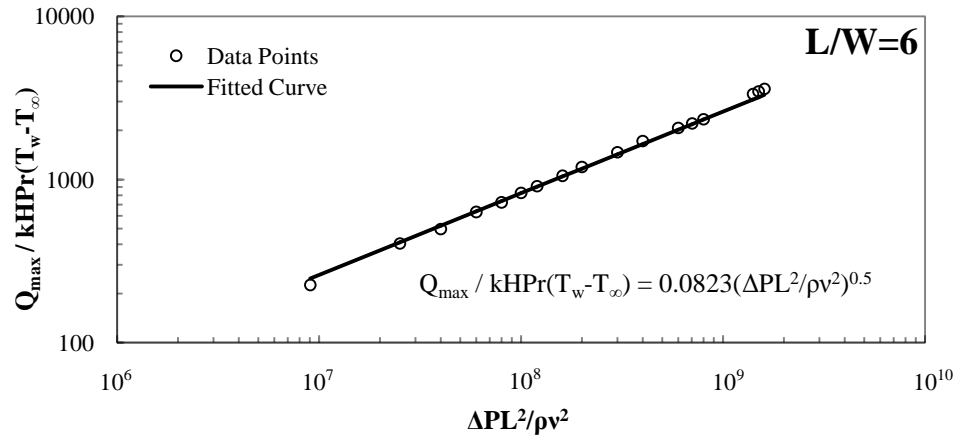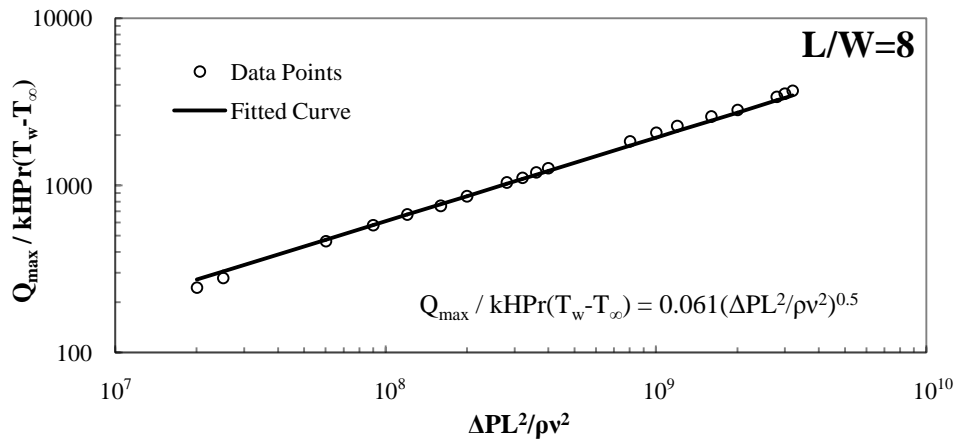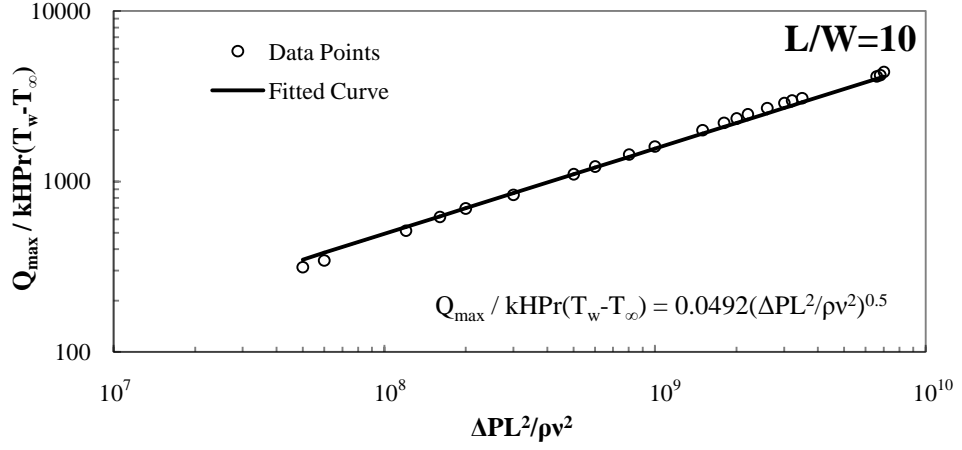
Figure 5.19 Maximum total heat transfer rate versus pressure drop (L/W=10)
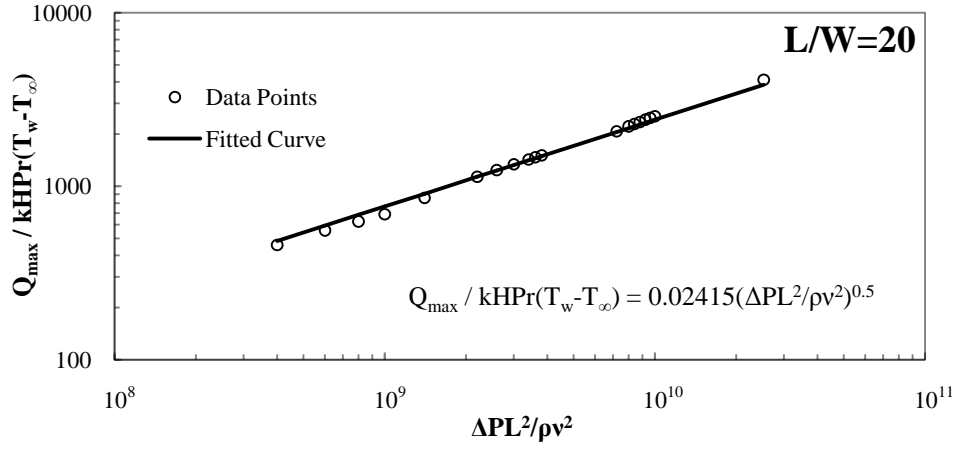
Figure 5.20 Maximum total heat transfer rate versus pressure drop (L/W=20)

To summarize the results, optimum spacing s_{opt}/L and maximum dimensionless heat transfer rate $\dot{Q}_{max}/kH\Pr(T_w - T_\infty)$ are related to dimensionless pressure difference group $\Delta PL^2/\rho v^2$ in terms of general expressions which are presented below:

$$\frac{s_{opt}}{L} = B\left(\frac{\Delta PL^2}{\rho v^2}\right)^{-0.25} \tag{5.15}$$

$$\frac{\dot{Q}_{max}}{kH\Pr(T_w - T_\infty)} = C\left(\frac{\Delta PL^2}{\rho v^2}\right)^{0.5} \tag{5.16}$$

Table 5.1 Values of coefficients B $\left(\dfrac{L}{W}\right)$ and C $\left(\dfrac{L}{W}\right)$ for different L/W ratios

	L/W							
	0.5	**1**	**3**	**5**	**6**	**8**	**10**	**20**
B	4.05	4.2	3.78	3.6751	3.65	3.61	3.57	3.48
C	0.85	0.45	0.1616	0.101	0.0823	0.061	0.0492	0.0241

where B and C are the constants that depend only on the parameter L/W. Values of coefficients B and C can be tabulated as in Table 5.1.

If the results for optimum spacing or width of the channels are progressed one step further, coefficients B and C are plotted with respect to parameter L/W in Figure 5.21 and Figure 5.22. Smooth curves passing through all of the points are also illustrated in the corresponding figures. Hence, the graphical relationships are acquired for the coefficients (B and C) as a function of L/W.
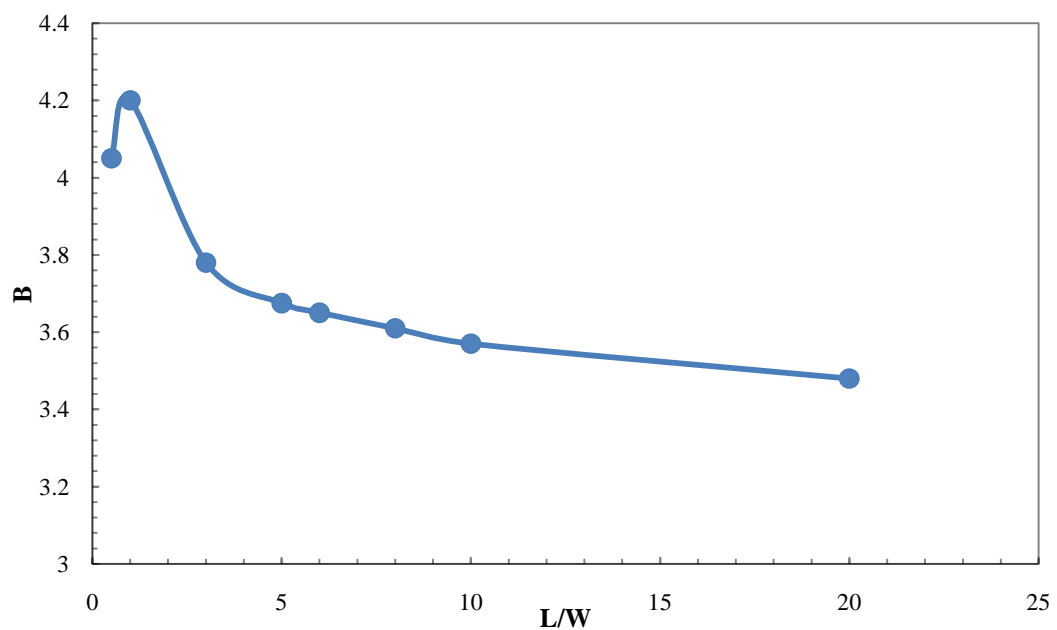

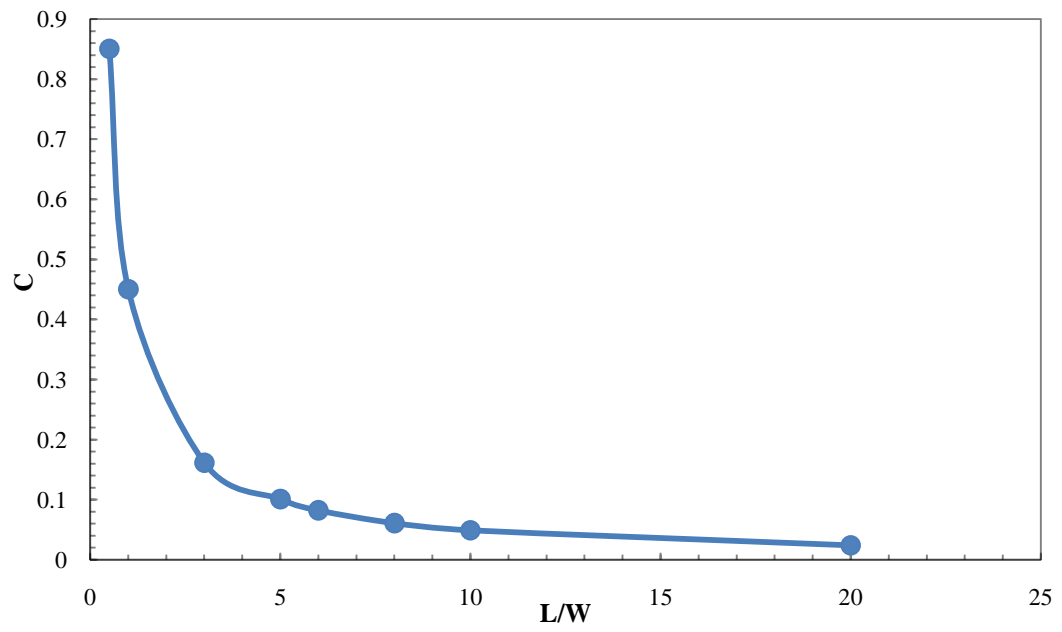
Figure 5.21 Coefficient, B, in equation (5.15), versus L/W

Figure 5.22 Coefficient, C, in equation (5.16), versus L/W

CHAPTER 6

CONCLUSION AND DISCUSSION

After the development of the graphs and the correlations in Chapter 5, the obtained results and their importance are to be discussed and assessed in certain aspects. Particularly, the possible errors associated with the numerical results are explained, and the findings in Chapter 5 are compared and validated with the two-dimensional studies of Bejan and Sciubba [8], and Yüncü and Ekici [14] in the current chapter.

First of all, the total error in the numerical estimation of the flow and heat transfer is called the residual error, which is determined after each iteration step. Residual error is defined as the relative approximation error averaged over all of the control volumes in the computational domain. It is mathematically expressed, by neglecting superscripts star (*) and prime (') in velocity and pressure components, as shown below:

$$E_P = \frac{\sum_{K=1}^{N_z-2} \sum_{J=1}^{N_y-2} \sum_{I=1}^{N_x-2} (P^n_{I,J,K} - P^{n-1}_{I,J,K})}{\sum_{K=1}^{N_z-2} \sum_{J=1}^{N_y-2} \sum_{I=1}^{N_x-2} P^n_{I,J,K}} \tag{6.1a}$$

$$E_u = \frac{\sum_{K=1}^{N_z-2} \sum_{J=1}^{N_y-2} \sum_{i=1}^{N_x-3} (u^n_{i,J,K} - u^{n-1}_{i,J,K})}{\sum_{K=1}^{N_z-2} \sum_{J=1}^{N_y-2} \sum_{i=1}^{N_x-3} u^n_{i,J,K}} \tag{6.1b}$$

$$E_v = \frac{\sum\limits_{K=1}^{N_z-2}\sum\limits_{j=1}^{N_y-3}\sum\limits_{I=1}^{N_x-2}(v^n_{I,j,K} - v^{n-1}_{I,j,K})}{\sum\limits_{K=1}^{N_z-2}\sum\limits_{j=1}^{N_y-3}\sum\limits_{I=1}^{N_x-2}v^n_{I,j,K}} \tag{6.1c}$$

$$E_w = \frac{\sum\limits_{k=1}^{N_z-3}\sum\limits_{J=1}^{N_y-2}\sum\limits_{I=1}^{N_x-2}(w^n_{I,J,k} - w^{n-1}_{I,J,k})}{\sum\limits_{k=1}^{N_z-3}\sum\limits_{J=1}^{N_y-2}\sum\limits_{I=1}^{N_x-2}w^n_{I,J,k}} \tag{6.1d}$$

$$E_\theta = \frac{\sum\limits_{K=1}^{N_z-2}\sum\limits_{J=1}^{N_y-2}\sum\limits_{I=1}^{N_x-2}(\theta^n_{I,J,K} - \theta^{n-1}_{I,J,K})}{\sum\limits_{K=1}^{N_z-2}\sum\limits_{J=1}^{N_y-2}\sum\limits_{I=1}^{N_x-2}\theta^n_{I,J,K}} \tag{6.1e}$$

, as also reported in equations from (4.31a) to (4.31e) without the error notations $E_{p,u,v,w,\theta}$. When the necessary conditions, indicated in equations from (4.31a) to (4.31e), are satisfied, the Gauss-Seidel and SIMPLE iterations are stopped. However, note that inequalities given by (4.31a), (4.31b), (4.31c) and (4.31d) should be simultaneously satisfied for the sufficient results in SIMPLE algorithm. At this point, it should be emphasized that the relative error limits have been determined to be as low as possible by the consideration of having reasonably low CPU times for the computations. In other words, relative residual errors in the numerical algorithm have been kept as low as possible by the specified error limits with reasonably low CPU times.

Residual errors are caused by the summation of two main types of numerical errors, which are known to be round-off and truncation errors [35]. Round-off error is because of the limited number of significant digits stored in the computer memory [35]. It can be reduced by increasing the number of significant digits in the numerical code. In this study, double precision, which provides a satisfactory precision with 15 significant digits [36], is assigned for the numbers. Therefore, the effects of round-off errors can be made negligible by the usage of double precision. Next, the second type of numerical error, truncation error, is involved in the numerical results for the reason that numerical methods are primarily developed from the approximation of

exact mathematical expressions, such as infinite series. The infinite series are cut after a certain expression, and this condition leads to the truncation errors in the solution. Therefore, the extent of the truncation errors mainly depends on the scheme used for the discretization of differential equations [35]. The undesirable effects of truncation error are alleviated by integrating non-uniform meshes, which are finer at the regions having high gradients for velocity and temperature, and grid adaptation, which has also been presented in Tables from 4.2 to 4.4, during the development of the numerical model.

After the description of the possible numerical errors and the precautions against their dangerous effects, the outcomes of the numerical solution can be compared with the findings of Bejan and Sciubba [8], and Yüncü and Ekici [14]. It can be recalled from Chapter 2 that both studies have been carried out for two-dimensional parallel boards having infinite widths (W) in y-direction. Therefore, their studies are represented by the special case "L/W=0" in the generalized solution of the current problem.

At this point, it should be appropriate to reconsider Figure 5.21 with additional points in Figure 6.1. The dashed curve in Figure 6.1 is given for the case in which the data from the current problem are joined with the numerical solution of Bejan and Sciubba [8] when "L/W=0". The other two points are the results from Bejan and Sciubba's approximate analytical solution (intersection of asymptotes) [8] and from Yüncü and Ekici's numerical analysis [14], respectively.

As clearly observed from Figure 6.1, a considerably smooth curve is generated when the results indicated in Figure 5.21 are combined with the Bejan and Sciubba's numerical result [8], which are suitable for infinite parallel plates. Hence, the outcome of the current numerical problem can be safely extended to the limiting case of "L/W=0". In fact, the numerical results obtained from this study are validated by the consistency of the extended dashed curve in Figure 6.1 with the curve in Figure 5.21, which is the continuous curve in Figure 6.1. As a result, the complete smooth curve with dashed extension in Figure 6.1 can be used for the design of three-dimensional thermal packaging systems for cooling purposes. In addition, when Figure 5.22 is investigated in detail, total heat transfer rate from the parallel boards

goes to infinity as L/W is approximated to zero. This condition is expected since "L/W=0" case means infinite area for heat generating surfaces and, by contrast, negligibly small area for insulated walls in three-dimensional working model.

The other limiting case is encountered when L/W goes to infinity. Unlike "L/W=0", heat generating surface area is almost zero, and insulated lateral surface area is relatively large in this case. As expected, total heat transfer rate from the boards becomes almost zero for the limiting case of infinite L/W value because of the small heat transfer area against large area of insulated walls. Furthermore, it is implied in Figure 6.1 that there is, most probably, an asymptote at about "B=3.3-3.4" for very large L/W values. It means that change of L/W does not affect significantly the determination of optimal spacing of parallel boards when L/W is designed to be very large. It may also be expected for the reason that variation of total heat transfer rate with respect to L/W is very small for large L/W values, as indicated from Figure 5.22.
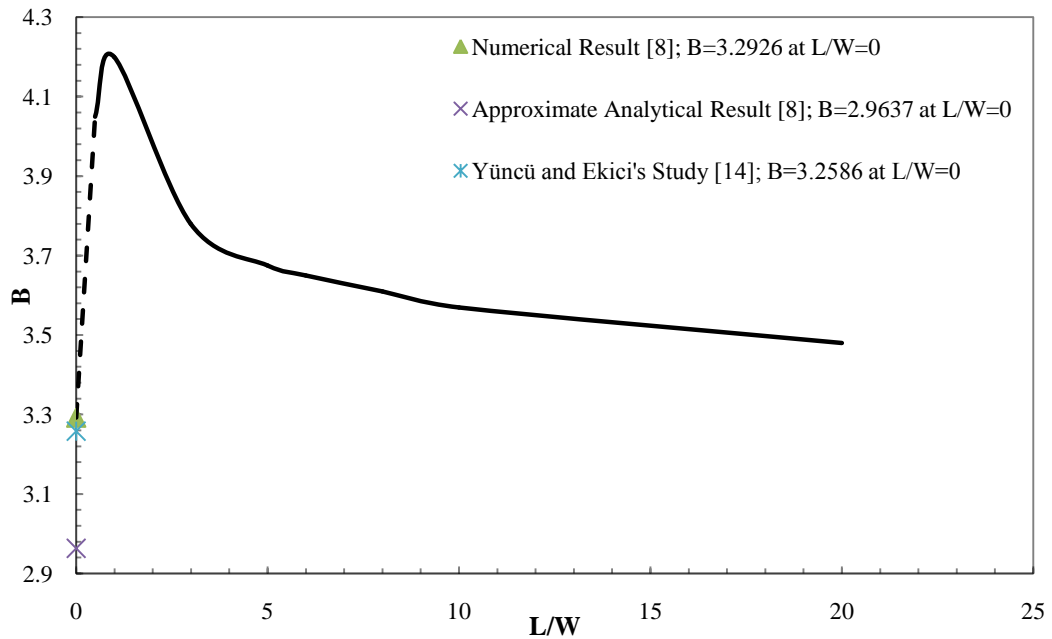

Figure 6.1 Coefficient, B, in equation (5.15), versus L/W in the current study and its comparison with the other studies in literature

To summarize, we conclude from the numerical results the following:

a) Theoretical expression for the optimum spacing of parallel heat generating isothermal boards stacked in a fixed volume of electronic package is found by the relation $s_{opt} / L = B(\Delta P L^2 / \rho v^2)^{-0.25}$. Coefficient B, which is included in the corresponding relation, is a function of L/W, and it is given in Figure 5.21 or Figure 6.1.

b) Theoretical expression for the maximum heat transfer rate from parallel heat generating isothermal boards stacked in a fixed volume of electronic package is found by the relation $\dot{Q}_{max} / kH \Pr(T_w - T_\infty) = C(\Delta P L^2 / \rho v^2)^{0.5}$. Coefficient C, which is included in the corresponding relation, is a function of L/W, and it is given in Figure 5.22.

c) The data obtained from the numerical solution yields a good agreement with the available results [8, 14] in literature.

REFERENCES

[1] Bar-Cohen, A., Watwe, A.A., and Prasher, R.S., Heat Transfer in Electronic Equipment, in Bejan, A., and Kraus, A.D., eds., *Heat Transfer Handbook*, John Wiley & Sons, USA, pp. 947-1027, 2003

[2] Bar-Cohen, A., Perelman, A., and Sabag, A., Bubble Pumped Convective Augmentation on Vertical Submerged Condenser Surfaces, (cited in) Bar-Cohen, A., Watwe, A.A., and Prasher, R.S., Heat Transfer in Electronic Equipment, in Bejan, A., and Kraus, A.D., eds., *Heat Transfer Handbook*, John Wiley & Sons, USA, pp. 947-1027, 2003

[3] National Electronics Manufacturing Institute, *Technology Roadmap*, (cited in) Bar-Cohen, A., Watwe, A.A., and Prasher, R.S., Heat Transfer in Electronic Equipment, in Bejan, A., and Kraus, A.D., eds., *Heat Transfer Handbook*, John Wiley & Sons, USA, pp. 947-1027, 2003

[4] Semiconductor Industry Association, *National Technology Roadmap for Semiconductors: Technology Needs*, (cited in) Bar-Cohen, A., Watwe, A.A., and Prasher, R.S., Heat Transfer in Electronic Equipment, in Bejan, A., and Kraus, A.D., eds., *Heat Transfer Handbook*, John Wiley & Sons, USA, pp. 947-1027, 2003

[5] Kakaç, S., Introduction to ASI on Cooling of Electronics, in Kakaç, S., Yüncü, H., and Hijikata, K., eds., *Cooling of Electronic Systems*, (cited in) Ekici, Ö., The Optimum Spacing Between Parallel Heat Generating Boards Cooled by Forced Convection, *Thesis for the Degree of Master of Science*, Middle East Technical University, p. 4, July 2001

[6] Yanagida, T., A Method for Calculating the Temperature Distribution of IC Packages on a PBC (Part I, Temperature Distribution in the Thermal Wake of an IC Package), (cited in) Ekici, Ö., The Optimum Spacing Between Parallel Heat Generating Boards Cooled by Forced Convection, *Thesis for the Degree of Master of Science*, Middle East Technical University, p. 5, July 2001

[7]   Ekici, Ö., The Optimum Spacing Between Parallel Heat Generating Boards Cooled by Forced Convection, *Thesis for the Degree of Master of Science*, Middle East Technical University, July 2001

[8]   Bejan, A., and Sciubba, E., The Optimal Spacing of Parallel Plates Cooled by Forced Convection, *International Journal of Heat and Mass Transfer*, Vol. 35, No. 12, pp. 3259-3264, 1992

[9]   Bejan, A., *Convection Heat Transfer*, 2nd edition, John Wiley & Sons, USA, p. 157, 1984

[10]   Bejan, A., *Shape and Structure From Engineering to Nature,* Cambridge University Press, Cambridge, 2000

[11]   Mereu, S., Sciubba, E., and Bejan, A., The Optimal Cooling of a Stack of Heat Generating Boards with Fixed Pressure Drop, Flowrate or Pumping Power, *International Journal of Heat and Mass Transfer,* Vol. 36, No. 15, pp. 3677-3686, 1993

[12]   Favre-Marinet, M., Le Person, S., and Bejan, A., Maximum Heat Transfer Rate Density in Two-Dimensional Minichannels and Microchannels, *Nanoscale and Microscale Thermophysical Engineering*, Vol. 8, Issue 3, pp. 225-237, 2004

[13]   Campo, A., Bounds for the Optimal Conditions of Forced Convective Flows Inside Multiple Channels Whose Plates are Heated by a Uniform Flux, *International Communications in Heat and Mass Transfer*, Vol. 26, No. 1, pp. 105-114, 1999

[14]   Yüncü, H., and Ekici, Ö., The Optimum Spacing Between Parallel Heat Generating Boards Cooled by Laminar Forced Convection, *Journal of Thermal Science and Technology*, Vol. 26, No. 2, pp. 1-10, 2006

[15]   Morega, A.M, and Bejan, A., Optimal Spacing of Parallel Boards with Discrete Heat Sources Cooled by Laminar Forced Convection, *Numerical Heat Transfer, Part A: Applications*, Vol. 25, Issue 4, pp. 373-392, 1994

[16]   Bejan, A., and Fautrelle, Y., Constructal Multi-Scale Structure for Maximal Heat Transfer Density, *Acta Mechanica*, Vol. 163, pp. 39-49, 2003

[17]   Bello-Ochende, T., Bejan, A., Maximal Heat Transfer Density: Plates with Multiple Lengths in Forced Convection, *International Journal of Thermal Sciences*, Vol. 43, No. 12, pp. 1181-1186, 2004

[18]   Furukawa, T., and Yang, W., Thermal Optimization of Channel Flows with Discrete Heating Sections, *Journal of Non-Equilibrium Thermodynamics*, Vol. 28, Issue 4, pp. 299-310, 2003

[19]   Bejan, A., *Entropy Generation Through Heat and Fluid Flow*, John Wiley & Sons, USA, 1982

[20]   Patankar, S.V., *Numerical Heat Transfer and Fluid Flow*, Hemisphere Publishing Corporation, Taylor & Francis Group, New York, 1980

[21]   Da Silva, A.K., Bejan, A., and Lorente, S., Maximal Heat Transfer Density in Vertical Morphing Channels with Natural Convection, *Numerical Heat Transfer, Part A: Applications*, Vol. 45, Issue 2, pp. 135-152, 2004

[22]   Bello-Ochende, T., and Bejan, A., Optimal Spacing for Mixed Convection, Transactions of the ASME, *Journal of Heat Transfer*, Vol. 126, Issue 6, pp. 956-962, 2004

[23]   Yilmaz, A., Büyükalaca, O., and Yilmaz, T., Optimum Shape and Dimensions of Ducts for Convective Heat Transfer in Laminar Flow at Constant Wall Temperature, *International Journal of Heat and Mass Transfer*, Vol. 43, No. 5, pp. 767-775, 2000

[24]   Tunc, G., and Bayazitoglu, Y., Heat Transfer in rectangular microchannels, *International Journal of Heat and Mass Transfer*, Vol. 45, No. 4, pp. 765-773, 2002

[25]   Muzychka, Y.S., Constructal Design of Forced Convection Cooled Microchannel Heat Sinks and Heat Exchangers, *International Journal of Heat and Mass Transfer*, Vol. 48, No. 15, pp. 3119-3127, 2005

[26]   Kakaç, S., Yüncü, H., and Hijikata, K., eds., *Cooling of Electronic Systems*, Kluwer Academic Publishers, Dordrecht, Netherlands, 1994

[27] Sathe, S., and Sammakia, B., A Review of Recent Developments in Some Practical Aspects of Air-Cooled Electronic Packages, Transactions of the ASME, *Journal of Heat Transfer*, Vol. 120, No. 4, pp. 830-839, 1998

[28] Versteeg, H.K., and Malalasekera, W., *An Introduction to Computational Fluid Dynamics: The Finite Volume Method*, 2nd edition, Pearson Education Limited, Harlow, Essex, United Kingdom, 2007

[29] Harlow, F.H., and Welch, J.E., Numerical Calculation of Time-Dependant Viscous Incompressible Flow of Fluid with Free Surface, *Physics of Fluids*, Vol. 8, pp. 2182-2189, 1965

[30] Shah, R.K., and London, A.L., *Laminar Flow Forced Convection Heat Transfer and Flow Friction in Straight and Curved Ducts – A Summary of Analytical Solutions*, (cited in) Shah, R.K., and London, A.L., *Laminar Flow Forced Convection in Ducts*, Academic Press, New York, p. 200, 1978

[31] Schmidt, F.W., Personal Communication, (cited in) Shah, R.K., and London, A.L., *Laminar Flow Forced Convection in Ducts*, Academic Press, New York, p. 204, 1978

[32] Curr, R.M., Sharma, D., and Tatchell, D.G., Numerical Predictions of Some Three-Dimensional Boundary Layers in Ducts, (cited in) Shah, R.K., and Bhatti, M.S., Laminar Convective Heat Transfer in Ducts, in Kakaç, S., Shah, R.K., and Aung, W., eds, *Handbook of Single-Phase Convective Heat Transfer*, John Wiley & Sons, USA, Chapter 3, 1987

[33] Bhattacharjee, S., and Grosshandler, W.L., The Formation of Wall Jet Near a High Temperature Wall under Microgravity Environment, *ASME National Heat Transfer Conference*, Vol. 96, pp. 711-716, 1988

[34] Petrescu, S., Comments on the Optimal Spacing of Parallel Plates Cooled by Forced Convection, *International Journal of Heat and Mass Transfer*, Vol. 37, No. 8, p. 1283, 1994

[35] Chapra, S.C., and Canale, R.P., *Numerical Methods for Engineers*, 5th edition (ISE edition), McGraw-Hill, Singapore, pp. 54-55, 2006

[36]   Deitel, P.J., and Deitel, H.M., *C++ How to Program*, Prentice Hall (Pearson Education Limited), Upper Saddle River, New Jersey, 2008